UPC   eit InnoEnergy   etha wind SUSTAINABLE BUSINESS   KTH VETENSKAP OCH KONST

Universitat Politècnica de Catalunya

Escola Tècnica Superior d'Enginyeria Industrial de Barcelona

Estimation of the wind energy resource in relation to orographic complexity in Finland: A comparison study of three conventional wind simulation software

MASTER THESIS

Master of Energy Engineering

Autor: Paola Israde Burrola

Director: Enrique Velo

Industrial supervisors: Staffan Asplund & Christian Granlund

September 2019

Estimation of the wind energy resource in relation to orographic complexity in Finland:

A comparison study of three conventional wind simulation software

Paola Israde Burrola

Abstract

The aim of this study is to provide a comparative study for three conventional software for wind resource assessment (WindPRO, WindSim and Zephy TOOLS) applied to a place with a low orographic complexity terrain (Korpinen), a place with a moderate slope (Lokan Tekojärvi) and a fictive case of a complex terrain where there is a current ski resort (Ylläs), all of them located in Finland. The main outcome parameter to be investigated in the simulations is the wind speed. Furthermore, the analysis of the outcome will give a hint of the suitability of each software depending on the different site conditions and input parameters.

Once the locations were defined, the input files for every software had to be prepared and processed in third software, such as QGis, OpenWind, Global Mapper and text editors in order to be handled in the correct extension for each software.

The results indicate that both WindPRO and WindSim manage to estimate the wind resource accurately when the terrain has a low orographic complexity. In this case, the linear model, without the ability to model turbulence is as good as the non-linear model in wind resource estimation terms. Zephy TOOLS overestimates the wind speeds in this type of terrain with only 0.40%. For the moderate slope, WindPRO and WindSim differ in only 0.13% while Zephy TOOLS over-predicts again the wind speed in 0.40%. For the site with complex orography, the three software present a significant difference of the wind estimation of around 1.35m/s between them.

Keywords: WindPRO, WindSim, Zephy TOOLS, complex terrain, wind resource assessment, CFD modelling.

Estimación del recurso de energía eólica en relación con la complejidad orográfica en Finlandia

Un estudio comparativo de tres software de simulación de viento convencionales

Paola Israde Burrola

Resumen

El objetivo de este estudio es proporcionar un estudio comparativo de tres software convencionales para la evaluación del recurso eólico (WindPRO, WindSim y Zephy TOOLS) aplicado a un lugar con un terreno de baja complejidad orográfica (Korpinen), un lugar con una pendiente moderada (Lokan Tekojärvi) y un caso ficticio de un terreno complejo donde hay una estación de esquí (Ylläs), todos ellos ubicados en Finlandia. El principal parámetro resultante a investigar en las simulaciones es la velocidad del viento. Además, el análisis de resultados dará una pista de la idoneidad de cada software dependiendo de las diferentes condiciones del sitio y parámetros de entrada.

Una vez que se definieron las ubicaciones, los archivos de entrada para cada software tuvieron que prepararse y procesarse en un tercer software, como QGis, OpenWind, Global Mapper y editores de texto para poder manejarlos en la extensión correcta para cada software.

Los resultados indican que tanto WindPRO como WindSim logran estimar el recurso eólico con precisión cuando el terreno tiene una baja complejidad orográfica. En este caso, el modelo lineal, sin la capacidad de modelar turbulencia, es tan bueno como el modelo no lineal en términos de estimación del recurso eólico. Zephy TOOLS sobreestima la velocidad del viento en este tipo de terreno con solo 0.40%. Para la pendiente moderada, WindPRO y WindSim difieren en solo 0.13%, mientras que Zephy TOOLS vuelve a sobreestimar de nuevo la velocidad del viento en 0.40%. Para el sitio con orografía compleja, los tres software presentan una diferencia significativa de la estimación del viento de alrededor de 1.35 m/s entre ellos.

Palabras clave: WindPRO, WindSim, Zephy TOOLS, terreno complejo, evaluación de recursos eólicos, modelado CFD.

Dedication

To mom & dad, Zaira, abi Blanca & abi Angela,

to Johan & David

I love you

Preface

This master thesis is the final project for the joint master's program in *Renewable Energy (RENE)*, accredited by the *European Institute of Innovation and Technology (EIT)* and *KIC InnoEnergy*, the leading engine for innovation and entrepreneurship in sustainable energy.

The double master's degree program for Renewable Energy leads to a *Master of Science*, from KTH: Royal Institute of Technology, Sweden and a *Master of Energy Engineering*, from UPC: Universitat Politècnica de Catalunya · BarcelonaTech, Spain.

This thesis has been carried out at the company *Etha Wind OY* in Vaasa, Finland.

Acknowledgements

Paola Israde Burrola
Vaasa, Finland. September 17, 2019

Contents

List of Figures

List of Tables

Acronyms

AEP Annual Energy Production. 45, 50, 64, 67

CFD Computational Fluid Dynamics. 24, 36, 38, 45, 46

EIA Environmental Impact Assessment. 114

LCOE Levelised Cost of Electricity. 108

MCD Measure Correlate Predict. 46

NLS National Land Survey of Finland. 59, 60

O&M Operations and Maintenance costs. 110

PD Public Display. 114

RANS Reynolds Averaged Navier-Stokes. 24, 36, 38
RIX Ruggedness Index. 43

WTGs Wind Turbine Generators. 45, 46, 51, 63, 64

Chapter 1

Introduction

The assessment of wind resource availability in a potential site is of high importance in the project development stage. Suitable places for wind power generation can be located with the assistance of professional software that models and predicts the wind behavior, allowing to estimate the power production. Such tools employ different flow models depending on the complexity of the terrain. For a flat and simple orography, where the wind resource assessment and energy estimations are uncomplicated, linear models give acceptable results. Conversely, for complex terrain, a non-linear Computational Fluid Dynamics (CFD) model is applied, introducing orography effects that can be adjusted to model wind flow in the boundary layer.

Among the popular commercial software employed by wind development consulting firms, **WindPRO** and **WindSim** stand out due to the veracity and reliability of the results. Alternatively, many other software developers continue innovating the models to obtain improved and more accurate results for the wind power assessment. That is the case of **Zephy TOOLS**, carrying an innovative mindset to revolutionize the use of computer modeling in the wind energy industry, and has developed a range of tools and services in the wind resource assessment branch using open-source and cloud-computing technology.

The accuracy of these software diverge due to the diverse simulation parameters. For this reason, it is of interest to produce an in-depth study of the outcome differences between linear and non-linear models used in wind power simulations and to evaluate the limitations of such computing tools concerning the chosen simulation parameters in order to determine which type of software is suitable for each specific type of landscape and how the simulation should be performed.

In this study, three different places in Finland will be estimated and compared in terms of wind resources availability, having different orography, from gentle and smooth to complex terrain and such results will be validated using authentic measurements from a real wind farm.

1.1 Aims and objectives

This study aims to provide a comparative study for three wind assessment software applied to an onshore place with a low orographic complexity terrain (Korpinen), an onshore place with a moderate slope (Lokan Tekojärvi) and a fictive case of a complex terrain where there is a current ski resort (Ylläs).

The main outcome parameter to be investigated in the simulations is the wind speed. Furthermore, the analysis of the outcome will give a hint of the suitability of each software depending on the different site conditions and input parameters.

1.2 Limitations

The information used for the simulations concerning the climatology was provided by Etha Wind OY, comprising real time data recorded with a met mast of 137m located at an existing wind farm in Finland. Due to privacy reasons, the real location cannot be revealed, but will be called *"Finlandia"* throughout this study.

Another constraint involves the use of a new software named *"Zephy TOOLS"*, for which there is not much information apart from their website. The lack of step-by-step guidance is time-consuming for the user, as many questions arise throughout the simulation process, not to mention the uncertainties of the results after a long computing time invested.

1.3 Dissertation research questions

- Which software provides more reliable and accurate results in terms of wind speed calculation for different complexity terrain sites?

- What are the advantages of using a CFD modelling software over a linear flow model?

- In terms of user experience, which software offers the least painless and more appropriate option?

- In terms of computational time, which software can provide suitable results in an acceptable time frame?

- In terms of visual results, which software provides sufficient and adequate outputs?

1.4 Literature review

Different authors have used the wind simulation software WAsP, WindSim and WindPRO to estimate different parameters. Still, research of this kind using both WindSim and WindPRO in Finland is nonexistent. Likewise, no information about research using Zephy TOOLS was found.

1.4.1 Latest research using WindSim

Johansson (2013) performed a comparison of wind resource calculations made with the software WAsP (linear model) and the CFD software WindSim over a Swedish hilly forested area. The results of the study suggest that WindSim can provide a slightly increased accuracy compared to WAsP, but CFD modeling does not automatically give more reliable modeling results. The results of WindSim were highly dependent on how the model was set up and therefore, more errors were observed in WindSim compared to WAsP. It also became clear for WindSim that a model in which the simulated wind shear coincided with the measured one, did not necessarily imply to produce good extrapolations of wind conditions from different towers. Furthermore, WAsP misjudged the effects of the topography and for any wind measurements on distinctive heights WAsP was likely to overestimate the wind conditions in the low-lying parts of the terrain.

Mancebo (2014) studied the behavior of an embankment in Hjardemål, Denmark using two different software, Meteodyn WT and WindSim to evaluate the vertical wind profiles given the site measurements. His results showed that Meteodyn WT predicts closer vertical wind profiles before the embankment, at and after, whilst WindSim predicts a closer wind profile just after the embankment. The discussion of his results is based on the limitations of both software tools, which have conditioned the comparison, including the lack of measurements at higher heights not allowing for an ampler comparison with reality, but software comparisons found a better convergence at higher heights.

1.4.2 Latest research using WindPRO

Dayal (2015) carried out an offshore wind resource assessment, site suitability and technology selection for Bligh Waters in Fiji using WindPRO, and performed energy calculations for a 10-12MW model offshore wind farm. A simple economic analysis was also included, comparing the results to the cost of energy generation by other renewable and conventional sources in Fiji, concluding the feasibility and competitive potential to invest into offshore wind farms to support the national electricity grid in Fiji. The objectives were achieved by assessing the offshore wind resources employing atmospheric reanalysis data from the WindPRO online database performing the data correlation using the Measure Correlate Predict module of WindPRO.

1.4.3 Latest research using both WindSim and WindPRO

Nilsson (2010) compared two wind simulation software to simulate energy production based on both the linear (WAsp) and a non-linear (WindSim) models. The orographic complexity was studied in Näsudden and Hunnflen, in Sweden, which have low orographic complexity and high orographic complexity respectively. The simulations were performed by a preparation process in WindPRO, followed by the actual simulations in the two simulation software. The results indicated that WAsP and WindSim estimate the energy production at a similar level which is close to the measured production when the orographic complexity is low. The WindSim simulation was very time consuming when comparing it to the WAsP simulation. When it comes to high orographic complexity, the results indicated that WindSim estimates the energy production in a very close range to the measured production. The WAsP simulation, however, overestimated the energy production about 40%. In the case with high orographic complexity, the results showed that a flow model that can calculate turbulence is needed. The model used in WindSim can model turbulence and therefore estimates an accurate energy production.

Simisiroglou (2012) estimated and compared the annual energy production for a site located in Greece, employing both wind farm design tools WindPRO and WindSim. For energy calculations in WindPRO, different roughness data and height contours were used and evaluated, resulting into 36 different energy estimations. The results show that the annual energy production for different parameters have a difference of 0.07% to 8.18%. Parameters introducing uncertainties and energy losses in the calculations were identified and quantified. Using the annual energy production, uncertainty and energy losses, the P_{50}, P_{75} and P_{90} were produced and compared for WindPRO and WindSim. These results indicate a good approximation in the estimated values for the investigated site, varying from 0.2% to 2.0%.

Timander and Westerlund (2012) performed a comparative study of two different approaches in wind energy simulations, whose aim was to investigate the performance of two commercially available tools. The study included the linear model by WAsP and the computational fluid dynamic model of WindSim. The place of study is a small wind farm located in Sweden featuring a fairly complex and forested terrain. The results showed similar estimations from both software and, in some cases, an advantage for WindSim. The site terrain was however deemed not complex enough to manifest the potential benefits of using the CFD model. It can be concluded that estimating the energy output in this kind of terrain is done satisfactorily with both tools. WindSim did, however, show a significant improvement in consistency at estimating the energy output from different measurement heights when using the forest module, compared to only using the standardized roughness length.

Woo et al. (2012) in their study, predicted the annual energy production of Gangwon (South Korea) wind farm for three consecutive years using WindPRO and

WindSim. The predictions from the linear code, WindPRO were compared with both the actual energy prediction presented in the clean development mechanism monitoring report of the wind farm and also the predictions from the CFD code, WindSim. The results from WindPRO were close to the actual energy productions and the errors were within 11.8% unlike the expectation. The reason for the low prediction errors was found to be due to the fact that although the wind farm is located in highly complex terrain, the terrain steepness was smaller than a critical angle (21.8°) in front of the wind farm in the main wind direction. Therefore, no flow separation was found to occur within the wind farm. The flow separation of the main wind was found to occur mostly behind the wind farm.

Maruf (2015) proposed three suitable places in Bangladesh for wind power development. Two of them were close to the coast line, proving that those sites were suitable for developing wind power projects. WindPRO, WindSim and WAsP were used for site suitability assessment, annual energy production estimations, wind resource mapping and site compliance. The results in site compliance show that the local climate is suitable for installation of wind turbines. The results with WindPRO and WindSim showed that the whole coastline is suitable for wind power development, and the results from WAsP revealed that the local climate is suitable for deploying modern wind turbines.

Chapter 2

Wind Power Fundamentals

This chapter presents the fundamentals and characteristics of wind energy, from its approximation, measurement, visualization and conversion. Also, two limitations for the power conversion of wind will be described in sections 2.5.1 and 2.7.

2.1 Estimations of winds

The dynamics of the air circulating in the atmosphere are governed by different driving forces such as the earth´s rotation, the gravity, sun radiation, ground´s friction and the air movement. The wind is thence, dependant on these forces. [19]

2.1.1 Driving forces in the wind

Different forces cause the air particles to move and create wind currents:

Gravitational force

The mass m contained in the particles of air in conjunction with the gravitational constant g (see figure 2.1) defines the gravitational force directed downwards according to equation (2.1).
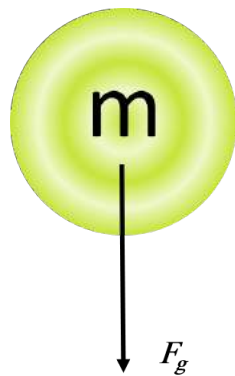
Figure 2.1:
Gravitational force

$$F_g = m\,g \qquad (2.1)$$

Pressure gradient force

This is the force produced when air with different pressures are placed next to each other. These differences occur in the atmosphere due to differences of densities in the air. Cold air is more dense than warmer air. The thickness of the atmosphere is higher when the air is warm, due to the fact that as air warms, the volume of air increases causing an expansion of the air, while cooling air has the contraction effect. A pressure difference is also visible when the air with different temperature are placed together. The high pressure air seeks equilibrium and moves towards low pressure areas, and this pressure gradient force (equation (2.2)) is the result of the pressure differences.

$$F_p = -\frac{1}{\rho}\frac{\partial p}{\partial n} \tag{2.2}$$

Where p is pressure, ρ is the air density and n is the normal to the isobars. The pressure gradient can be seen in figure 2.2.
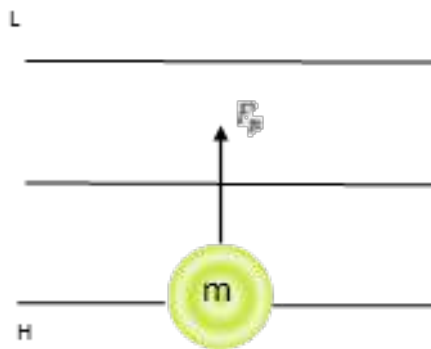
Figure 2.2: Pressure gradient force directed towards the low pressure area L

Coriolis force

It is an apparent force, relative to the earth´s surface that leads to deviation of moving objects to the right in the Northern hemisphere and to the left in the Southern hemisphere due to the earth´s rotation. The Coriolis force is described by equation (2.3).

$$F_c = \pm f u \tag{2.3}$$

Where $f = 2\omega sin(\varphi)$, ω the angular speed of the earth´s rotation, φ the latitude and u the wind speed. [20]

Centrifugal force

Is the apparent outward force on a mass when it is rotated. The direction of the centrifugal force is always outward away from the axis, since the Earth´s rotates

in a fixed axis (see figure 2.3). Hence, it is opposite to the direction of gravity at the equator and it´s zero at the poles. The centrifugal force is defined according to equation (2.4).

$$F_{cent} = m\frac{u^2}{r} \tag{2.4}$$

where r is the radius of the direction change. [21]
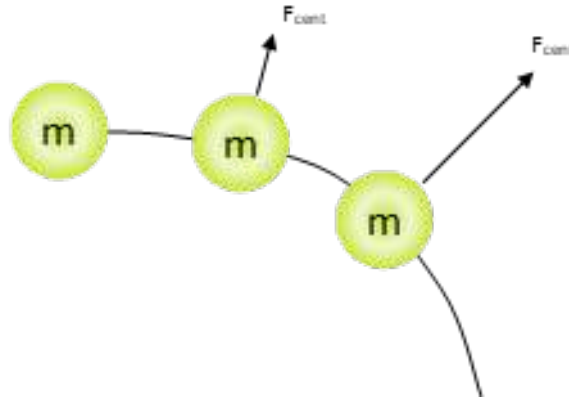
Figure 2.3: Centrifugal force affecting the air parcel

Friction force

Friction is defined as the force resisting the relative motion of solid surfaces, fluid layers and material elements sliding against each other. This force is a function of the wind speed and the *roughness length z_0*, which is the height above the ground at which the wind speed is theoretically equal to zero. [22]

$$F_f = -ku \tag{2.5}$$

With:

$$k = f(z_0) \quad \text{and} \quad z_0 = ze^{-\frac{ku}{u_*}} \tag{2.5a, b}$$

Where z stands for the height and k is the Von Karmans constant and u_* is the friction velocity.

The roughness lengths and classes will be further described in section 2.2.

2.1.2 Balanced forces

The wind moves in a 3-Dimensional direction driven by the forces previously described in subsection 2.1.1. These forces act in the vertical and horizontal plane, and a force balance can be developed for the wind.

Hydrostatic balance

In the vertical direction, the gravitational force and the vertical pressure act on the air mass. Thus, when putting together, the forces reach equilibrium state, known as the *hydrostatic balance* (equation (2.6)). Likewise, the centrifugal force is neglected as the air remains static.

$$F_g = F_p \qquad (2.6)$$

Geostrophic balance

At high altitudes around 1000m, the geostrophic balance is a fair resemblance for the wind speed and direction, and is used by WAsP and WindSim as a base for extrapolating winds at these heights. The geostrophic balance describes two forces acting in the air mass, composed by the Coriolis force and the pressure gradient force. The first one makes the wind move to the right of the motion in the northern hemisphere or to the left in the southern hemisphere while the latter one is always directed towards low pressure and perpendicular to the isobars, as shown in figure 2.4.

When the pressure gradient force and the Coriolis force are equal, the *geostrophic* wind appears, which means that the wind moves parallel to the isobars, and this is unaltered by the ground friction. [19]
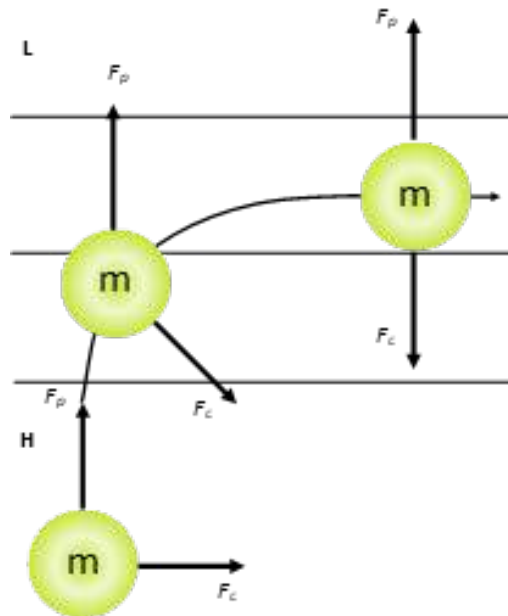
Figure 2.4: The pressure gradient force is equal to the Coriolis force

Gradient balance

The wind should move in a straight line without any direction change for the geostrophic balance to function, otherwise (as usual), the centrifugal force effects have to be considered. The centrifugal force is always acting perpendicularly to the direction change, as in figure 2.3.

Guldberg-Mohn balance

For conditions close to the surface, a revision of the geostrophic balance needs to be applied to account for the friction in the balance. The wind decreases since the friction force opposes to it, diminishing the Coriolis force as it is dependent on the wind speed. As a result, reduced wind speed will cross the isobars with an angle determined by the strength of the friction force and hence the roughness length of the surface because of the powerless Coriolis force.

2.1.3 The logarithmic velocity profile

This is an estimation of the vertical wind profile, and acts independently of the above-mentioned balances and is calculated as shown in equation (2.7).

$$u = \frac{u_*}{k} ln \frac{z}{z_0} \tag{2.7}$$
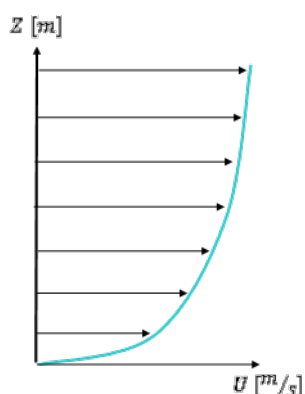
Figure 2.5: The logarithmic velocity profile

Atmospheric stability

The atmospheric stability is a factor that determines how well can the atmosphere cope with the vertical movement of air, and can be measured through the environmental *lapse rate*, which is the rate of temperature decrease due to elevation as well as with the *adiabatic rate*, which determines the rate of when the air cools and compresses or heats and decompresses without interchanging heat with the surroundings. [14]

The adiabatic lapse rate is a constant of $9.8°C/km$, but the saturated adiabatic lapse rate will variate and depend on the latent heat released during condensation of the air. Temperature affects significantly this rate. Aside from this, the water vapor in the air decreases considerably as it arises and when water condenses, resulting in less heat released. Atmosphere stability or instability is a complex

phenomenon conducted by factors such as temperature, pressure, humidity and momentum. It varies over time and it is never constant at a certain location. [16]

***Absolute stable atmosphere**: when the environmental lapse rate is lower than the moist adiabatic rate, the atmosphere is absolute stable. An air parcel displaced upward by an adiabatic process would be denser than its environment and would tend to sink back to its degree of origin. [14]

***Neutral stable atmosphere**: the atmosphere is neutral stable When the environmental lapse rate is equal to either the moist adiabatic rate at saturated conditions or the dry adiabatic rate at unsaturated conditions. In essence, the air parcel will be cooled or heated with the same rate as its surroundings and in this manner have the same weight.

***Absolute unstable atmosphere**: this is a state of instability that depends upon whether or not the rising air is saturated and happens when the environmental lapse rate is higher than the dry adiabatic rate. In this case, an elevated air parcel cools slower than the environmental lapse rate, being warmer and lighter than the surroundings. It rises further until an unstable equilibrium state is reached and a lowered air parcel continues sinking until unstable equilibrium is reached.

***Conditional stable atmosphere**: this occurs when the environmental lapse rate lies between the moist and dry adiabatic rates. The atmosphere is usually in a conditionally unstable state. This means that when air is unsaturated, the atmosphere is stable and when air is saturated, the atmosphere is unstable. [23]

Many factors cause instability. One is a steep environmental lapse rate coming from cool air aloft (brought on by cold advection, the environmental lapse rate or both) coupled with warm air at the surface (caused by daytime solar heating, warm advection, or a warm surface). Another factor that affects instability is mixing, which increases warming below and cooling higher up in the atmosphere. Likewise, lifting enhances instability; when a layer of air is forced to rise it becomes more unstable since the top layer cools more swiftly than the bottom, steepening the environmental lapse rate. This effect is boosted even more when the lower layer of the lifted parcel is moist and the upper layer is dry. In this instance, lesser lifting is required to steepen the environmental lapse rate. This effect is known as *convective instability* and is associated with heavy storms.

Temperatures

Potential temperature is usually used in meteorology since it explains temperature alterations due to the altitude, but specifically due to the pressure. It is part of the Obukhov length, described in section 2.1.3 on the following page. The potential temperature is the temperature that a parcel of dry air would achieve if it was

adiabatically taken to a certain standard pressure, defined in equation (2.8).

$$\theta = T \left(\frac{p_*}{p} \right)^{R/c_p} \tag{2.8}$$

Where T is temperature, p is pressure, p_* is a standard reference pressure ($\approx$ 1 bar), R is the individual gas constant and c_p is the specific heat capacity.

The *virtual temperature* is another useful parameter, which is the temperature a dry air parcel would obtain if its pressure and density were the same as for a specific parcel of moist air. The virtual temperature is defined in equation (2.9).

$$T_v = \frac{T(1 + r_v/\epsilon)}{1 + r_v} \tag{2.9}$$

Where r_v is the mixing ratio and ϵ is the ratio of the gas constants for air and water vapor ($\approx$ 0.622). The mixing ratio is the mass fraction of an atmospheric constituent, normally water vapor to dry air. The virtual temperature is useful when the dry air equation of state has to be applied for moist air. The dry bulb temperature is in this case substituted with the virtual temperature. [24]

Obukhov length

The Obukhov length also known as the *Monin-Obukhov length*, refers to the characteristic height scale of the dynamic sub-layer and connects thermal, dynamic and buoyant processes. This is an important factor for stable or unstable surface layers, and is incorporated as well in the Monin-Obukhov theory, which presents a modified version of the logarithmic law (equation (2.7)). In this model, a wind speed profile in a stratified surface layer can be obtained with equation (2.10).

$$v_{wind,z} = \left(\frac{u_*}{k} \right) \left[ln \left(\frac{z}{z_0} \right) - \psi_m(z/L) \right] \tag{2.10}$$

Where the function ψ_m depends on the fraction Z/L known as the *dimensionless Obukhov length*, often denoted as ζ. The other variables follow the ones in eq. (2.7).

The principal contributor of the generation of turbulent kinetic energy is the wind share at heights below the L, and above it, the buoyant forces are the responsible ones. For atmospheres with neutral stratification,the Obukhov length is zero while it has positive and negative values for stable and unstable stratification in the atmosphere, respectively. Furthermore, the *dimensionless Obukhov length* is regularly used as a stability parameter, ranging from 1 to 5 for stable stratification

and -5 to -1 for unstable stratification. Also, a value of $\zeta = 0$ is used for statically neutral stability. The Obukhov length is described with equation (2.11).

$$L = \frac{-u_*^3 \bar{\theta}_v}{k_c g \overline{(w'\theta_v')}_s}$$

(2.11)

Where u_* is the friction velocity, θ_v is the virtual potential temperature (can be obtained using the potential temperature in equation (2.9)), k_c is the Von Karman´s constant (0.41), g is the gravitational acceleration, and $\overline{(w'\theta_v')}_s$ is the surface kinematic virtual potential temperature flux. w is the vertical velocity over the surface, while w' is the instantaneous and the average velocity. The same applies to θ_v'. The surface kinematic virtual potential temperature flux is obtained by averaging over the surface. [25]

The over-lines in the variables indicate average values.

The value of ψ_m in equation (2.10) is the integration of the stability function ϕ_m, whose values will depend on it stability as seen in equation (2.12)

$$\begin{cases} \phi_m(\zeta) = 1 + \beta_1\zeta & \zeta > 0 \ (stable) \ (typical \ value \ \beta_1 = 4.7) \\ \phi_m(\zeta) = (1 - \gamma_1\zeta)^{-1/4} & \zeta < 0 \ (unstable) \ (typical \ value \ \gamma_1 = 15) \end{cases}$$

(2.12)

Reasonable default values are $|L| > 1000$ for neutral atmosphere, $200 < L < 1000$ for stable atmosphere and $0 < L < 200$ for a very stable atmosphere. $0 > L > -200$ for a very unstable atmosphere and $-200 > L > -2000$ for an unstable atmosphere. Depending on the stability of the atmosphere the wind profile in the higher elevations differs considerably (see figure 2.6)
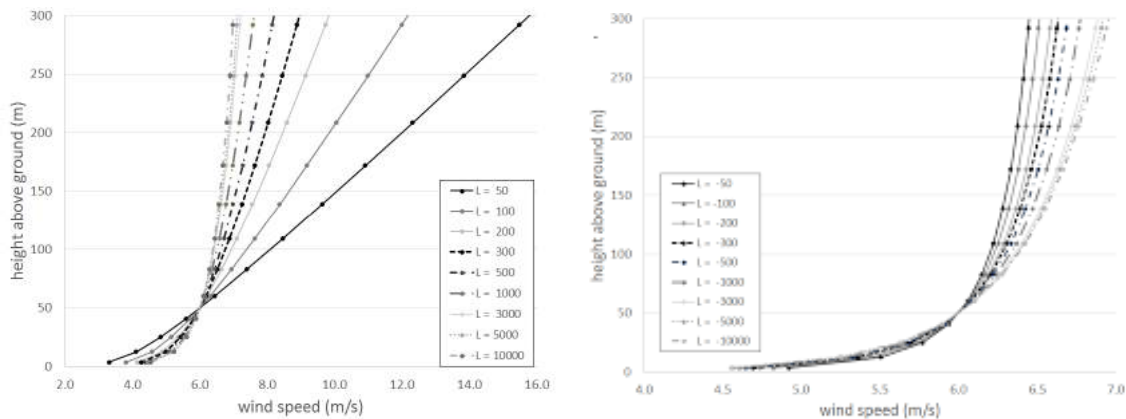
Figure 2.6: Wind speed profile for different Monin-Obukhov lengths

2.2 Roughness and wind share

The wind speed and the turbulence level are strongly influenced by the earth´s surface roughness and obstacles in the terrain due to the friction. The wind speed profile follows the pattern of low speeds at the ground level and increases positively as a function of the height above ground until it reaches the speed of the not obstructed flow at the upper height of the boundary layer. There are some peculiar circumstances where the wind diminishes with the height, e.g. with temperature inversion in a quiet wind environment. There are some mathematical formulas to roughly evaluate the wind speed profile, known as the *wind shear*. One of these is the *log wind profile* in equation (2.13). [26]

$$v_{wind,z} = \left(\frac{u_*}{k_c}\right) ln \left(\frac{z}{z_0}\right) \qquad (2.13)$$

Where $v_{wind,z}$ is the wind speed at height z, z_0 is the surface roughness, k_c is the Von Karman's constant and u_* is the friction velocity, which is simply a shear stress expressed in the unit of velocity. Equation (2.13) applies for cases with a neutral surface layer. Also, it is possible to calculate the wind speed of a place given the same information of another with equation (2.14). This formula is useful for instance, to estimate the wind speed at a certain wind turbine hub height and it is a function of the surface roughness z_0, describing the equivalent height above ground where the wind speed is theoretically zero. These values are given depending on the different types of terrain and are displayed in table 2.1.

$$\frac{v_{wind,z_1}}{v_{wind,z_2}} = \frac{ln(z_1/z_0)}{ln(z_2/z_0)} \qquad (2.14)$$

Table 2.1: Roughness lengths for different types of terrain

Terrain description [27]	Roughness length	Terrain description [28]	Roughness length
Very smooth, ice or mud	0.00001	Water areas (lakes, fjords, open sea)	0.0001
Calm open sea	0.0002	Sand surfaces (smooth)	0.0003
Blown sea	0.0005	-	-
Snow surface	0.003	Snow surfaces (smooth)	0.001
Lawn grass	0.008	Mown grass	0.008
Rough pasture	0.01	-	-
Fallow field	0.03	Farmland with very few buildings and trees	0.03
Crops	0.05	Farmland with an open appearance	0.05
Few trees	0.1	Farmland with a closed appearance	0.1
Many buildings, hedges, few buildings	0.25	Suburbs	0.5
Forest and woodlands	0.5	Forest	0.8

A high roughness length diminishes the wind speed at a higher extent than a low roughness length. As a result, areas with high roughness length will have higher friction force, e.g.dense forests than in places with low roughness length, e.g. water. The *roughness classes* are defined in terms of the roughness length, as shown in table 2.2.

Table 2.2: Roughness length and Roughness class

Roughness Class RC	Roughness Length [m]	Terrain description [29]
0	0.0002	Water surface
0.5	0.0024	Completely open terrain with a smooth surface such as concrete runways in airports, mowed grass
1	0.03	Open agricultural area without fences and hedgerows and very scattered buildings. Only softly rounded hills
1.5	0.055	Agricultural land with some houses and 8m tall sheltering hedgerows within a distance of ~1250m
2	0.1	Agricultural land with some houses and 8m tall sheltering hedgerows within a distance of ~500 m
2.5	0.2	Agricultural land with many houses, shrubs and plants, or 8m tall sheltering hedgerows within a distance of ~250m
3	0.4	Villages, small towns, agricultural land with many or tall sheltering hedgerows, forests and very rough and uneven terrain
3.5	0.8	Larger cities with tall buildings
4	1.6	Very large cities with tall buildings and sky scrapers

WindPRO uses the roughness classification established by the European Wind Atlas [30] (table 2.2), which is a digital version of wind statistic data, and it contains material about the meteorological model, the wind resource assessment as well as the location of turbines.

The *power law* is also another mathematical model to estimate the wind share, defined by equation (2.15), where $v_{wind,H}$ stands for the estimated wind at height H, v_0 is the measured wind speed at height H_0 and α is the wind share exponent, heavily regulated by the site characteristics and ambient conditions, such as elevation, time of day, wind speed, temperature, season, nature of the terrain among others, which might be sometimes complicated to calculate.

$$v_{wind,H} = v_0 \left(\frac{H}{H_0} \right)^{\alpha} \tag{2.15}$$

2.3   Displacement height

The airflow over a forested area is lifted in comparison to the airflow over open terrain, thus when objects are placed above ground level in forested areas, an altered relation to the ground level concerning the airflow will occur. The nominal height above ground will consequently be larger than the effective height experienced by the object. To account for this effect, a zero plane displacement height is brought in (see figure 2.7).

Displacement is defined as the height at which the mean velocity is zero due to large obstacles such as buildings and dense vegetation, such as forests. When they are close to the wind turbine, these obstacles can certainly decrease the hub height of the wind turbine by increasing the height necessary above ground level to attain a specific wind speed. The displacement height is presumed to be equal

to 2/3 to 3/4 the height of the surrounding vegetation, depending on how dense it is.
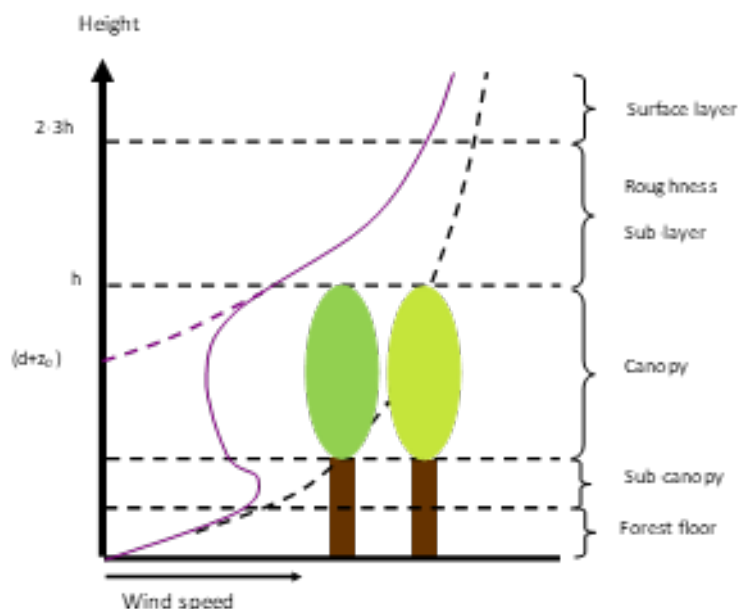
Figure 2.7: Displacement height

2.4 Orography

The orography is a crucial factor to take into account when creating a wind flow model since the wind share profiles theory is relevant to flat terrain and is not directly applicable to landscapes with sudden changes in elevation. Places with these sudden changes in elevation are usually preferred for placing wind turbines because of the strong winds. The air that flows into the hill gets compressed and accelerates as it moves to the top until it reaches the lower pressure side behind the hill. The airflow might, however, become turbulent and separated depending on the roughness of the slope, the incidence angle and the flatness of the summit, which is less suitable for a wind turbine installation. The modeling of flow separation in WAsP (used in WindPRO) does not consider the viscosity of the fluid, which means that the fluid will follow the terrain. To account for this, the *RIX index* can be used (see section 3.2 on page 43). [31]

2.4.1 Obstacles

An object that obstructs the flow motion and creates turbulence and reduced wind speeds is considered an obstacle, and they can be both natural objects such a bluff of trees or artificial structures, such as buildings.

Figure 2.8: Obstacles affecting the wind profile

2.5 Conversion of wind energy

Wind turbines convert the kinetic energy from the wind into mechanical power, which can be used for specific assignments (such as pumping water) or this mechanical power can be converted into electricity by a generator.

A wind turbine transforms energy in the wind into electricity using the aerodynamic force initiated by the rotor blades. The air pressure on one side of the blade decreases when the wind flows across the blade. The difference in air pressure across the two sides of the blade creates both lift and drag. The force of the lift is stronger than the drag, making the rotor to spin. The rotor is connected to the generator, either directly or through a shaft and a gearbox that speed up the rotation. This translation of aerodynamic force to the rotation of a generator produces electricity. [32]

2.5.1 Power in the wind

It is possible to determine how much power can be extracted from the wind, by using the kinetic energy E from the moving air, with a certain mass m and a given speed v_{wind}, as in equation (2.16).

$$E = \frac{1}{2}mv_{wind}^2 \tag{2.16}$$

The power that can be obtained by the wind P_{wind} (equation (2.17) can be obtained from the kinetic energy equation and the mass flow of the air, which is a function of the wind speed, the density ρ and the swept area A.

$$P_{wind} = \frac{1}{2}\rho A v_{wind}^3 \tag{2.17}$$

Betz limit

There is a limit of how much kinetic energy can be extracted from the wind, and such theory is known as the *Betz limit*. The Betz limit embodies the maximum

theoretical potential for wind energy conversion by any free-standing device in any free-flowing fluid stream. It does not depend on certain constraints, neither is connected to the fluid properties nor the device assembly. The Betz limit is not a function of the air temperature or humidity either. [1]

No wind turbine can reach a higher aerodynamic efficiency than *16/27*, which is approximately *59.3%*. Nonetheless, despite this limit cannot be reached, the aerodynamic efficiency of a modern wind turbine is very superior. For instance, a commercial wind turbine manufactured by Vestas, the $V150 - 4.2MW$ is configurable to achieve the optimum power curve. The configurations maximize annual energy production of the individual turbines in the wind park, while adhering to the operational envelope of 20 year design lifetime. [33]

In operation, there are similarly other forms of losses in a wind turbine, e.g. friction losses which will decrease the turbine efficiency further.

To define the efficiency of a wind turbine, a typical parameter used is the *power coefficient* C_p, which is the electrical power output P_{output} from the wind turbine divided by the wind energy input, P_{wind}, as stated in equation (2.18).

$$C_p = \frac{P_{output}}{P_{wind}} = \frac{P_{output}}{\frac{1}{2}\rho A v_{wind}^3} \tag{2.18}$$

The C_p value can be found in the datasheet of every wind turbine, supplied by the manufacturer and generally comes together with the power curve of the wind turbine which is a graphical representation of the power output at the operating wind speed. This is measured according to the *IEC 61400-12*, which is a standard for measuring power curves. The power curve is defined according to this standard and states that the normal air density ($1.225kg/m^3$) is to be employed. In case the air density at the site differs from this value, a corrected power curve needs to be applied. For so doing, the IEC 61400-12 standard considers that the power output at all wind speeds is dependent on the velocity and density according to equation (2.16). Based on this assumption, equation (2.19) can be derived and expresses how the wind speed is dependent on the density. Here u_{site} is the wind speed at the site with density ρ_{site} and u_{std} is the wind speed for the standard density ρ_{std}.

$$u_{site} = u_{std} \left(\frac{\rho_{std}}{\rho_{site}} \right)^{1/3} \tag{2.19}$$

By interpolating the corrected power curve to fit the standard wind speeds, it is possible to obtain a density corrected power curve (with the standard wind speed values) and the new wind speeds for the site, which is displayed along with the standard power output. [31]
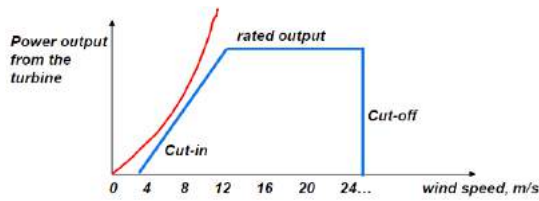
Figure 2.9: Cut-in and cut-out wind speeds [1]

EMD International A/S has identified some restrictions in this method, which conducted to an enhanced method grounded on the IEC 61400-12 named *"New WindPRO correction"* [31]. The correction method for the density assumes the same aerodynamic efficiency for all wind speeds, which is inaccurate and most conspicuous for wind speeds around rated power. The "New WindPRO correction" contains an exponent, seen in equation (2.19) to account for this limitation. Other significant parameters are the *cut-in, cut-out* and *rated wind speed* (see figure 2.9). Cut-in speed refers to the speed at which the turbine starts producing electricity. Cut-out speed is the speed at which the wind turbine shuts off to protect itself against strong wind speeds. Lastly, the rated wind speed denotes the minimum wind speed at which the wind turbine can produce its maximum power output.

2.5.2   Power control of the wind

Controlling the power output of the wind turbine can be executed by two concepts: pitch and stall regulation. Intending to reduce the power output with a pitch regulated turbine, the blades pitch out of the wind to reduce the lift force and the rotation speed and thus the power output (see figure 2.10). *"Pitching"* means that a blade can flip around its longitudinal axis, thus being able to maintain a certain angle of attack at varying wind speeds, effectively regulating the lift without increasing the drag.
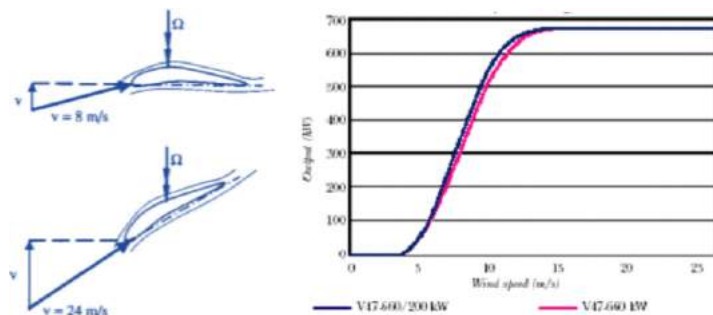
Figure 2.10: Pitching of the blades [1]

The pitching of blades allows for smooth and optimal power regulation of the rotor at any wind speed. However, it has a more complicated mechanical arrangement in the rotor hub (such as pitch motors, bearings and control system), which add costs and may decrease the reliability of the turbine. Most of the early commercial turbines were stall controlled (which were robust but with lower costs), while most of the modern turbines are pitch controlled, optimized for the best performance and smooth power quality throughout the operational spectrum of wind speeds.

"Stall" occurs at large angles of attack and triggers a violent turbulent flow behind the wing profile, with increasing drag and a gradual loss of lift (see figure 2.11). In this case, stall can be both passive or active. In the case of a passive stall, the

rotor blades are anchored in a fix angle. When the wind speed arrives at a precise level, the momentum around the blades rises and the lifting power drops, and so does the power output. In the case of an active stall, the rotor blades pitch into the wind in order to diminish the lift force and consequently, the power output.

The stall is used in the first-generation wind turbines, typically below 1 MW rated power. It needs to be combined with a direct grid connection, holding the rotor at a constant speed of rotation regardless of wind speed. Among the major drawbacks, the impossibility to maintain a perfectly stable power output, the simplicity and robustness are traded off to an inferior performance and very high loads at high winds.
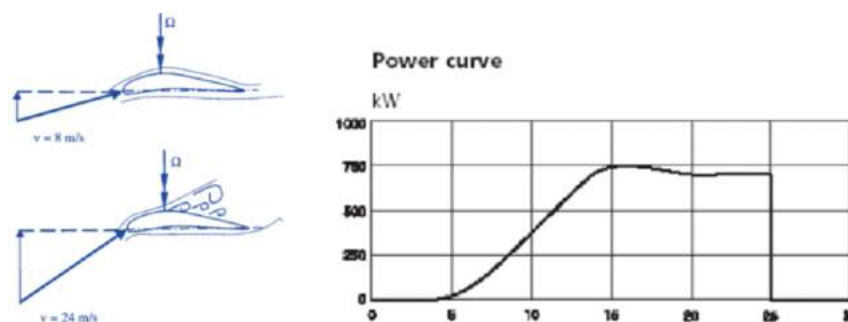
Figure 2.11: Stall of the blades [1]

The different types of control of the blades are displayed in figure 2.12.
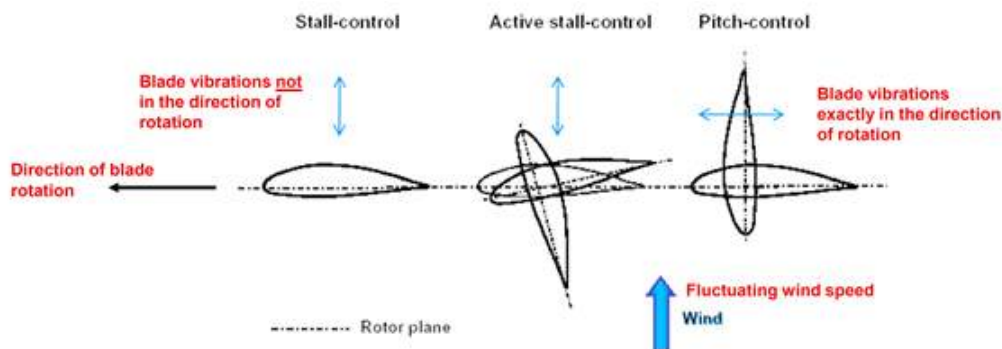
Figure 2.12: Pitch vs. stall aeroelastic performance [1]

2.6 Turbulence

Contrary to the laminar flow, which is stable and has constant boundary conditions, a turbulent flow follows a chaotic and random pattern, with unpredictable and changing flow properties, such as velocity. [10]

A technique to measure the turbulence level at a position is the *turbulence intensity*, defined as the root mean square of the turbulent velocity fluctuations u' and the

mean velocity U, as seen in equation (2.20). When there is available information about the time series of wind data, the turbulence intensity is defined as the wind standard deviation divided by the mean wind speed measured during 10 minutes.

$$I = \frac{u'}{U} = \frac{\sqrt{\frac{1}{3}({u'_x}^2 + {u'_y}^2 + {u'_z}^2)}}{\sqrt{U_x^2 + U_y^2 + U_z^2}} = \frac{\sqrt{\frac{1}{3}(u'^2 + v'^2 + w'^2)}}{\sqrt{U^2 + V^2 + W^2}} \qquad (2.20)$$

Turbulence plays an important role for wind turbine applications, because it is associated with fatigue loads on the components of the structure. Higher turbulence levels result in more fatigue loads to the structure. Therefore, it is crucial to account for this phenomenon previous to the selection of wind turbine, site and layout. Turbulence can be conceived from various sources:

- **Orographic**: any change in atmospheric conditions caused by a change in elevation, primarily due to mountains, can create turbulence.
- **Roughness**: generated by deviations in the direction of the normal vector of a real surface from its ideal form
- **Turbine**: generated in the wakes downstream of a turbine
- **Obstacles**: turbulence can also be formed by the presence of objects within the terrain

In WindPRO, the turbulence produced by the turbine is taken into account, but ambient turbulence produced from roughness and orography has to be entered either from measurements or by the user.

Likewise, in WindSim, turbulence is taken into account using various types of two-equation models like the k-ϵ model described in section 3.1.2 on page 38.

Moreover, Zephy Tools is specialized in developing numerical tools for Computational Fluid Dynamics, and its calculator offers the possibility to access to different turbulence models.

2.7 Wake effect

The wake effect is a sophisticated phenomenon developed downwind of a wind turbine and is a result of the physical laws of the wind energy conversion. Based on the fact that energy can neither be created nor consumed, it can be observed that since a wind turbine generates electricity from the energy in the wind, the wind will be slowed down and consequently the wind speed downwind of the rotor will be reduced and turbulent once the energy in the wind is converted. The wind leaving the turbine has a lower energy content than the wind arriving in front of the turbine.

A wind turbine will always cast a wind shade in the downwind
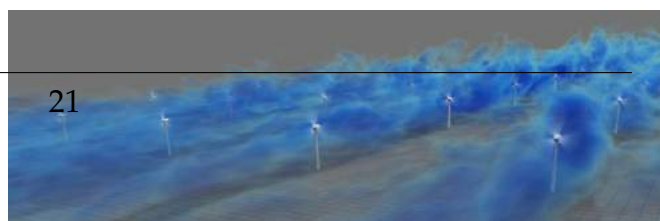
direction, an extended trail of wind which is rather turbulent and slowed down when compared to the wind facing forward the turbine. The area affected by this phenomena is defined as the wake (figure 2.13). Wind turbines in parks are usually spaced at least three rotor diameters from one another in order to avoid too much turbulence around the turbines downstream. In the prevailing wind direction turbines are usually spaced even farther apart. [34]

2.7.1 Park layout

Ideally, sitting turbines as distant as possible in the prevailing wind direction would be desirable. However, the determining factors for spacing are mainly the land use and the electrical grid connection costs. As a rule of thumb, turbines in wind parks are frequently spaced somewhere between 5 and 9 rotor diameters apart in the prevailing wind direction and between 3 and 5 diameters apart in the direction perpendicular to the prevailing winds.

In figure 2.14, three rows of five turbines each in a fairly typical pattern are displayed. The turbines (white dots) are placed 7 diameters apart from each other in the prevailing wind direction and 4 diameters apart in the direction perpendicular to the prevailing winds.
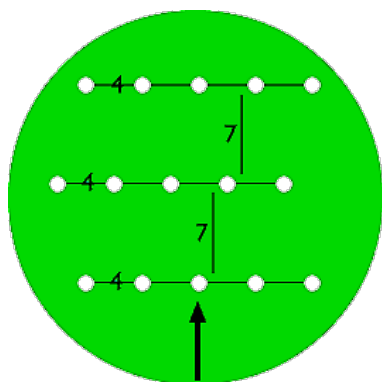
Figure 2.14: Wind farm layout [1]

According to section 2.5.1, the Betz limit states that a wind turbine can only use around 59% of the wind energy. This is accomplished when the free stream air velocity is decelerated with 2/3. The free stream air velocity behind the turbine is therefore only 1/3 of the velocity in front of the turbine. From this remaining kinetic energy, less energy can be extracted and many losses appear in the generation. Energy loss from the wake effect knowing the wind turbine rotor, the wind rose, the Weibull distribution and the roughness in the different directions can be estimated by manufacturers or developers. Typically, the energy loss will be about 5%. [34]

2.7.2 Wake models

The wake behind a wind turbine has a repercussion on the downstream turbine when it is affected by the modified wind flow. This effect regulates the electricity output adversely and might as well boost the failure rate of the turbines within the wind farm. It is thus decisive to predict the level of impact to better optimize farm layout and to appropriately estimate the decrease in energy output by considering a wake model into the calculations.

The first wake models developed in the 1980s were based on explicit analytic expressions. These models require minor computational power, due to high costs at that time. Nowadays the analytic models are still being used, as they have demonstrated satisfactory results when modeling single wakes and small farms. Nonetheless, they are not contemplating the atmospheric stability effects nor the near wake development. [35]

The commercial CFD software WindSim has implemented the analytical wake models from *Jensen, Larsen* and *Ishihara*. WindPRO integrates into the PARK module (see section 4.2) both the Jensen and the Larsen model (recommended by WindPRO) and a third model called *Eddy Viscosity model*. Zephy Tools considers the empirical model of Park-Jensen in its calculations for now and they are currently working on a CFD wake model using the actuator disk, to lower the uncertainties.

These models are single wake models, which means that the interaction between multiple turbines has to be further calculated by empirical correlations as it is not resolved by the models itself. [31]

N.O. Jensen wake model

The Jensen model is preferred in WindPRO and Zephy TOOLS, and is altered to incorporate various turbines and hub heights in the same wind farm layout. Also, the center-line of the wake is assumed to follow the terrain. This model is based on momentum deficit theory, where the wake radius is assumed to expand linearly. Equation (2.21) is employed to calculate the wind speed deficit behind a turbine in relation to the thrust coefficient C_t, where ξ is the wake decay constant, v_{wind} is the velocity of the free stream, r is the rotor radius, x_r is the downstream distance from the rotor, u_{wake} is the wake velocity at x_r meters downwind of the rotor and C_t is the thrust coefficient which is derived for the specific wind turbine model employed and depends on the wind speed. C_t values are supplied in WindPRO along with the information for a particular wind turbine model.

$$1 - \frac{u_{wake}}{v_{wind}} = \frac{1 - \sqrt{1 - C_t}}{\left(1 + \frac{\xi x_r}{r}\right)^2} \qquad (2.21)$$

The ξ constant represents the expansion of the wake from the rotor and has a default value of $0.075m$, describing an opening angle of $4°$. A minimal impact on the results can be observed when the wake decay constant is changed. Nonetheless, it has been determined that the value differs depending on the turbulence in the area. The turbulence level is dependent on the roughness of the terrain, and so the wake decay constant will range from $0.04m$ to $0.1m$. [31]

Equation (2.22) is used for combined wake calculations, where the velocity deficit is acquired by two or more wakes, and can be combined by using the sum of squares. n is the number of turbines upstream. For a downwind turbine partly placed inside a wake is determined by the fraction of the overlapping area to the rotor area of the downwind turbine.

$$\left(1 - \frac{u_{wake}}{v_{wind}}\right)_n = \sqrt{\sum_{m=1}^{n-1}\left(\left(1 - \frac{u_{wake}}{v_{wind}}\right)_{mn}\right)^2} \tag{2.22}$$

G.C. Larsen wake model

The Larsen model is a semi-analytical model derived from Prandtl's rotational symmetric turbulent boundary layer equations. The model is conservative for close spacing and can thus be adjusted to enhance the correctness of the near wake with semi-empirical descriptions applying a double peak velocity profile. It is advisable to use the model with wake loading according to the European Wind Turbine Standards II project in 1999. [36]

Eddy viscosity wake model 1986

Also known as the *Ainslie wake model* determines the wake velocity decay using the Reynolds Averaged Navier-Stokes equation and the eddy viscosity approach. The rotor is assumed to be axisymmetric and the flow incompressible. A numerical solution to the differential equation is attained by employing a Crank-Nicholson scheme and replacing the differential equations with finite difference approximations. [31]

Ishihara japanese model

Wake models are classified into two categories, analytic CFD based model. Analytic models benefit from the viewpoint of wind farm design due to its simplicity and computational speed. Existing analytic wake models assume that the rate of wake recovery is constant. Therefore, one single model cannot be used for both onshore and offshore wind farms.

In Japan, several wind farms are constructed nearby the coast, where the ambient turbulence fluctuates significantly depending on the wind direction, indicating

the need for a universal wake model applicable to any ambient turbulence and
thrust coefficient. A new universal wake model was developed by taking the
effect of turbulence on the rate of wake recovery into account. The model well
predicts the wake for any ambient turbulence and thrust coefficient C_t. [37]

2.8 Wind speed distributions

Wind speed distributions are frequently used to express the annual available
wind energy. These distributions are predicted employing wind maps, site mea-
surements or computer analysis. Statistical functions or tables can present the
distribution as well.

Figure 2.15 presents the relative distribution $h(v)$ of wind speed v in Lokan Teko-
järvi (read more in section 5.1.2). This distribution illustrates how often a specific
wind speed occurs. It is immediately noticeable that the wind energy potential in
this place is very high.
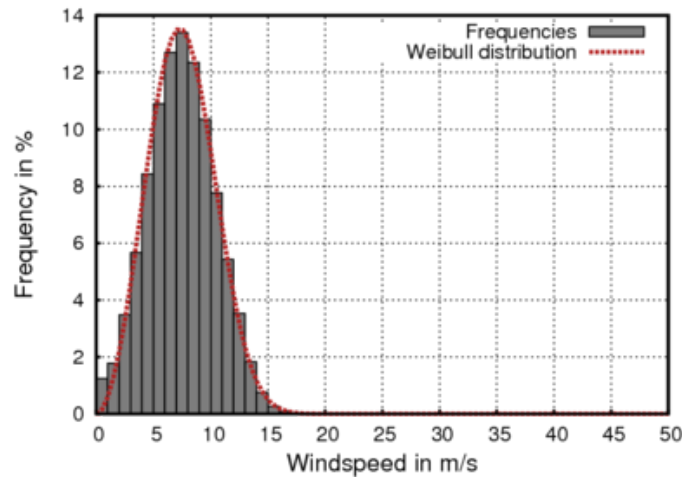
Figure 2.15: Weibull distribution of Lokan Tekojärvi obtained from WindSim

The wind speed measurement interval can originate uncertainties in the predic-
tion of wind speed frequency distributions. If the average of the wind speed is
registered exclusively every 10 minutes or even every hour, additional calcula-
tions on wind generator yield can produce significant errors since the energy of
the wind is not linearly dependant on the wind speed. Recording the average
of the wind speed cubed provides a solution for avoiding such error. The mean
wind speed can be simply calculated with equation (2.23). [38]

$$\bar{v} = \sum h(v) \cdot v \tag{2.23}$$

With:

$h = \dfrac{\text{fraction of time wind speed is between v and } (v+\Delta v)}{\Delta v}$ and $\displaystyle\int_0^\infty h \cdot dv = 1$

Nevertheless, the mean wind speed describes partially the potential of a site, as the wind distribution might be continuous wind or extended quiet periods interspersed with periods of extremely high wind speeds. The wind energy in both events can be completely different, but the mean wind speed is generally used to indicate the site quality. Wind maps of the mean wind speed are available for most countries (e.g. Troen and Lundtang Petersen (1989)).

The wind can variate depending on the location. For instance, in coastal areas, a mean wind speed of $6m/s$ or more is common whereas in inland areas it can be below $3m/s$. Mountainous regions also have favorable wind conditions. Nowadays it is possible to estimate wind speeds even for locations where no measurements have been recorded through digital wind maps and computer programs (e.g. Risø National Laboratory, 1987).

A wind speed frequency distribution provides more appropriate information about the wind conditions of a certain site than the mean wind speed and it can be given as statistical functions or as tables with wind speed intervals. The most typical statistical functions used for wind power calculations include the *Weibull* and the *Rayleigh* distributions. The Weibull distribution of wind speed v with shape parameter k and scale parameter a is given by equation (2.24):

$$f_{Weibull}(u) = \frac{k}{A} \left(\frac{u}{A} \right)^{k-1} exp \left(- \left(\frac{u}{A} \right)^{k} \right) \tag{2.24}$$

Where $f(u)$ is the frequency of occurrence of wind speed u, k is the shape parameter and A is the scale parameter, which depends on every site. [30]

The mean wind speed can be approximated from the Weibull parameters as in equation (2.25):

$$\bar{u} = a \cdot \left(0.568 + \frac{0.434}{k} \right)^{1/k} \tag{2.25}$$

The parameter a for $k = 2$ can be obtained from the mean wind speed as in equation (2.26):

$$a_{k=2} = \frac{\bar{u}}{0.886} \approx \frac{2}{\sqrt{\pi}} \cdot \bar{u} \tag{2.26}$$

If a is substituted in the Weibull distribution and $k = 2$ is used, the *Rayleigh distribution* is obtained, as shown in equation (2.27). Such distribution requires the average wind speed as a parameter. The distribution for different mean wind speeds can be seen in figure 2.16. [38]

$$f_{Rayleigh}(u) = \frac{\pi}{2} \cdot \frac{u}{\bar{u}^2} \cdot exp \left(\frac{\pi}{4} \cdot \frac{u^2}{\bar{u}^2} \right) \tag{2.27}$$
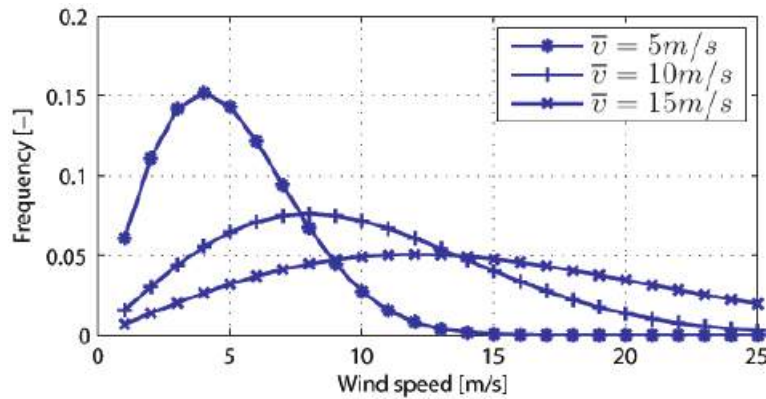
Figure 2.16: Rayleigh distributions for various mean wind speeds v [3]

2.9 Wind measurement

For successful planning and implementation of wind energy projects, a meticulous understanding of the wind characteristics at the potential sites is fundamental. Key information is required for analyzing a site, including the speed and direction of the prevailing wind at different time scales. Likewise, ecological factors could sometimes help pinpoint a candidate site for wind power project development. Wind data from the adjacent meteorological stations provide a better understanding of the wind spectra available at the site, but for an accurate analysis, the wind direction and velocity at the particular site have to be measured with proper and reliable instruments.

2.9.1 Ecological indicators

Eolian features are the formations on the land surface caused by a constant strong wind, which can indicate the behavior of the wind in a prevailing area. An example of such features is dunes, whose particles when gathered and transported by the wind flow, are deposited back when the wind speed diminishes. By recognizing the particle size that was carried and deposited along with the distance, the average strength of the wind in that place can be estimated. Similarly, biological indicators such as deformation of trees and bushes can be observed and studied as a result of strong winds in the region; such indicators are present mostly in valleys, coasts and mountains.

According to Mathew (2007), deformations of trees due to the wind effect fall into 5 categories:

- **Wind brushing** is evident when the trees are off their leaves, and it happens due to the leeward bending of branches and twigs of the trees, implying the presence of light wind, which is not favorable for wind energy conversion.
- In **flagging**, the branches are stretched out to leeward, with the possible stripping of upwind branches. Wind speeds corresponding to the flagging

effect are attractive for energy conversion.

- In **wind throwing**, the trunk and branches of the tree bend away from the coming wind, indicating the existence of stronger wind.
- Under **clipping**, the lead branches of the tree are restrained from growing to its normal height due to strong wind.
- In **wind carpeting**, the trees are clipped even at a very low height with extreme winds.

Based on these deformations, the intensity of wind is illustrated in figure 2.17, showing the top and front views of the tree trunk. (0) means no deformation due to the wind, (i) is brushing, (ii) is light flagging, (iii) is moderate flagging, (iv) stands for strong flagging, (v) is both flagging and clipping, (vi) is throwing and flagging and (vii) is extreme flagging. Still, this method needs to be calibrated with long term wind data for a given tree variety because the degree of the deformation might differ from one tree species to another. Once such calibration is available, the wind speed range can be straightforwardly estimated based on these biological indicators. [39]
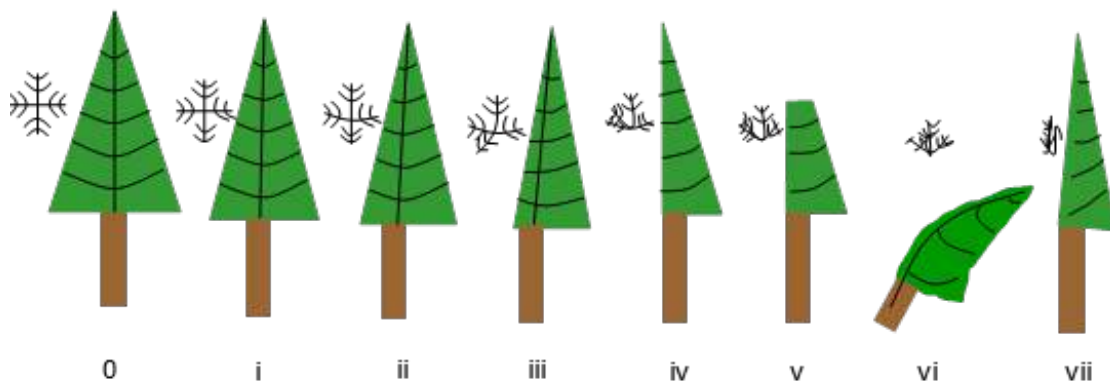
Figure 2.17: Biological rating scales for the wind speed

2.9.2 Anemometers

The final selection of the site needs to be based on field measurements. Anemometers are devices fitted on tall masts used for such wind measurements, placed either at the turbine hub height or below it. In the latter case, the surface shear has to be acknowledged and the wind measurements have to be corrected to manifest the wind speeds at hub height. Sensitive, reliable and properly calibrated anemometers should be used for wind measurements since the power is certainly susceptible to the wind speed. Mathew (2007) described 4 types of anemometers based on their working principle:

- **Rotational anemometers**: cup and propeller anemometers
- **Pressure type anemometers**: pressure plate, pressure tube and sphere anemometers
- **Thermoelectric anemometers**: hot-wire and hot plate anemometers

- **Phase shift anemometers**: ultra sonic and laser doppler anemometers

Cup anemometers

This device is popular among the wind energy measurements and consists of 3 or 4 equally spaced conical or hemispherical cups attached to a centrally rotating vertical axis, as displayed in figure 2.18. The drag force (displayed in equation (2.28)) imposed by the wind is responsible for generating the motion along the axis.

$$F_D = C_D \cdot \frac{1}{2} \cdot A_c \rho_a v_{wind}^2 \tag{2.28}$$

Where C_D is the drag coefficient, A_c is the area of the cup exposed to the wind, ρ_a is the air density and v_{wind} is the wind speed.

Figure 2.18: Cup anemometer [4]

As the drag coefficient on the concave side of the cups is greater than on the convex side, the cup with its concave side facing the wind experiences more drag force. As a result, the cups begin to rotate around its central axis. The rotational speed of the anemometer is directly proportional to the wind speed, thus a calibration to sense and directly record the wind speed can be done.

Even though such measuring devices are usually robust and long-standing, capable of favorably withstand harsh conditions, they still have some constraints. It accelerates rapidly as the wind speed increases, but retards slowly while the wind diminishes. Hence, the cup anemometers generate unreliable results in wind gusts. Furthermore, any variation in air density will also affect the measurements, as can be seen in equation (2.28). Despite these limitations, the cup anemometers are extensively used as measuring devices both in meteorology and in wind energy applications. [39]

Pressure plate anemometers

The pressure plate anemometer was the first kind of anemometer and comprises a swinging plate attached at the end of a horizontal arm. This is in turn anchored on a vertical axis that can freely rotate. It also contains a wind vane to keep the plate facing the wind direction. The pressure applied by the wind to the plate provokes it to pivot inward. As the distance at which the plate swings inward depends on the wind velocity, it can be calibrated to measure the wind speed directly. The pressure plate anemometer gives truthful results in gusty winds, unlike the cup anemometer. [39]

Hot-wire anemometers

It uses a very fine wire electrically heated up to some degrees above the ambient. Air flowing via the wire has a cooling effect on the wire. As the electrical resistance of most metals is dependent upon the temperature of the metal, a relationship can be obtained between the resistance of the wire and the flow speed. The hot-wire anemometer, while intensely delicate, has an immensely high-frequency response and fine spatial resolution when compared to other assessment methods, and as such is almost globally employed for the detailed study of turbulent flows. [40]

Laser doppler anemometer

The laser Doppler anemometer uses a beam of light from a laser which splits into two beams, with one propagated out of the anemometer. Particulates flowing along with air molecules near where the beam exits reflect or backscatter the light back into a detector, where it is contrasted to the original laser beam. A Doppler shift for measuring wind speed in the laser light is produced by the particles in great motion, and is used to calculate the speed of the particles, and thence the air around the anemometer. [40]

Examples of these anemometers are the remote sensing techniques *SODAR* and *LIDAR*, doppler effect instruments using sound and light, respectively:

- **SODAR**: SOund Detection And Ranging, or *'acoustic radar'*. A SODAR is a ground-based remote sensing instrument that sends a short acoustic sinusoidal pulse ($\approx$ 50ms) into the atmospheric boundary layer and waits for return signals, assessing the sound waves scattered back by turbulence generated by the thermodynamic structure of the atmosphere. The intensity and the doppler shift of the returns are important to determine wind speed and direction and the turbulent structure of the lower atmosphere. A three-dimensional vertical wind profile can be acquired by SODARs consisting of 3 or more beams at different angles to the vertical. Mono-static SODAR is a common device, at which receivers and the transmitter and placed in a

single unit. The monostatic SODAR is given by equation (2.29):

$$P(R) = P_0 A L \sigma(R) exp^{\left(\frac{-2aR}{R^2}\right)} \tag{2.29}$$

Where $P(R)$ is the power obtained from a distance R, P_0 is the effective transmitted power, A is the effective area of the receiver, L is the length of the acoustic pulse in space and σ is the acoustic reflectivity at distance R. The exponential is the transmission term (between 0-1), where α is the average molecular attenuation coefficient of sound in air over the distance R and factor 2 indicates a two-way transmission path. [41]

- **LIDAR**: LIght Detection And Ranging, or *'laser radar'*. A LIDAR is an optical remote sensing instrument that transmits a laser beam into the atmospheric boundary layer and estimates the scattered radiation which is received back. It can be positioned both at ground level and airborne. LIDARs can detect radiation in the ultraviolet, visible and infrared regions of the electromagnetic spectrum, interacting differently with the different physical processes within the atmosphere. Therefore, differing scattering processes allows an array of information about the atmospheric boundary layer to be inferred, including temperature, atmospheric composition and wind. A slight discrepancy of the laser beam can be interpreted as an insignificant beam width up to a few hundred meters for a continuous wave LIDAR, and up to tens of kilometers for pulsed LIDARs, permitting high resolution even at these heights. The former systems count on detector focusing to resolve vertical distance, while the latter applies signal timing. A backscattered LIDAR signal can be described as in equation (2.30).

$$P(R) = K \, G(R) \, \beta(R) \, T(R) \tag{2.30}$$

Where K is the performance of the system, $G(R)$ is the range-dependent geometric factor, $\beta(R)$ is the backscatter coefficient at distance $R0$ and $T(R)$ is the transmission factor, which describes how much light is lost from the LIDAR to distance R and back. [41]

Wind direction measurements and charts

The direction of the wind is an important factor in wind energy projects, apart from the wind speed. If the major share of the wind energy comes from a particular direction, it is necessary to avoid any obstructions that could influence the flow from this direction. Nowadays, modern anemometers are regularly equipped with wind direction measuring devices along with wind speed simultaneously. It is possible to combine information of both wind speed and direction in the form of a wind rose chart, which indicates the distribution of wind in different directions. Typically, the rose chart is divided into 8, 12 or 16 equally spaced sectors depicting

the different directions. Three different probabilities are displayed in the wind rose charts. [39]

- The percentage of time for which wind is received in a specific direction.
- The average strength of the wind spectra, defined as the product of such a percentage of time and the average wind velocity in this direction.
- The available energy from different directions defined as the product of the percentage of time and the cube of the wind speed.

Most of the software for wind calculations automatically plot wind frequency roses for visualization of the wind characteristics. Such a wind rose chart is presented in figure 2.19.
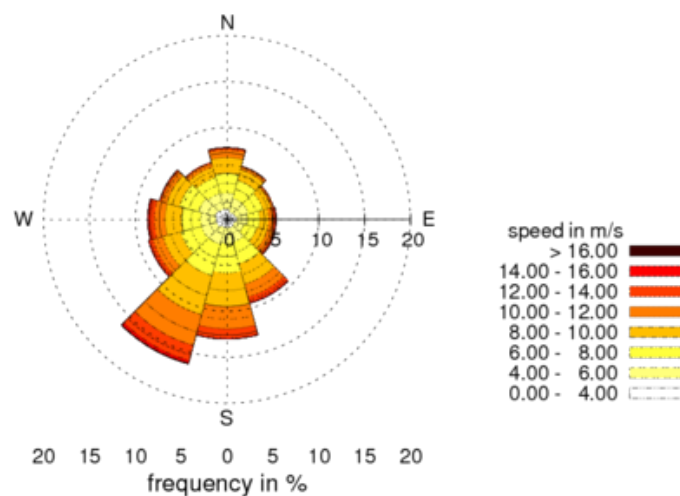
Figure 2.19: Wind rose of Lokan Tekojärvi generated by WindSim

Meteorological mast

The meteorological mast, commonly known as the *met mast* is a tower where the measuring equipment is installed. Ideally, the met mast should have the same high as the hub height of the wind turbines to be installed in the area. Nonetheless, due to economic factors, shorter masts are normally used.

The equipment installed on the met mast can include anemometers placed at different heights, a weather vane to record the direction of the wind, a barometer and a thermometer. The information collected is stored in a *data logger*. Auxiliary features can usually be found in a met mast, such as solar panels, a protective lightning pole on top, anti-vandalism fence and the foundation.

For accurate estimations, at least a year of data has to be recorded, but longer measurements ranging from 2 to 5 years present minor uncertainties and capture more accurately the fluctuations and variability of the wind in the area. [42]

Chapter 3

Computational Fluid Dynamics

3.1 Flow models

In this section the linear and non-linear models will be described, as well as the sub-models that comprise them. A comparison between the models is presented.

3.1.1 Linear model

Troen and Lundtang Petersen (1989) first described the linear model used in WAsP, which is based on the wind atlas model that combines a physical model with a statistical model. [30]

Physical model

The atmospheric boundary layer is the one closest to the ground and extends up to about 100m to more than 2km depending on the weather. The lowest part of this layer is known as the *surface layer*, which represents around 1/10 of the boundary layer depth. It is possible to model the wind profile over a flat and reasonably homogeneous terrain at high wind speeds by using the logarithmic law described in equation (3.1):

$$u(z) = \frac{u_*}{\kappa} ln \frac{z}{z_0} \tag{3.1}$$

Where z_0 is the surface roughness length, $u(z)$ is the wind speed above ground level at height z, κ is the Von Karman constant set as 0.40, and $u*$ is the air friction velocity.

For high wind speeds over a homogeneous terrain, a logarithmic wind law is applied using equation (3.2), due to the fact that even at moderate wind speeds,

deviations from the logarithmic profile might occur when the elevation exceeds a few meters.

$$u(z) = \frac{u_*}{\kappa}[ln\frac{z}{z_0} - \psi\frac{z}{L}]$$ (3.2)

This equation contains an empirical stability function, $\psi = \frac{z}{L}$, that compensates for lower wind speeds and surface heat flux. L is the Monin-Obukhov length which is obtained with equation (3.3).

$$L = \frac{T_0}{\kappa g}\frac{C_p U_*^3}{H_0}$$ (3.3)

Where g the acceleration of gravity, c_p is the heat capacity of air at constant pressure and T_0 and H_0 are the surface absolute temperature and heat flux, respectively.

The geostrophic wind is also incorporated in the geostrophic drag law for those winds in the atmospheric boundary layer that can be considered to arise from pressure differences. This is a balance between the geostrophic wind and the friction velocity, as seen in equation (3.4):

$$G = \frac{u_*}{\kappa}\sqrt{(ln\frac{u_*}{f z_0} - A)^2 + B^2}$$ (3.4)

For the non-neutral stability conditions, constants A and B become functions of the atmospheric stability parameter μ in equation (3.5)

$$\mu = \frac{\kappa u_*}{fL}$$ (3.5)

- **Stability sub-model:** the effects of varying the surface heat flux on the logarithmic wind profile are usually neglected as they are considered unimportant for low wind speed ranges. With this model, the stability of the atmosphere can be described by using the root-mean-square of the heat flux. For stable and unstable conditions, equation (3.6) is applied:

$$\psi(\frac{z}{L}) = \begin{cases} (1 - 16\frac{z}{L})^{1/4} - 1 & \text{if conditions are stable} \\ -4.7\frac{z}{L} & \text{if conditions are unstable} \end{cases}$$ (3.6)

- **Roughness change sub-model** : When there are changes in the roughness of the terrain, the logarithmic wind profile has to be compensated in order to balance for these changes as the logarithmic wind profile is valid exclusively for homogenous terrain conditions. The height of the internal boundary layer changes when the roughness changes as well, which means that the wind profile above the boundary layer before the change will be unaltered but the wind profile below will get affected, as seen in figure 3.1.
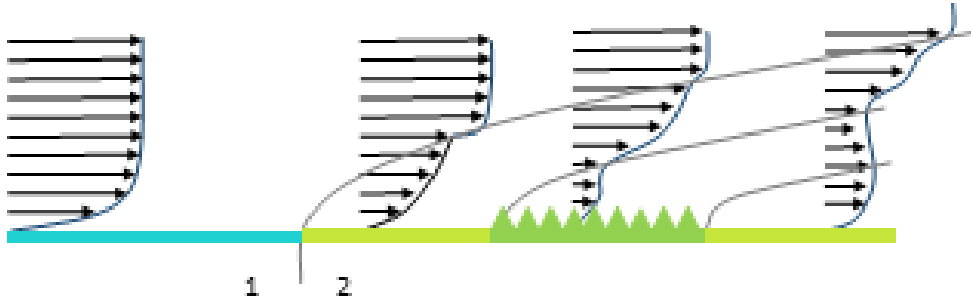
Figure 3.1: Wind profile alteration due to roughness change

It is empirically possible to model the change of surface friction velocity u_{*2} by using the relation (3.7) containing the surface stress upwind from the change u_{*1} which can be derived from matching of neutral wind profiles at the height h:

$$\frac{u_{*2}}{u_{*1}} = \frac{ln\frac{h}{z_{01}}}{ln\frac{h}{z_{02}}} \tag{3.7}$$

Also, the perturbed profile can be modeled using three logarithmic parts, shown in equation (3.8)

$$u(z) = \begin{cases} u'\frac{ln(z/z_{01})}{ln(c_1h/z_{01})} & for z \geq c_1h \\ u'' + (u' - u'')\frac{ln(z/c_2h)}{ln(c_1/c_2)} & for c_2h \leq z \leq c_1h \\ u''\frac{ln(z/z_{02})}{ln(c_2h/z_{02})} & for z \leq c_2h \end{cases} \tag{3.8}$$

Where $u' = (u_{*1}/\kappa)ln(c_1h/z_{01})$, $u'' = (u_{*2}/\kappa)ln(c_2h/z_{02})$ and $c_1 = 0.3$, $c_2 = 0.09$.

- **Shelter sub-model:** The wind profile is affected by all the obstacles around a wind turbine, and these might range from small sand grains and tree leaves to large trees and big buildings. They are all considered already in the roughness model described in chapter 3.1.1. Nearby a particular obstacle, at distances proportionate to the height of the obstacle and at heights correspondingly similar to the height of the barrier, the wind profile is perturbed, particularly in the downstream wake, thus the object must be treated independently since the characteristics of the object apply a significant influence on the effects in the wake immediately behind a dull object.

The shelter model covers the deviation due to large obstacles such as buildings, that generate wakes behind them and depends on the geometry of the object, its porosity and size, as well as the angle of incidence of the wind. In order to calculate the decrease in wind speed behind an obstacle, an empirical equation (3.9) is used:

$$\frac{\Delta u}{u} = 9.8\left(\frac{z_a}{h}\right)^{0.14}\frac{x}{h}(1 - P_{eta})\,\eta exp(-0.67\eta^{1.5}) \tag{3.9}$$

Where $\frac{\Delta u}{u}$ is the decrease in wind speed, z_a is the height considered , x is the downstream distance, P_{eta} the porosity, h the height of the obstacle and η is defined according to equation (3.10):

$$\eta = \frac{z_a}{h}\left(\frac{0.32}{ln(h/z_0)}\frac{x}{h}\right)^{-0.47} \tag{3.10}$$

- **Orographic sub-model:** similar to the sub-models above mentioned the orographic model corrects measured wind data due to inhomogeneities in the height variations around the met mast and turbine. For so doing, the model introduces a horizontal grid radially expanded from the met mast to the turbine, using polar representation. In figure 3.2, the radial grid size is lowest at the center and is expanded by a constant factor of 1.06 outwards for each grid cell, allowing to have a better resolution at the point of interest.
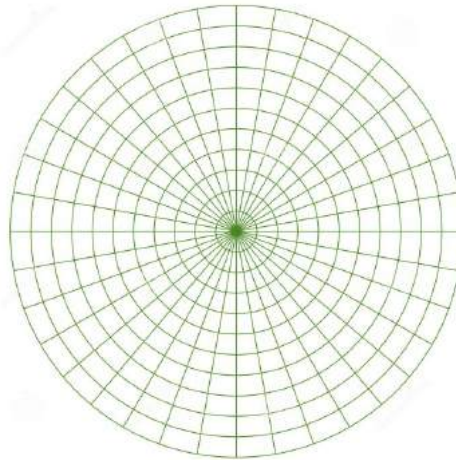
Figure 3.2: The radial grid

Statistical model

It is well known that both the speed and direction of the wind are rapidly changing over time. The mechanisms that cause the wind to blow are in contrast changing just moderately with time, as the weather changes. Additionally to the accelerated change at a single point, speed and direction change from point to point at any given moment. The wind variations are therefore the result of the turbulence in the atmospheric boundary layer.

The representation of the frequency distribution of wind speed in a simple form can be expressed as Weibull distribution, seen in equation (2.24).

3.1.2 Non-linear model

A CFD non-linear model based on Reynolds Averaged Navier-Stokes (RANS) equations with a turbulence model such as the $k - \epsilon$ or a modified version, is used in both WindSim and Zephy TOOLS.

The non-linear model described in this chapter is based on Versteeg and Malalasek-era (2007). An iterative method is required to solve the partial differential equations since the physical phenomena are complex and non-linear. During the iteration process, six flow variables are solved: three velocity components, pressure, turbulent kinetic energy and turbulent dissipation rate. Each variable has to be solved to achieve a converged solution.

Navier-Stokes equations 3.1 (equations (3.12) through (3.14)) apply for continuous substances and are based on the principle of conservation of mass, momentum and energy for a control volume. The governing equations of the flow of a compressible Newtonian fluid are presented in table 3.1.

Table 3.1: Equations governing the flow of a Newtonian compressible fluid [10]

Continuity	$$\frac{\partial \rho}{\partial t} + div(\rho \mathbf{u}) = 0$$	(3.11)
x-momentum	$$\frac{\partial(\rho u)}{\partial t} + div(\rho u \mathbf{u}) = -\frac{\partial p}{\partial x} + div(\mu \ grad \ u) + S_{Mx}$$	(3.12)
y-momentum	$$\frac{\partial(\rho v)}{\partial t} + div(\rho v \mathbf{u}) = -\frac{\partial p}{\partial y} + div(\mu \ grad \ v) + S_{My}$$	(3.13)
z-momentum	$$\frac{\partial(\rho w)}{\partial t} + div(\rho w \mathbf{u}) = -\frac{\partial p}{\partial z} + div(\mu \ grad \ w) + S_{Mz}$$	(3.14)
Energy	$$\frac{\partial(pi)}{\partial t} + div(\rho i \mathbf{u}) = -p \ div \ \mathbf{u} + div(k \ grad \ T) + \mathbf{\Phi} + S_E$$	(3.15)
Equations of state	$$p = \rho R T \quad and \quad i = c_v T$$	(3.16)
General transport	$$\frac{\partial(\rho \phi)}{\partial t} + div(\rho \phi \mathbf{u}) = div(\Gamma \ grad \ \phi) + S_\phi$$	(3.17)
	$$\mathbf{\Phi} = \mu \left\{ 2 \left[\left(\frac{\partial u}{\partial x}\right)^2 + \left(\frac{\partial v}{\partial y}\right)^2 + \left(\frac{\partial w}{\partial z}\right)^2 \right] + \left(\frac{\partial u}{\partial y} + \frac{\partial v}{\partial x}\right)^2 + \left(\frac{\partial u}{\partial z} + \frac{\partial w}{\partial x}\right)^2 + \left(\frac{\partial v}{\partial z} + \frac{\partial w}{\partial y}\right)^2 \right\} + \lambda(div \ \mathbf{u})^2$$	(3.18)

Where $\mathbf{u}$ is the velocity vector with its components (u, v, w) in x, y and z- direction respectively, ρ is the density, μ represents the dynamic viscosity for relating stresses to linear deformations (using λ for volumetric deformations) and $S_{Mx,y,z}$

is the source term for momentum per unit time and volume. Body forces on the control volume such as centrifugal forces, Coriolis forces or electromagnetic forces can be accounted in the latter source term. The *k* parameter accounts for the conductivity of the fluid and ϕ (defined in equation (3.18)) is a dissipation function that comes from the introduction of the Newtonian model where viscous stresses are expressed as gradients of velocity components. C_v denotes the specific heat and finally, S_i is the source term for energy per unit time and volume. Equation (3.17) is known as the transport equation and it is used as an initiating point when performing calculations with the finite volume method. This equation is the conservative form of all fluid equations expressed with the general flow variable and contains the rate of change term and the convective term on the left-hand side together with the source and diffusive term on the right-hand side.

Equations showed in table 3.1 apply to laminar flows, and model the instantaneous behavior of the flow. However, in reality, turbulent flows appear more often. For so doing, solving the RANS equations to resolve turbulent fluctuations and time-averaged properties is performed. The Reynolds Averaged Navier-Stokes shown in 3.2 are used in many CFD software packages. They share many common terms with the Navier-Stokes equations presented in table 3.1, but new terms that incorporate products of fluctuating velocities and which are associated with convective momentum transfer due to turbulent eddies are introduced. In these equations, the tilde stands for the density-weighted variables because the density might fluctuate, but for free turbulent flows where root-mean-square velocity fluctuations can reach 20% of the mean velocity, density fluctuations do not start to affect the turbulence until Mach numbers of around 1 are reached. [10]

Hence, the effects of density fluctuations are imperceptible but the changes in the mean density are not. Equations are displayed in table 3.2.

Also, six extra turbulent stresses in the velocity components appear, known as the *Reynolds stresses* shown in equations (3.24a-c) and (3.25a-c). The terms in the RANS equations that involve the turbulent shear stresses are generally gigantic in comparison to the viscous stresses that appear in turbulent flows. Therefore, a turbulence model is desired.

Modeling of turbulence

In order to simulate the turbulence, three different categories for numerical simulation of turbulent flows can be found: Turbulence models for the RANS equations, large-eddy simulations and direct numerical simulations. Turbulent flows are complex when it comes to eddies of a different time and length scales interacting dynamically. For WindSim and Zephy TOOLS, the associated turbulence models are of interest. These models describe the Reynolds stresses, and they are categorized by the number of transport equations that need to be solved along with the RANS equations. These models are displayed in table 3.4. These models form the basis of standard turbulence calculation procedures in currently available commercial CFD codes.

Table 3.2: Equations governing the turbulent compressible flows [10]

Continuity:

$$\frac{\partial \rho}{\partial t} + div(\bar{\rho}\tilde{\mathbf{U}}) = 0 \tag{3.19}$$

Reynolds averaged Navier-Stokes equations:

$$\frac{\partial(\bar{\rho}\tilde{U})}{\partial t} + div(\rho\tilde{U}\tilde{\mathbf{U}}) = -\frac{\partial \bar{P}}{\partial x} + div(\mu \, grad \, \tilde{U}) + \left[-\frac{\partial(\overline{\bar{\rho}u'^2})}{\partial x} - \frac{\partial(\overline{\bar{\rho}u'v'})}{\partial x} - \frac{\partial(\overline{\bar{\rho}u'w'})}{\partial x} \right] + S_{Mx}$$
$$\tag{3.20}$$

$$\frac{\partial(\bar{\rho}\tilde{V})}{\partial t} + div(\rho\tilde{V}\tilde{\mathbf{U}}) = -\frac{\partial \bar{P}}{\partial y} + div(\mu \, grad \, \tilde{V}) + \left[-\frac{\partial(\overline{\bar{\rho}u'v'})}{\partial x} - \frac{\partial(\overline{\bar{\rho}v'^2})}{\partial y} - \frac{\partial(\overline{\bar{\rho}v'w'})}{\partial z} \right] + S_{My}$$
$$\tag{3.21}$$

$$\frac{\partial(\bar{\rho}\tilde{W})}{\partial t} + div(\rho\tilde{W}\tilde{\mathbf{U}}) = -\frac{\partial \bar{P}}{\partial z} + div(\mu \, grad \, \tilde{W}) + \left[-\frac{\partial(\overline{\bar{\rho}u'w'})}{\partial x} - \frac{\partial(\overline{\bar{\rho}v'w'})}{\partial y} - \frac{\partial(\overline{\bar{\rho}w'^2})}{\partial z} \right] + S_{Mz}$$
$$\tag{3.22}$$

Scalar transport equation:

$$\frac{\partial(\bar{\rho}\tilde{\Phi})}{\partial t} + div(\rho\tilde{\Phi}\tilde{\mathbf{U}}) = div(\Gamma_\Phi \, grad \, \tilde{\Phi}) + \left[-\frac{\partial(\overline{\bar{\rho}u'\varphi'})}{\partial x} - \frac{\partial(\overline{\bar{\rho}v'\varphi'})}{\partial x} - \frac{\partial(\overline{\bar{\rho}w'\varphi'})}{\partial x} \right] + S_\Phi \tag{3.23}$$

- **The k-ϵ model**:

The k-ϵ model allows for the transport of turbulence properties employing convection and diffusion, as well as for the production and destruction of turbulence, e.g. in recirculating flows. Therefore, it is necessary to consider statements regarding the dynamics of turbulence and the mechanisms that affect the turbulent kinetic energy. Two transport equations in the form of partial differential equations are considered, as seen in table 3.4, accounting for both the turbulent kinetic energy k as well as the rate of dissipation of turbulent energy ε.

This model assumes that the turbulent viscosity μ_t is isotropic, which means that the ratio between the Reynolds stresses and the mean rate of deformation is equal in all directions.

The sum of the turbulent kinetic energy k (eq.(3.28)) and the mean kinetic energy K (eq. (3.27)) results in the instantaneous kinetic energy k_i (eq. (3.26)).

Table 3.3: Reynolds stresses

$$\tau_{xx} = -\rho\overline{u'^2} \qquad \tau_{yy} = -\rho\overline{v'^2} \qquad \tau_{zz} = -\rho\overline{w'^2} \qquad \text{(3.24a-c)}$$

$$\tau_{xy} = \tau_{yx} = -\rho\overline{u'v'} \qquad \tau_{xz} = \tau_{zx} = -\rho\overline{u'w'} \qquad \tau_{yz} = \tau_{zy} = -\rho\overline{v'w'} \quad \text{(3.25a-c)}$$

Table 3.4: Turbulence models

Turbulence model	Additional transport equations
Mixing length model	0
Spalart-Allmaras model	1
k-ϵ model	2
k-w model	2
Algebraic stress model	2
Reynolds stress model	7

$$k_i = K + k \tag{3.26}$$

$$K = \frac{1}{2}(U^2 + V^2 + W^2) \tag{3.27}$$

$$k = \frac{1}{2}(\overline{u'^2} + \overline{v'^2} + \overline{w'^2}) \tag{3.28}$$

Deducing the time-averaged transport equations that govern the RANS equations for mean and turbulent kinetic energy is possible since the rate of dissipation of turbulent kinetic energy ε comes as a term in the governing equation of k. Turbulent kinetic energy gets dissipated due to the smallest eddies in the flow, which exert work against viscous stresses. Also, other properties including ϵ can be performed for all other turbulence properties, but these equations can be complex and with immeasurable terms. Thus, the k-ϵ consists of the following two equations: [10]

Table 3.5: k-ϵ model equations

$$\frac{\partial(\rho k)}{\partial t} + div(\rho k\mathbf{U}) = div\left[\frac{\mu_t}{\sigma_k}\,grad\,k\right] + 2\mu_t S_{ij} \cdot S_{ij} - \rho\varepsilon \tag{3.29}$$

$$\frac{\partial(\rho\varepsilon)}{\partial t} + div(\rho\varepsilon\mathbf{U}) = div\left[\frac{\mu_t}{\sigma_\varepsilon}\,grad\,\varepsilon\right] + C_{1\varepsilon}\frac{\varepsilon}{k}2\mu_t S_{ij} \cdot S_{ij} - C_{2\varepsilon}\rho\frac{\varepsilon^2}{k} \tag{3.30}$$

With:

$$\mu_t = \rho C_\mu\frac{k^2}{\varepsilon} \tag{3.31}$$

$$\sigma k = \frac{\mu_t}{\Gamma_k} \quad \text{and} \quad \sigma\varepsilon = \frac{\mu_t}{\Gamma_\varepsilon} \tag{3.32a, b}$$

In equation (3.32a, b), the terms for σk and $\sigma\varepsilon$ are known to be the *Prandtl numbers* and they associate the diffusivities of ϵ and k. Also, the term S_{ij} designates a matrix with the terms of deformation, as it can be seen in equation (3.33):

$$S_{ij} = \begin{bmatrix} S_{xx} & S_{xy} & S_{xz} \\ S_{yx} & S_{yy} & S_{yz} \\ S_{zx} & S_{zy} & S_{zz} \end{bmatrix} = \begin{bmatrix} \frac{\partial U}{\partial x} & \frac{1}{2}\left[\frac{\partial U}{\partial y} + \frac{\partial V}{\partial x}\right] & \frac{1}{2}\left[\frac{\partial U}{\partial z} + \frac{\partial W}{\partial x}\right] \\ \frac{1}{2}\left[\frac{\partial U}{\partial y} + \frac{\partial V}{\partial x}\right] & \frac{\partial V}{\partial y} & \frac{1}{2}\left[\frac{\partial V}{\partial z} + \frac{\partial W}{\partial y}\right] \\ \frac{1}{2}\left[\frac{\partial U}{\partial z} + \frac{\partial W}{\partial x}\right] & \frac{1}{2}\left[\frac{\partial V}{\partial z} + \frac{\partial W}{\partial y}\right] & \frac{\partial W}{\partial z} \end{bmatrix} \tag{3.33}$$

It is necessary to calculate the Reynolds stresses, and for so doing, the Boussinesq relationship in equation (3.34) is applied:

$$\tau_{ij} = -\rho\overline{u_i' u_j'} = \mu_t\left(\frac{\partial U_i}{\partial x_j} + \frac{\partial U_j}{\partial x_i}\right) - \frac{2}{3}\rho k\delta_{ij} = 2\mu_t S_{ij} - \frac{2}{3}\rho k\delta_{ij} \tag{3.34}$$

The term δ_{ij} refers to the *Kronecker delta*:

$$\delta_{ij} = \begin{cases} 0 & i \neq j \\ 1 & i = j \end{cases}$$

- **The RNG k-ϵ model:**

This model describes the effects of small-scale turbulence as a result of a haphazard forcing function in the Navier–Stokes equation. The RNG procedure methodically dismisses the small scales of motion from the governing equations by expressing their effects in terms of larger-scale motions and a modified viscosity. The mathematics behind the model is remarkably abstruse, as shown in equations (3.35) to (3.36):

Table 3.6: RNG k-ϵ model equations

$$\frac{\partial(\rho k)}{\partial t} + div(\rho k\mathbf{U}) = div\left[\alpha_k\mu_{eff}\, grad\, k\right] + \tau_{ij} \cdot S_{ij} - \rho\varepsilon \tag{3.35}$$

$$\frac{\partial(\rho\varepsilon)}{\partial t} + div(\rho\varepsilon\mathbf{U}) = div\left[\alpha_\varepsilon\mu_{eff}\, grad\, \varepsilon\right] + C_{1\varepsilon}^*\frac{\varepsilon}{k}\tau_{ij} \cdot S_{ij} - C_{2\varepsilon}\rho\frac{\varepsilon^2}{k} \tag{3.36}$$

With:

$$\tau_{ij} = -\rho\overline{u_i' u_j'} = 2\mu_t S_{ij} - \frac{2}{3}\rho k\delta_{ij} \tag{3.37}$$

and

$$C_\mu = 0.0845 \qquad \alpha_k = \alpha_\varepsilon = 1.39 \qquad C_{1\varepsilon} = 1.42 \qquad C_{2\varepsilon} = 1.68$$

3.1.3 Boundary conditions

RANS equations are solved numerically in a geometrical domain divided into small cells forming a mesh, in which equations are applied for every single cell by an iteration method until convergence is reached. Different types of meshes can be generated according to the software, and for some cases where the topography is very detailed e.g. terrain irregularities, a more refined mesh around the studied area is desired. However, a better resolution area requires an intense computational capacity, resulting in longer computing time but higher accuracy.

Different boundary conditions are applied at the borders depending on the boundary, but the same logarithmic wind profile as described in the wind energy and linear model sections, equations (2.7) and (3.1) is established, as well as the profiles of k and ε used in the turbulence model. [14]

In order to apply the boundary conditions, a 3-dimensional model is used to preset a ground structure, length, width and height. The 6 conditions described in table 3.3, shown in equations (3.24a-c) and (3.25a-c) are computed for every cell in the model. At the ground of the model (figure 3.3a), no air is supposed to pass through and in the top (figure3.3b) either the pressure is fixed, meaning that a homogeneous pressure is extended along a plane of a chosen height or no friction is set, so that no air can pass through the wall. Finally, the geostrophic balance described in section 2.1.2 is applied at a constant wind speed above the top boundary layer (figure 3.3c). Temperature can as well alter the atmospheric stability depending on the site and conditions, as described in section 2.1.3.
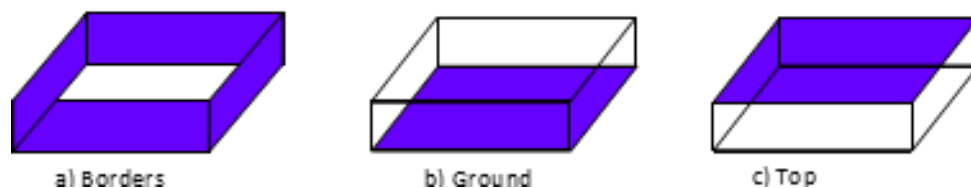
Figure 3.3: Boundary conditions

Statistical model

The non-linear model can process data in two ways, either as frequency tables or as time series during a period of time. The first ones contain wind speeds and directions in summarized tables while the latter case is fundamental wind speeds and directions measured in a period of time, e.g. every minute, providing with more accurate information about the conditions at the site.

3.2   Distinctness in the models

It is known that when terrain slopes are around 30% or 17°, flow separation is generated, provoking the wind to accelerate up the hill and resulting in high wind speeds (see figure 3.4).
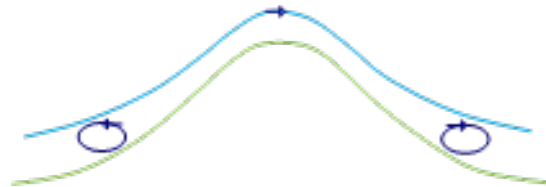
Figure 3.4: Wind separation due to high angle slope [5]

The linear approach assumes the attached flow and hence over-predicts the hill shape speed-up effect of a very steep hill, as seen in figure 3.7. This model generally considers an increasing speedup effect when slope increases, meaning that if the met mast is located in a flat plane terrain and the turbine is to be placed on a steep hill (initiating flow separation), an over-prediction might occur, correspondingly to the opposite case in the reverse direction, leading to an under-prediction. The major difference in the models is the way the software treats this flow separation, as they can differently account for this phenomenon while modeling complex terrain sites. The linear approach cannot account for this separation and treats the flow as attached over the hill, as shown in figure 3.5. Non-linear models can account for this separation, as they include the turbulence model (see figure 3.6).
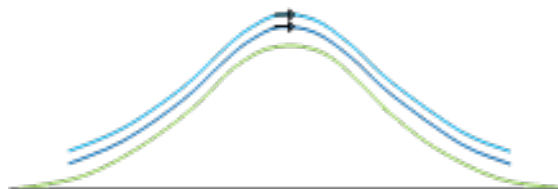
Figure 3.5: Behaviour of wind in the linear model [5]

Figure 3.6: WAsP estimation of flow over steep inclines (left) and real wind flow separation (right) [5]

A way to forecast the magnitude of the errors for under and over estimations when the surrounding terrain differs for both reference and predicted sites is the

delta-RIX methodology. The Ruggedness Index is the percentage fraction of the terrain within a certain distance from a site which is steeper than a defined critical slope and gives a coarse measure of the extent of flow separation. If the delta RIX value is negative, an expected under-prediction will be seen and a positive value will result in an expected over-prediction of wind speed. [5]
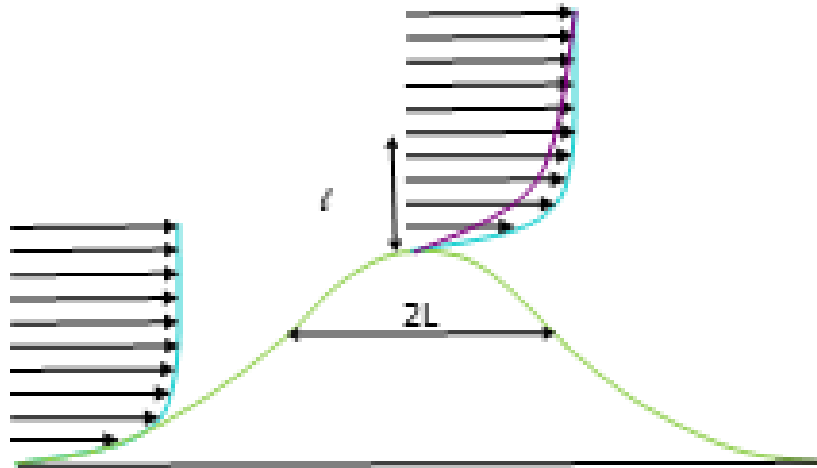
Figure 3.7: The speed up effect

Chapter 4

Software for wind farm layout optimization

Analytic and numerical models are implemented in order to calculate the wind resource. In this case of study, WAsP is the analytic model used by WindPRO for the Annual Energy Production calculation, which will be compared with the numerical model WindSim. Four different software were used to execute the simulations of the wind farms and the power generation:

- – WAsP
- – WindPRO

- – WindSim
- – Zephy Tools

4.1 WAsP

WAsP is a linear model for wind resource assessment and energy yield calculations for wind turbines and wind farms, developed by Risø laboratories in Denmark [30]. In WAsP it is possible to range from various wind applications such as wind analysis or sitting of wind turbines and power production calculations, and it is used for sites located in different kinds of terrain all over the world. When it comes to horizontal and vertical extrapolation, WAsP uses the built-in linear IBZ model, adequate for simulations for flat to moderately complex terrain. However, when the terrain is very complex, a CFD model is advisable to use. [43]

4.2 WindPRO

This module-based software is suitable for wind energy project development and planning of both single Wind Turbine Generators and large wind farms. With this numerical model, it is possible to simulate the vertical wind composition within the atmospheric boundary layer. This Danish software provides trustworthy calculations to provide an accurate assessment for financing purposes. WindPRO incorporates different energy modules:

- **METEO**: is an advanced import and analysis module for measured wind data which calculates the energy yield of WTGs considering on-site wind information. It is possible to prepare wind data for wind statistics generation with WAsP as well as visually inspect time series, gunshot diagrams, directional distributions among others.

- **MODEL**: used for modeling wind flow of vertical and horizontal extrapolations on a site. This module is supported by calculation tools such as WAsP, ATLAS and CFD. ATLAS is a tool already integrated into WindPRO and it is used when simple terrain calculations are needed, but roughness and elevation models are previously required. CFD calculations are not performed in WindPRO, so it is necessary to import the prepared CFD model into the software.

- **MCD**: used for long-term correction of measured data which uses different calculations methods, which include linear regression, matrix, Weibull scale and wind index. The output contains a wind statistic produced with WAsP/WAsP-CFD based on the long term corrected wind data and terrain information. This can be input directly in a PARK calculation or for a wind resource map calculation.

- **PARK**: is based on the previous models METEO and MODEL, this module calculates the energy production of a wind farm, containing array losses. This flexible tool allows to mix between different WTGs and different hub heights in the same calculation, which makes fast and easy the testing of several different layouts against each other.

- **LOSS AND UNCERTAINTY**: an efficient and structured way of addressing issues to be considered before a wind farm project reaches a bankable level. Takes into account an annual production at exceeding levels between P_{50} and P_{99}, and the potentiality to improve for systematic errors such as in complex terrain (RIX [1] correction) or to calculate the losses for various curtailment.

- **OPTIMIZE**: employed to enhance the layout of the wind farm concerning energy production or the operation mode plan to meet the established requirements. [31]

---

[1]Ruggedness Index is an objective measure of the extent of steep slopes in an area

4.3   WindSim

This Norwegian-developed tool is a CFD wind simulation software based on the non-linear flow model based on the 3D Reynolds Averaged Navier-Stokes partial differential equations described in section 3.1.2, whereby only the mean flow is solved and all eddies [2] are modeled together with the effect of turbulence models on the mean flow. These equations model fluid flows with more complex physics in terms of the non-linear transport equations for conservation of mass and momentum, which can be done by a meshing system. The solver inside WindSim can apply and model the wind conditions at each of the cells in the generated mesh system. [44]

WindSim is suitable for evaluating and optimizing wind farm production and efficiency, mapping of wind resources and is peculiarly useful when the site consists of a complex orography or with complex local climatology. The software is divided into modules which will be described as follows:

- **TERRAIN**: a 3D area around the planned wind farm is created by loading and modifying terrain grid data in .GWS format, defined by height contour and terrain roughness. A 2D data sheet with elevation and roughness need to be specified in advance into WindSim. A numerical model is performed where a meshed grid measures a specific area, and it is possible to create *grid refinement* where the spacing of the nodal points are closely packed at the area of interest, and increasingly spaced away from the refined area to the boundary (see figure 4.2). By applying this method, it is possible to obtain a higher resolution in the area of interest while still having a considerable number of cells. Refinement is only performed in the final nested layer, in order to prevent further nesting. It is important to consider the computational time required to reach a solution, as it is exponentially proportional to the number of cells in the grid. When the nesting technique is utilized, several smaller models are created from the original one, which proves to be time-efficient in terms of computational times required. Besides, when grid refinement is applied, the necessary computational times increase substantially. [45]
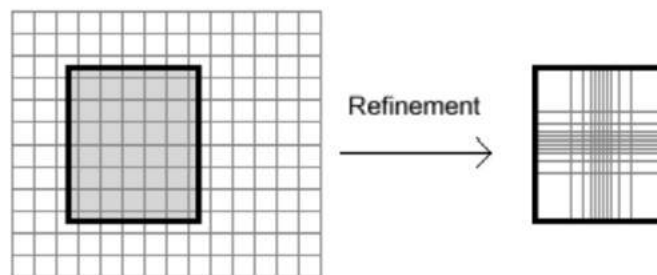

Refinement

Figure 4.2: WindSim cell refinement

---

[2]The swirling of a fluid and the reverse current created when the fluid is in a turbulent flow regime

In some cases a physical solution cannot be attained since the solution diverges instead of converging. This could be caused by of quick changes in the inclination between adjacent cells, such as in narrow valleys or sharp hill peaks. WindSim prevents divergence by using a technique called *terrain smoothening*, which automatically smoothens the terrain where the changes in the inclination are greater than a specific set value. The terrain gets slightly altered but can be tolerated as usually, these locations are not suitable for placing wind turbines.

It is also possible to achieve convergence by *orthogonalizing the grid*. The normal configuration extend the grid vertically along straight lines, but when this approach is used, the grid gets rearranged into lines that extends vertically in curved lines, targeting to be perpendicular to the ground. As a result, the cells will be less tilted with high inclinations. This feature is recommended when inclination angles surpass 50°. [45]

By default, the forest is disregarded in WindSim, but it is possible to be considered by associating a roughness height with the given forest characteristics. Once the roughness height has been determined, forest height is also needed, whose default value is 30m. Also, one can store all the forest characteristics under specific keywords in the grid file, from where the data will be taken afterward. For instance, *forest porosity* will have an allowed value between 0 (a fully blocked area) and 1 (a fully open area). Finally, the forest cell count in the vertical direction can have a set value, which is simply the difference between the set value for the entire simulation and the cell count for the forest.

- **WIND FIELDS**: this module produces the wind database and simulates how the terrain influences the wind. By using several numerical models, WindSim can solve the Reynolds Averaged Navier-Stokes differential equations using the $k - \varepsilon$ turbulence model, solving the variables of pressure, turbulence kinetic energy, velocity, and turbulent dissipation rate, as well as temperature for more complex models. Besides, the Coriolis force can also be included in the simulation for the turbulence model.

  In this module, the boundary and initial conditions need to be specified in the form of a vertical velocity profile which can be done either by setting a wind profile based on the log law, which depends on the roughness (and if the temperature is involved, also the atmospheric stability) or employing the nesting technique, which is often the recommended option, as the first one assumes an infinite flat landscape outside the computational domain as boundary conditions.

  It is possible to activate the temperature equations in the wind fields module so that different boundary and initial conditions are established depending on what kind of initialization is preferred. These equations can be initialized either by setting a value for the Monin-Obukhov length (described in section 2.1.3) or by assuming a log profile at the inlets. In the first case, a linear temperature gradient is assumed in the atmosphere whereas, in the second,

the temperature gradient is assumed constant throughout the atmosphere.

There are two numeric solvers that WindSim incorporates. The coupled solver, a multi-grid solver that simultaneously solves the hydrodynamic variables in a whole-field manner. The other option is the segregated solver based on the Patankar-Spalding SIMPLE (Semi-Implicit Method for Pressure Linked Equations) algorithm, which solves the velocity and pressure parts of the flow equations separately.

With the segregated solver, it is possible to solve a larger model compared to the coupled solver but might, however, need around 10 times the number of iterations as for the coupled solver, and hence the segregated solver should be used when longer computational times can be agreed. WindSim has incorporated a convergence wizard, useful When convergence is complicated to achieve. [45]

- **OBJECTS**: in this module, objects are placed within the model, such as turbines, climatologies and transferred climatologies. For visualization purposes various geometrical objects that can also be placed within the 3D terrain model as well. These objects can be set to be visible or invisible so that they are or not taken into account in the energy and wind resource calculations. A transferred climatology means a virtual collection of measurements obtained from a real climatology and the numerical database from the simulation, which allows simulating and mapping various wind conditions in different areas. Furthermore, it can also be set in the objects module specifications such as the power curve, hub height, rotor diameter, rotational speed and the direction towards which the wind turbines are rotating. [45]

- **RESULTS**: this module extracts 2D horizontal planes from the output of the Wind Field module generated during the wind field simulations. Flow variables such as direction, wind speed, the vertical component of the wind turbulence and intensity can all be viewed in the results module. Results can also be displayed for a specific particle in the model, which can be employed to high-risk areas to estimate if recirculation may occur. another feature of WindSim is the possibility of normalizing the results against either a scalar value or against the nearest climatology. [45]

- **WIND RESOURCES**: the wind resource module produces a wind resource map of the modeled area generated from the wind resources weighted against measurements, which can be later used in the energy calculations. An area classification feature is also included within this module and can locate appealing areas in the model, in terms of wind speeds and size. Likewise, this module can determine the possible power production in these areas.

Regarding the wake effects, WindSim has incorporated three analytic models that are particularly attractive in terms of reduced computational times compared to CFD based models. The Jensen model, the Larsen model and

the model proposed by Ishihara, Yamaguchi and Fujino. The wake models use the results generated in the wind fields module in WindSim to calculated the velocity deficit after the turbines. For more details, see section 2.7.2. [45]

- **ENERGY**: The Annual Energy Production can be calculated for all turbines in the project as well as the wake losses associated with each of them. Flexibility is a feature in the energy module, as different park layouts can be modeled and compared, along with more than one climatology option. The climatologies can be given in the form of frequency distribution and its Weibull distribution, resulting in the calculation of the electricity production in both cases.

  In the energy module, the air density at the turbine locations needs to be set, since the wind turbine power curve is provided for a given density value. If these values may differ, a correction factor is then applied. Two methods for correcting the power curve for an alternative density are used, according to the IEC standard EN 61400-12. One of them is for pitch-regulated turbines, where the original power curve is applied and the wind speed is corrected. The correction can be calculated by the wind speed times the fraction $\frac{air\ density\ AEP}{air\ density\ power\ curve}$ at the power 1/3. The other case is for stall-regulated turbines, where the density fraction is multiplied with the reference power curves. After the calculations have been made, the vertical wind profiles can be exported in an ASCII file and viewed for every wind turbine position. Additionally, the rotor profiles are as well available for export. [45]

4.4 Zephy TOOLS

This is a French software written by Zephy-Science, a subsidiary of AZIUGO. It uses a 3D Reynolds Averaged Navier- Stokes solver. The non-linear transport equations for mass, momentum and energy are therefore solved considering a steady-state and isotherm incompressible fluid. The non-linear Reynolds stress tensor is modeled by the $k - \epsilon$ dual equation closure scheme, based upon coupled transport equations for the turbulent energy density k and the turbulent dissipation rate ϵ.

It is an innovative software that runs in the Ubuntu environment with an open-source scheme. Zephy CFD uses OpenFOAM open-source solver as the software CFD core. For windows users, it is necessary to install a virtual Ubuntu environment to host Zephy TOOLS on any Windows version.

Zephy TOOLS requires the user to create an account in order to access the graphical user interface. If the account is not recognized, no cloud computation will be possible. [46]

4.4.1 Pre-processing

The first step for any new project is a *Pre-processing* stage, where all the processing parameters to be calculated have to be entered. They include:

- **Orography** The orography data needed for CFD projects can be loaded either in the format *.xyz* and *.map*.

  It is possible to define simple-case orography files directly in ZephyTOOLS, defining simple and double gaussian hills.

- **Roughness** The roughness data needed for CFD projects can be loaded either in the format *.xyr* and *.map*.

  It is possible to define simple roughness files directly in Zephy TOOLS, with a homogeneous roughness length having a circular zone in the middle with a different homogeneous roughness length.

- **Picture** Georeferenced pictures can be uploaded in order to use them as background in the maps and iso-heights plots. Georeferenced pictures are *.png* files with a *.pngw* text file associated, which contains the georeference information. Such files can be generated using *QGis*, which is a free open-source software.

- **Masts** The met masts locations are inputted with a *.zsmast* extension. Each line in it corresponds to a different mast, and for each mast, Zephy CFD needs the following information separated with white space:

  - X and Y: mast coordinates
  - Label: the mast name.

- **LIDARs** The lidars locations are inputted using the *.zslidar* extension. Each line in it corresponds to a different lidar and the following information, separated with white space is needed:

  - X and Y: lidar coordinates [m]
  - Angle: lidar scanning angle [deg]
  - Label: the lidar name.

- **Wind turbines** The wind turbines locations are inputted with text files with a *.zswt* extension. Each line in it corresponds to a different wind turbine and needs to have the following information, separated with white space:

  - X and Y: turbine coordinates
  - Label: turbine name
  - Group: a group name, to associate *.wtg* files to the WTGs by a group.

- **Result points** A *point* entity is an additional single result point in the domain whose results will be saved and has the *zspoint* extension. Each line in it corresponds to a different result point, for which a point entity will be defined. The following information separated with white space is needed:

- – X and Y: point coordinates [m]
- – Height: point height above ground [m]
- – Label: point name.

- **Mesoscale points** A *meso* entity describes a point for which wind data from a mesoscale model will be downscaled. A mesoscale point file has the *.zsmeso* extension and each line in the file corresponds to a different mesoscale point, for which a meso entity will be defined with the following information, separated with a white space:

  - – X and Y: point coordinates [m]
  - – Height: point height above ground [m]
  - – Mesoscale resolution: mesoscale model resolution [m]
  - – Resolution: the resolution [m]
  - – Label: point name.

- **Mappings** A *mapping* describes an area for which it will be possible to visualize Iso-heights results, export wind resource grids and export Iso-heights results, either as georeferenced pictures or *.xyz* files. A mapping file is saved with *.zsmapping* extension, and each line in it corresponds to a different mapping, for which a 2D result grid will be defined. For each area Zephy CFD needs the following information, separated with a white space:

  - – X_1, X_2, Y_1, Y_2: mapping corners coordinates [m]
  - – Resolution: the resolution of the result grid [m]
  - – Height: height of the result grid [m]
  - – Diameter: rotor diameter for calculating wind shear
  - – Label: the name of the mapping

- **Multi-data** It is possible to define several input files into one, using the *multi-data* format with the *.zsmulti* extension. The format contains one item per line, with the type of the entity being the first information on the line and the other values separated by a white space. Such entity identifiers are:

  - * Masts: mast
  - * Wind turbines: wt
  - * Points: point
  - * Mesoscale points: meso
  - * Mappings: mapping
  - * Orography: oro
  - * Roughness: rou

- **Climatology** A *climatology* is the wind data associated with a point in the CFD domain, which is to be extrapolated to the rest of the domain by using CFD results. Currently, there are two possible wind data file formats for Zephy CFD:

  1) *.tab* file
  2) *.zsvd/.zsvds* time series file with the following information:

  - – Line 1: Comments

- Line 2: *X*-coordinate *Y*-coordinate height
    - Line 3: Georeference
    - Line 4 and onwards: Values separated by white space.

  For *.zsvd*: Wind speed column and wind direction column.
  For *.zsvds*: Wind speed column, wind direction column and standard deviation column.

- **Generator** The power curve data needed by Zephy CFD for yield assessments can be loaded in standard *.wtg* files. [47]

4.4.2   ZephyCloud

Zephy TOOLS gives direct access to ZephyCloud, AZIUGO's cloud computing platform which allows running simulations in the online machines from cloud providers. [46]

4.4.3   ZephyCoins

Zephy TOOLS rents online machines for its cloud service and has developed a business model in which users have to purchase and use cloud credits for pay-as-you-go access to ZephyCloud. These cloud credits are called *ZephyCoins*. All ZephyCoins Ƶ have the same purchase price but different core-hour values depending on the type of account the user has:

- Premium Users: All Ƶ are Gold Coins
- Freemium Users: All Ƶ are Bronze Coins

$$1 \text{ Gold } Ƶ = 5 \text{ Bronze } Ƶ$$

The fully functional ZephyTOOLS software is freely accessible at any time. However, what makes it stand out is its cloud-computing capacity, which is charged on a cores-per-hour basis, with prices increasing with calculation time and number of processors utilized. The used calculation resources are charged in ZephyCoins, with a price of 4€ and the amount of ZephyCoins, spent per calculation will depend on the type of account chosen by the user. [46]

4.4.4   Main modules

The next step is to select the module for which the computer process will be launched either locally or on ZephyCloud. There are three modules available in Zephy TOOLS, including the *Zephy WDG* wind data generator for meso-scale projects, the *Zephy WDP* wind data processor for wind data analysis and the *Zephy CDF* wind modelling for micro-scale projects. [46]

Zephy CFD

The software is based on the opensource OpenFOAM CFD solver, powered by cloud computing servers currently using Amazon Web Services. This approach overcomes the main limitations of traditional CFD methods by providing more accurate, reliable and faster wind farm modeling simulation results. The different steps of a ZephyCFD new project are recapitulated as follows:

- **LOAD**: before the numerical calculations, the 3D calculation domain needs to be discretized into a mesh, using orography and land cover data. This section uploads the input files which were defined for the project.

- **ANALYSIS**: it analyses the topography inputs loaded in the previous section and combines them with the climatology files to perform a climatology-based RIX analysis at each point of interest. Besides, it calculates a parameter called *ZIX*, which indicates of the overall complexity of the site, allowing ZephyCFD to adapt its automatic specifications in the next steps.

- **MESHING**: this is one of the key steps of the CFD process and conducts the discretization of the calculation domain. ZephyCFD uses an unstructured mesh, which allows increasing mesh resolution at points of interest without considerably increasing the overall mesh size. Furthermore, the meshing is done in a cylindrical domain, allowing to keep the same grid for different wind directions, unlike cartesian-coordinate grids which always have to be set perpendicular to the incoming flow.

  Zephy TOOLS advises to create two different meshes in order to optimize the convergence of the calculations:

  - A low-resolution mesh used to evaluate the wind characteristics for the non-prevailing directions according to the measured wind roses.
  - A high-resolution mesh used to evaluate the wind characteristics for the prevailing directions according to the measured wind roses.

- **CALCULATIONS**: in this part, the user can either allow the software to choose automatically the wind sectors to calculate and the CFD parameters to use, or customize them manually with in-depth access to many parameters (solver, initialization, boundaries, turbulence, etc).

  The convergence can then be monitored in real-time, even for calculations running in the cloud. Calculations can be stopped and restarted as much as needed to ensure convergence.

- **ROSE**: once all the different wind sectors have been calculated, the results are combined into a single model of the domain. For each wind characteristic, the relations between a reference point and the other points in the domain are estimated (speed-up ratios, direction deviations, etc), by interpolating linearly between the available wind sector CFD results.

- **EXTRAPOLATIONS**: a climatology file has to be associated with each Rose generated in the previous step. Thus such wind data can be extrapolated by the Rose to the rest of the domain, obtaining the final wind estimations.

  In this section, 6 variables can be chosen: Speed Rose, Energy Rose, Inclination Rose, Absolute TI Rose, Histogram and Wind Rose.

  In the page of results, 6 variables can be chosen as well: Velocity, Flow Inclination, Turbulent Intensity, Weibull Scale Parameter, Weibull Shape Parameter and Wind Power Density.

- **YIELD ASSESSMENT**: Once wind extrapolations are available, it is possible to assess the expected annual yield for the project's wind turbine layout, resulting in the final production estimations. Therefore, it is necessary to associate the *.wtg* files to the project's wind turbines either by setting a single power curve for the whole farm or differentiating the turbine by one or by groups. Many different results can be exported as tables, particularly the production estimations along with the associated turbine-wise uncertainties. [48]

Chapter 5

Methodology

Three commercial wind energy calculation software will be evaluated and compared in three sites with different characteristics in Finland, in order to investigate their reliability and accurateness. WindPRO together with WAsP, WindSim and Zephy TOOLS are used to perform the wind flow calculations.

5.1 Site selection

Finland (figure 5.1) was covered by a thick layer of ice during the last Ice Age. About 10,000 years ago when the ice sheet melted, it gouged the surface of the land and left in its wake countless rivers, streams and islands, along with an approximated 188,000 lakes (see figure 5.2a). Nearly 60,000 of such lakes are wider than 200 m. With more than 70% of the land covered by thick forest, Finland is predominantly flat. In the southern areas, countless clear water lakes are far and wide, as water seems a more typical sight than land. Northwards of the Arctic Circle, the terrain rises into low mountains and hills of Lapland. Haltitunturi is the country's highest point, located at 1,328 meters above sea level, which stands on the edge of its border with Norway (see figure 5.2b). [49]

Figure 5.1: Finland

The geography of Finland can variate from North to South. Therefore, it is interesting to investigate what happens when the same site is simulated using different software. Three places were selected based on their elevation, placing the met mast and the wind turbine in a) a flat terrain with a quite gentle slope, b) a moderate slope and c) a steep slope along with an extra study case for a d) real case.

(a) Finnish lakes

(b) Haltitunturi

Figure 5.2: Site selection

5.1.1 Korpinen

Korpinen is a rather large lake in the Iijoki area, located in the region of Northern Ostrobothnia (see figure 5.3). A quite gentle hill was found around this area with a fairly smooth terrain and not many elevated areas around that might influence the prevailing wind. Therefore, it was interesting to see what results can be obtained.
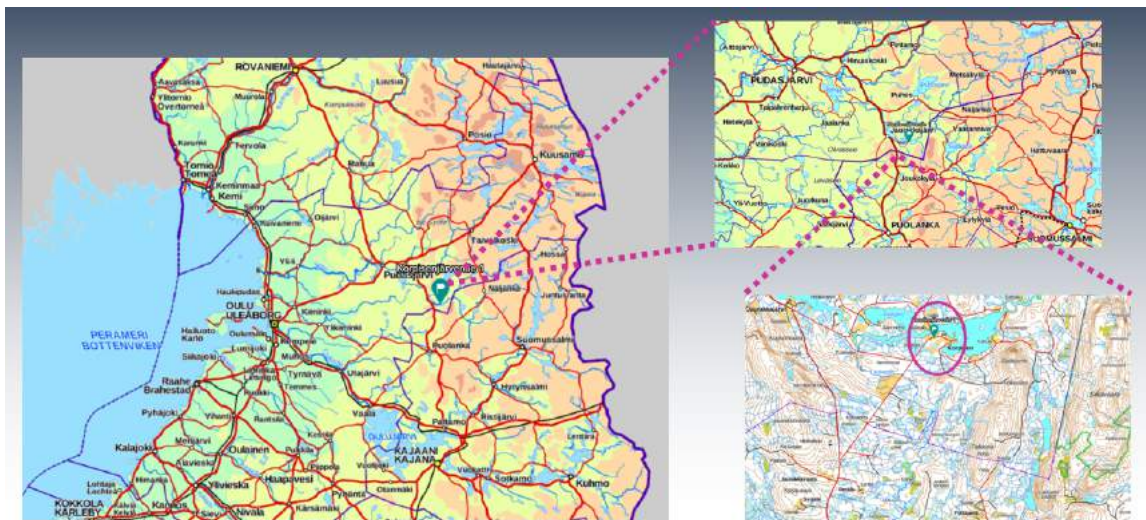

Figure 5.3: Korpinen location [6]

5.1.2 Lokan Tekojärvi

Located in the upper reaches of Luiro in Sodankylä in the region of Lapland (figure 5.4), Loka artificial lake is the largest reservoir of the European Union. At the lowest water level (240 m), the surface of the reservoir is 216 km^3 and at the highest level (245 m) 418 km^3. The filling of the Loka reservoir began in 1967. [50]

Northwards of the lake, a mountain with a moderate slope was selected for the simulation. 86 meters of height difference separate the met mast from the turbine, as well as a linear distance of 2700 meters between them.
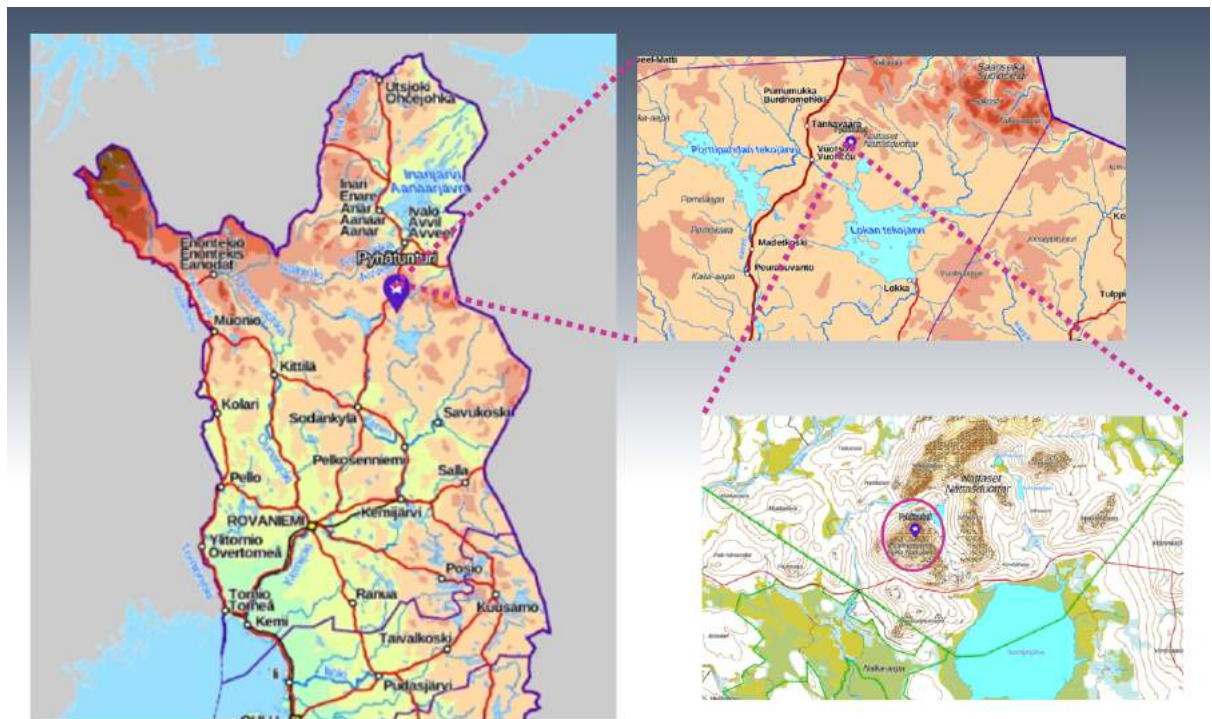
Figure 5.4: Lokan Tekojärvi location

5.1.3 Ylläs

Yllästunturi is a 719 m high mountain located in the western Lapland municipality of Kolari (figure 5.6). Ylläs is a popular ski area with two ski resorts connected, on the Ylläsjärvi side, the Sport Resort Ylläs and on the Äkäslompolo side Ylläs-Ski. For skiers, the high Ylläs and six wild fells in the area offer endless freedom of choice from smooth slopes to steep valleys covered with deep snow. There are 63 managed slopes in the resort, as seen in figure 5.5, where almost 50% of them reach at least 1 km and some 8 slopes are around 2-3 km long. Similar lengths and height differences cannot be not found elsewhere in Finland. [51]

Figure 5.5: Ski resort in Ylläs

This site was selected as a fictitious case just to determine how much power it could be obtained in such a location, in case any ski resort would not exist.
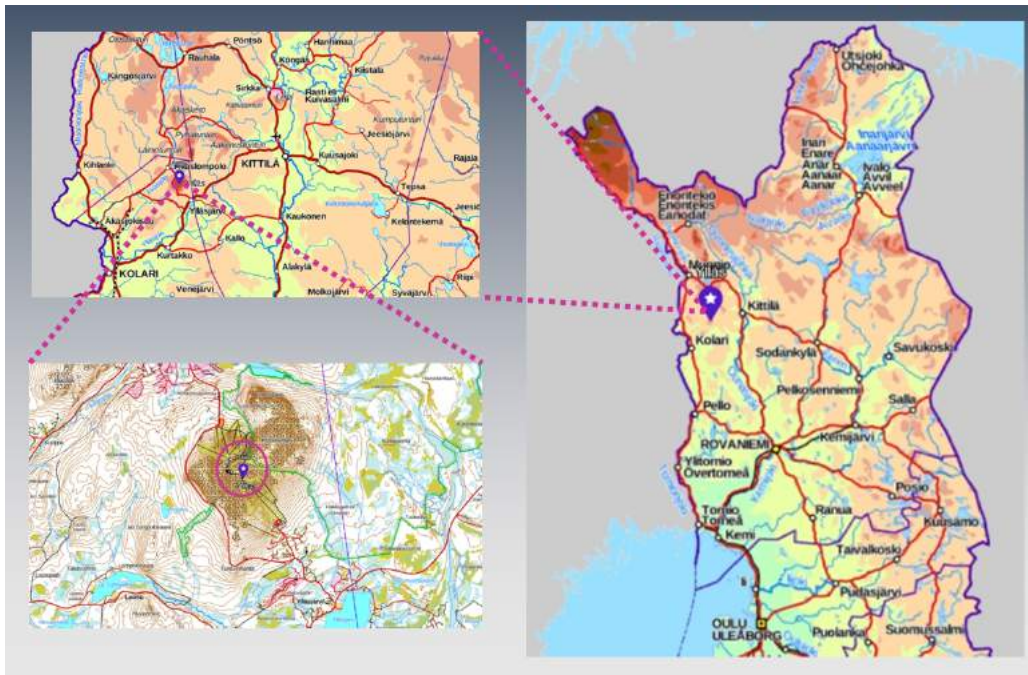
Figure 5.6: Ylläs location

5.1.4 Finlandia

The *Finlandia* wind power plant is located somewhere in the north of Finland comprising around 1,300 hectare area. Due to privacy issues, the exact location cannot be revealed in this study. The wind data utilized through this study was provided by this wind power plant.

5.2 Data treatment

Once a site is selected, some data need to be obtained before importing them into any software. Necessary inputs for the software have to be previously obtained and processed in a certain format. Some of them include topographic maps, height contours, roughness lines, met mast wind data or wind atlas, vegetation height, sensors for noise calculations, sensors for flicker calculations and turbine database.

5.2.1 Elevation

The elevation of a geographic location is its height above or below a fixed reference point. The term elevation is mainly used when referring to points on the Earth's surface. A topographical map containing the height contours of a site located in Finland can be obtained in the National Land Survey of Finland (NLS) website [52]. The case area needs to be selected in the map, and when zoomed in, the map

gets divided into quadrants, using the *ETRS-TM35FIN* coordinate system, where the sectors needed can be selected. An elevation model of 10m was chosen, and it can be downloaded in the *.ASCII Grid* format.

5.2.2   Topographic map

A topographic map is a type of map characterized by large-scale detail and quantitative representation of relief, usually using contour lines. Traditionally, a topographic map shows both natural and man-made features. For a Finnish region, this map can be obtained as well from the NLS website, by selecting the topographic map option, which can provide two different map scales, 1:100,000 and 1:250,000. Two files are downloaded with the extensions *.png* and *.pgw*.

5.2.3   Roughness

Surface roughness is a component of surface texture, quantified by the deviations in the direction of the normal vector of a real surface from its ideal form. If these deviations are large, the surface is rough but when they are small, the surface is smooth. Roughness plays an important role in determining how a real object will interact with its environment (see more details at section 2.2 on page 14). In the Finnish Environmental Institute website *SYKE*, it is possible to download maps for the spatial environment, in this case, *"Maanpeite"* (ground cover) has to be selected. It contains information of the cartography Corine 2018 that responds to the latest pan-European terrestrial land-use coverage coordinated through the European Environment Agency and aimed at identifying priority areas to protect ecosystems and natural resources. When the download is completed, a series of files are transferred but only the file in the extension *.tif* called *Clc2018_Fl20m_laatikko.tif* with 20m resolution data is needed. [53]

Global Mapper is the software used for transforming maps. For the roughness grid, the previously *.tif* file has to be selected, so that a roughness grid from the land cover layer is created. The Clc map can contain a very large area for a site. For roughness, the recommended area to choose is 10 to 15km away from the site in each direction. Before running the roughness raster layer calculation based on the Etha Roughness Length table, one can specify bounds or enter coordinates. As a result, the raster layer calculation is only done for the chosen area, and a raster layer for the colors that are identified in the map is created. This new file is saved in the *.asc* format.

Finally, the roughness raster layer previously prepared is placed in Global Mapper. It is necessary to "Create area features from equal values", in order to convert the current raster layer to the polygon layer according to the roughness lengths placed in the grid data. The resulting layer is then exported as a *shapefile* format.

In **WindPRO** it is possible to obtain a roughness map based on closed lines online. The area types needs to be specified one by one, making sure that the introduced

values correspond to the *roughness length* and not the *roughness class*, as seen in figure 5.7. Also, a background area type with a value of 0.7 [3] needs to be created.
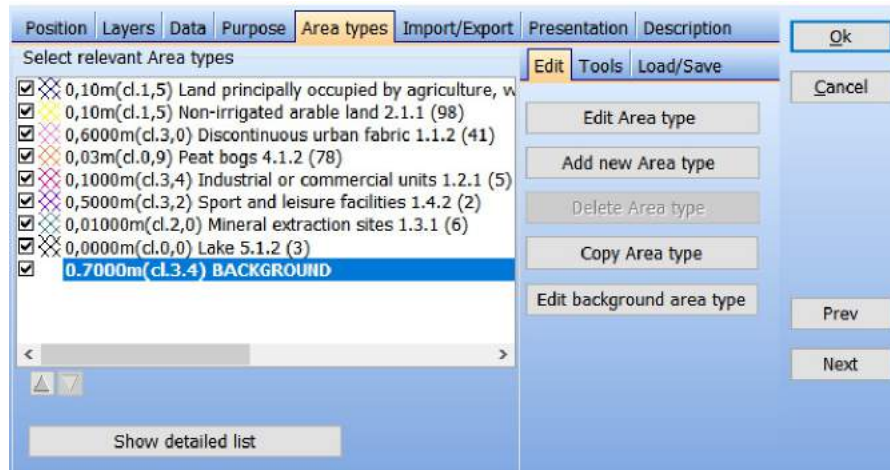

Figure 5.7: Selection of roughness lengths and classes in WindPRO

In **WindSim** the roughness comes together with the elevation in the *.wgs* file, which can be previously prepared in global mapper. A picture of the roughness generated in the software is shown in figure 5.8a.

In **Zephy TOOLS** the roughness needs to be imported in the software together with all the data to be used, and it has to follow the specifications explained in section 4.4.1 on page 51. An example of the visualization of the roughness areas created in this software can be observed in figure 5.8b.
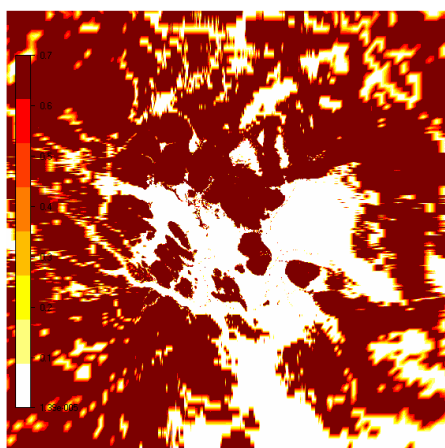
(a) Roughness map in WindSim
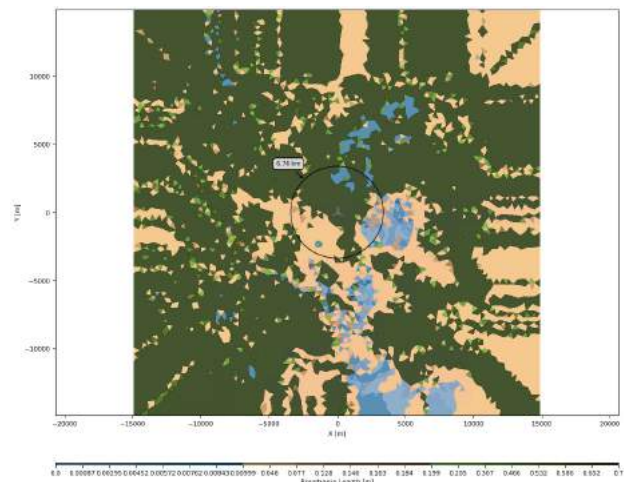
(b) Roughness map in Zephy TOOLS

Figure 5.8: Roughness maps in WindSim and Zephy TOOLS for Lokan Tekojärvi

---

[3]As an approximation, the roughness length is approximately one-tenth of the height of the surface roughness elements. For example, short grass of height 0.01m has a roughness length of approximately 0.001m. Surfaces are rougher if they have more protrusions. Forests have much larger roughness lengths than tundra, for example

5.2.4   Wind measurement and wind turbine

Information on a real site time-varying based on wind measurements for 20 years recorded information was provided by Etha Wind OY. This data was used for all the sites to get comparable results between the locations and software.

The wind turbine from Vestas V150-4.2MW, which stretches nearly a quarter of a kilometer into the air and is one of the highest producing onshore low wind turbines in the industry was selected for this project (figure 5.9). A hub height of 150m was used as well.

Figure 5.9: Vestas V150-4.2 [7]

5.3   Simulation procedure

In this section, the procedure followed in every software will be explained in detail.

5.3.1   Simulations in WindPRO

Site data

When creating a new project in WindPRO, the orography map needs to be imported and saved in a new layer, defined as *"elevation"*. Another layer can be created with the name of *"roughness"*, where the symbol *"insert area data (polygons)"* is selected and edited as seen in section 5.2.3 (see right bottom side of figure 5.10) . In the same layer, a *line object* needs to be created, with the purpose of generating roughness lines. Is important to mention that all of these layers and items are created in the *"objects"* section.
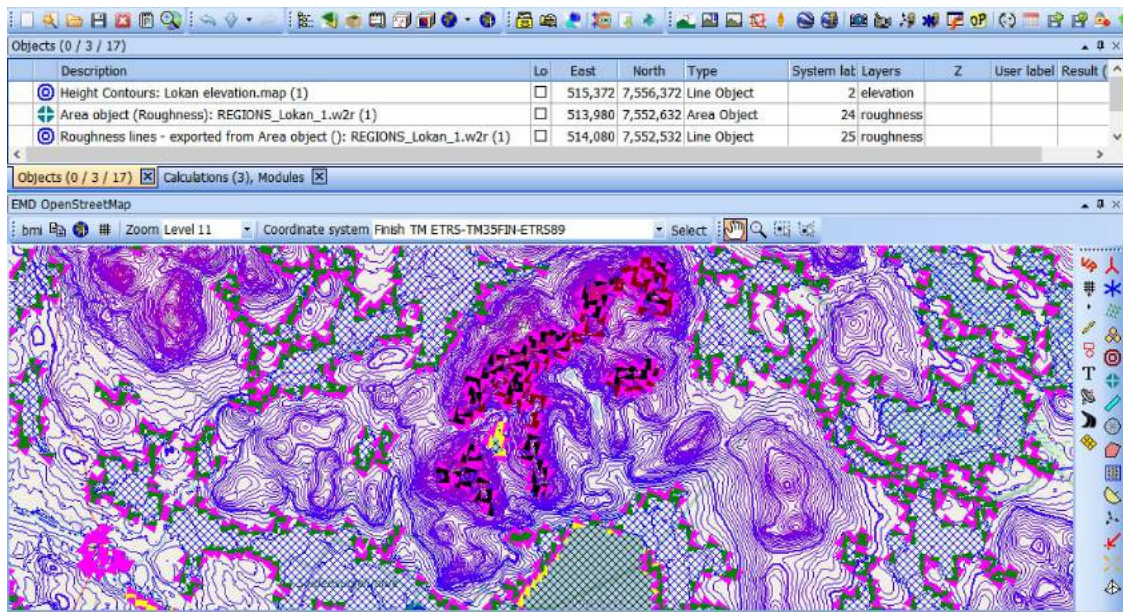
Figure 5.10: Elevation and roughness in WindPRO for Lokan Tekojärvi

Sitting of turbines

Wind Turbine Generators can be either imported as a shapefile or placed one by one. WindPRO contains an extensive list of the most common wind turbines types, containing the power curves, cut in and cut out wind speeds, power control, etc. The hub height needs to be defined by the user.
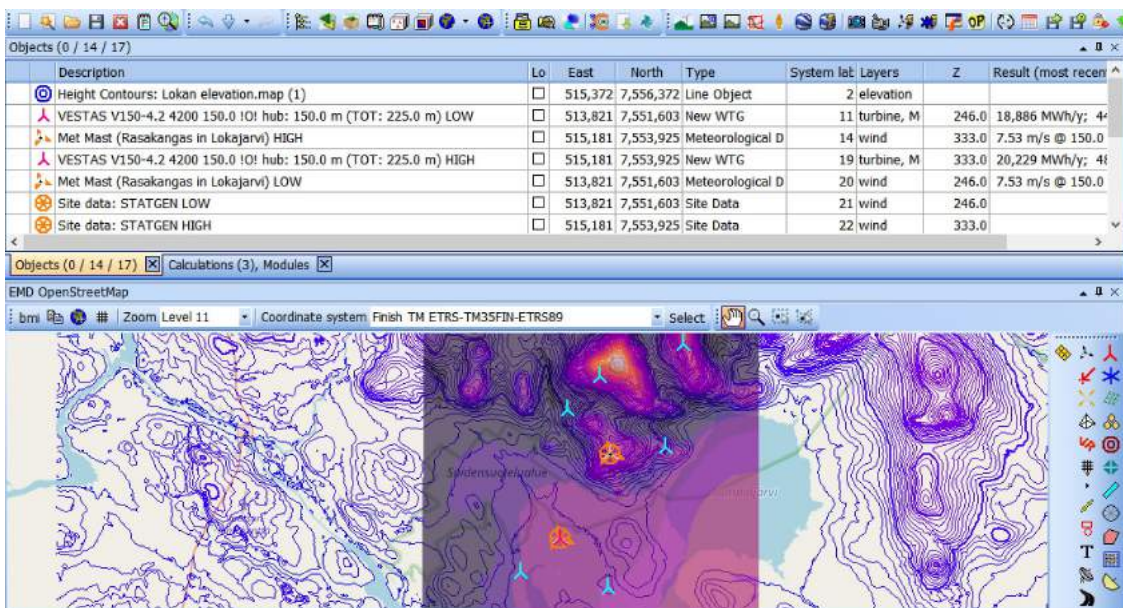

Figure 5.11: Placement of turbines and met masts in WindPRO for Lokan Tekojärvi

Wind data

In the wind data layer, the meteorological data can be imported. Generally, the data used consists of on-site measurements from met masts, which are frequently shorter than the hub height. In order to have more accurate results, the user has to specify in WindPRO the height [m] of the wind data measurements to be the same as the hub height to be simulated (also the displacement height, if considered), so that an extrapolation of the data is performed and more precise results can be obtained. Also two more objects need to be introduced in this layer by selecting the symbol *"insert site data (for energy calculations)"*. One will be use for *STATGEN* (generation of wind statistics) and the other for *RESGEN* (calculation of wind energy resources), as seen in figure 5.12.

Figure 5.12: Climatology options in WindPRO

Calculations and results

Once all the objects are created, the calculations can be executed. For a start, the *STATGEN* calculation can be selected. Subsequently, the *PARK* calculation will provide information about the production analysis, the wind curve analysis, the wind data analysis, the wind turbines distances, the time varying AEP, the scaling info and the map. In this section, the climatology needs to be selected, either as a wind statistic based calculation or as time series depending on the type of information available. Then, the WTGs have to be selected as well as the met mast with its corresponding heights. Finally, the *RESOURCE* module will generate a map in the area of study, where it can be displayed parameters such as the mean wind speed [m/s], specific energy [$kWh/m^2/year$], specific wind energy [W/m^2], WTG production [$MWh/year$], height above sea level [m] and specific WTG production [$kWh/m^2/year$]. It can show both a 2D and 3D map of the place including the wind turbines and met masts, such as the ones in figures 6.4, 6.7 and 6.2.

Figure 5.13 provides an overview over the logical sequence of the simulation process described in the above sections, from preparation to simulation in WindPRO. The diagram on the left applies for the other software as well.
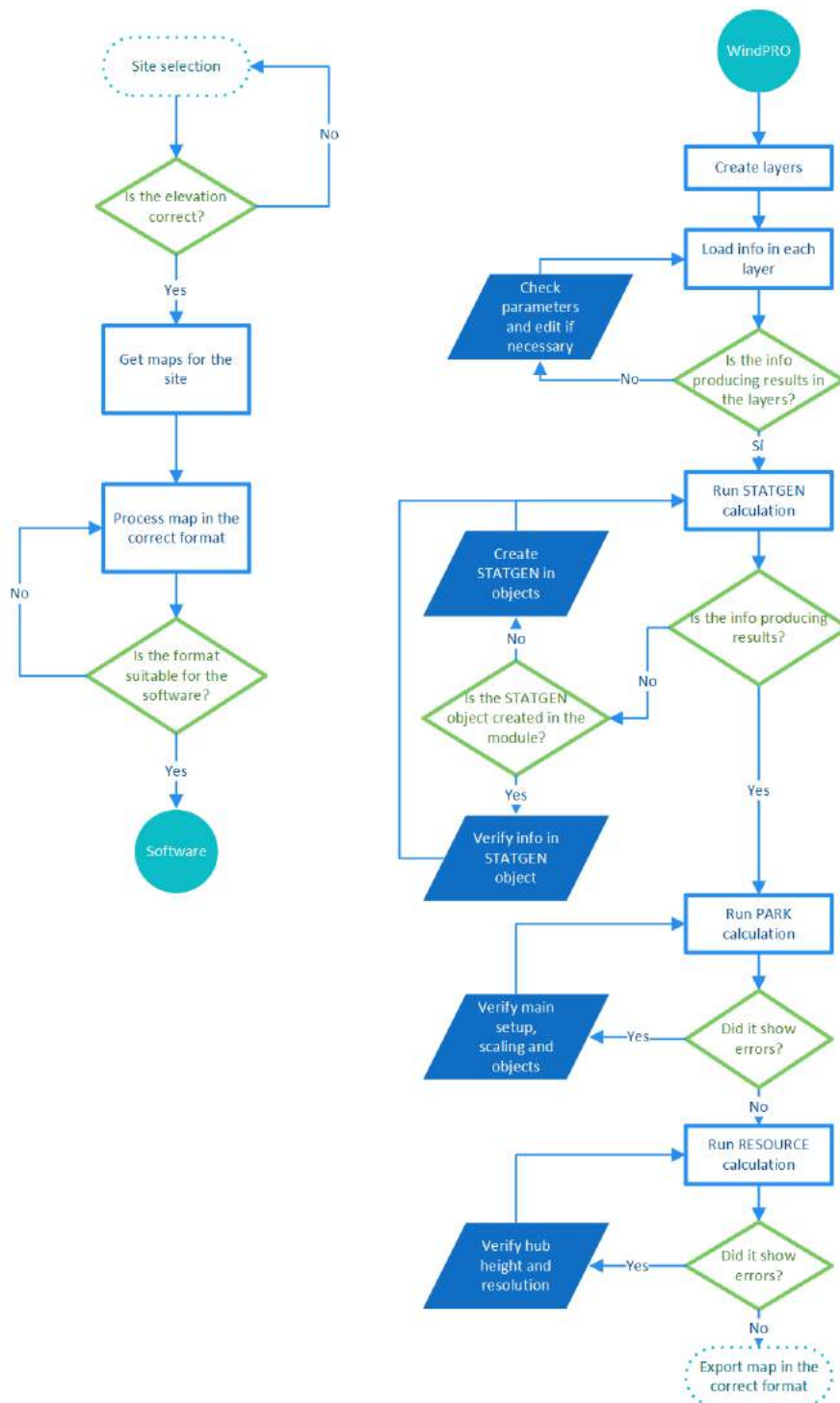
Figure 5.13: Methodology followed to get wind maps in WindPRO

5.3.2   Simulations in WindSim

Terrain

Once the file with the roughness and elevation is uploaded, the properties of the terrain can be selected. It is possible to specify whether there will be a refinement area or not by writing the coordinates. Also the maximum number of cells to be calculated. Equation (5.1) shows how the maximum number of cells are determined.

$$n_x n_y n_z \leq n_{max} \tag{5.1}$$

Particular consideration has to be addressed, being in the first place that the time of the simulation is exponentially proportional to the number of cells. Secondly, as the grid consists of numerous diminutive cubes with a certain length in both x and y direction and a certain height in z direction, then the area in the conversion of the *.map* file into *.gws* format has to be chosen as a square, so that x and y would be relatively equal in size. The number of cells in z direction should be picked so that the three dimensional cell is as close to a unit cube, e.g. with $x = y = z$. Indeed, the ratio between the length and the height of the cube shall nevermore outpace 10 to complete the simulation without divergence. For this study, 5 million cells were selected. [14]

Last but not least, the forest needs to be set up, adding the roughness height of 0.7 (corresponding to the background area type defined for windPRO in section 5.2.3).

Wind fields

This is the most time-consuming module in WindSim, so it is crucial to select the correct parameters for the calculations from the beginning. In the boundary and initial conditions, WindSim selects 12 uniform angle sectors as a default and the right of the boundary layer needs to be specified. In the physical model, the potential temperature can be selected. The *Monin-Obukhov length* was used for these calculations. The reference temperature is 288 as a default. The wind speed in reference height is obtained from WindPRO, as well as the density value after the PARK calculation. For the turbulence model, the *RNG k-ϵ* was used. Finally, in the calculation parameters it is necessary to select the number of iterations. In this case, the more iterations, the more computational time required but the better convergence.

Objects

In the park layout it is possible to position turbines, climatologies and transferred climatologies. For the turbines, the power curve, the hub height and the rotor diameter have to be specified, as well of the coordinates for each of them. For the climatology, the file in the *.tws* format is selected. After running the module, the park layout with the objects can be visualized, as in figure 5.14 for Lokan Tekojärvi.
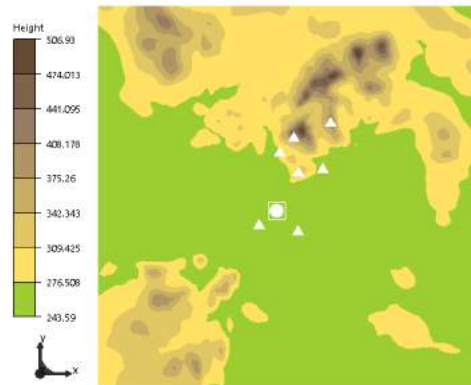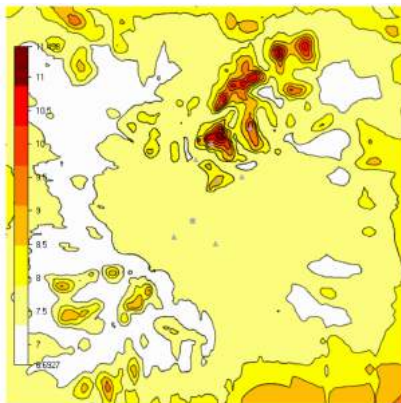

Figure 5.14: WindSim objects

Wind resources

In this module, the *wake model 1* was selected and the air density will be the same as in the wind fields. The results can be exported in both the *ASCII* format and the *WAsP* format as *.rsf* or *.wrg*. A visualization for Lokan Tekojärvi wind resources generated by WindSim can be seen in figure 5.15.

Figure 5.15: WindSim wind resources

Energy

Finally, in the energy module (displayed in figure 5.16) the Annual Energy Production can be calculated, based on the power curve for each turbine and the speed-up adjusted climatology.

Figure 5.17 provides an overview over the logical sequence of the simulation process described in the above sections, from preparation to simulation in WindSim.
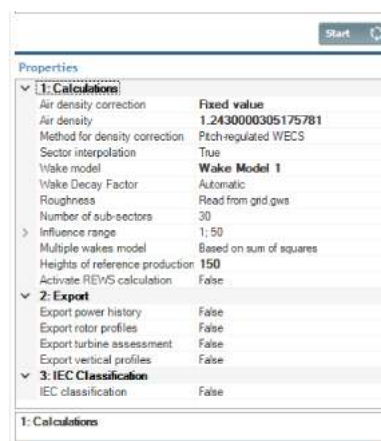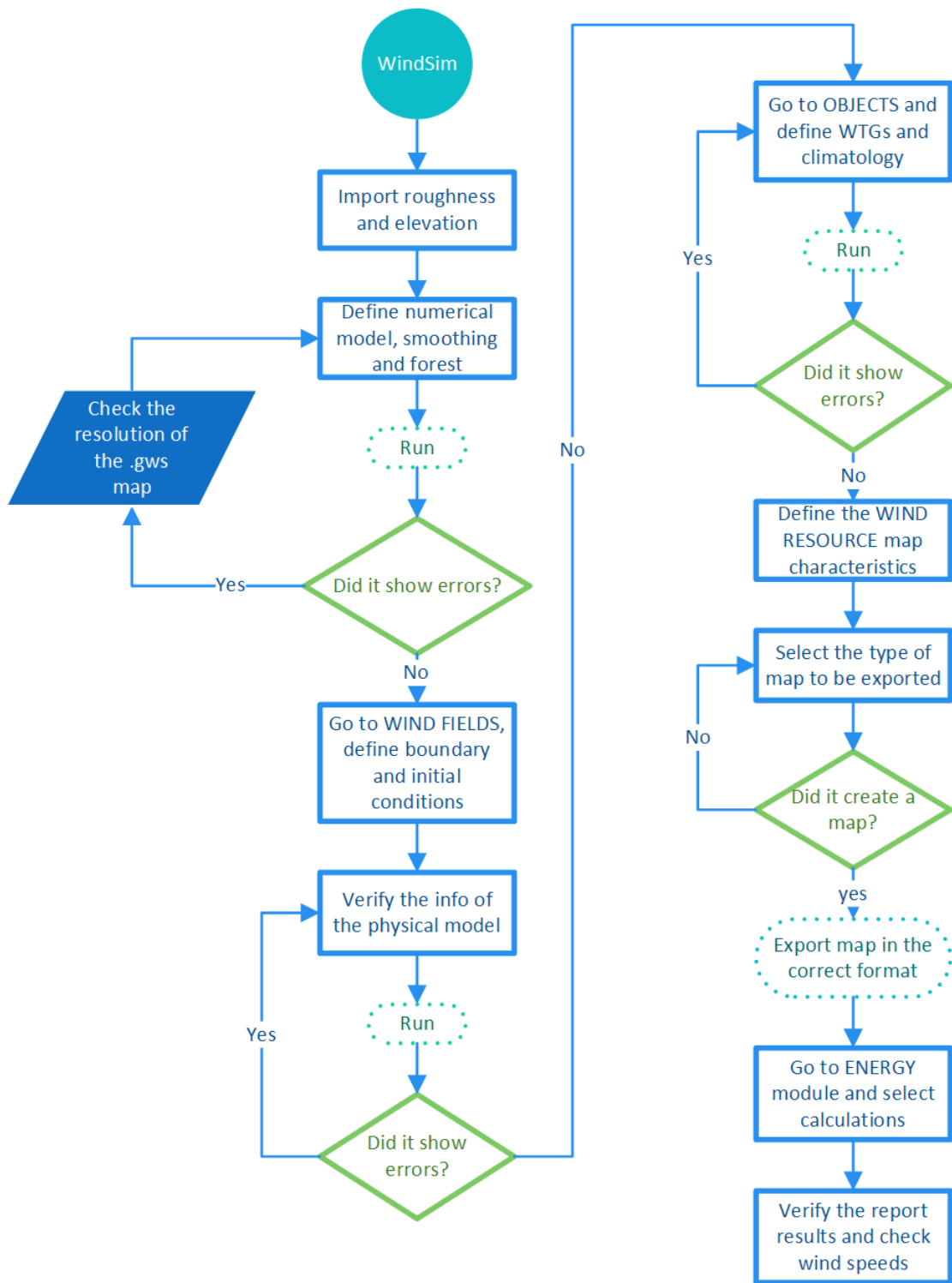

Figure 5.16: WindSim energy module

Figure 5.17: Methodology followed to get wind maps in WindSim

5.3.3 Simulations in Zephy TOOLS

Main menu and input files

To access to the Zephy TOOLS work space, it is necessary to log in with the user name and password provided by the software. Then, before starting any new project, all the data to be used need to be uploaded in the *"input files"* section, seen in figure 5.18

Figure 5.18: Main menu for importing new files in Zephy TOOLS

Afterwards, the documentation can be imported, selecting either one by one or a single file containing all the files in the format *.zsmulti*.

Load

Once loaded all the data, the user verifies that all the files are visible in the main page. If so, now the *LOAD* bottom can be clicked. For this and all the subsequent modules, the *number of processors* of the machine needs to be specified and the *queue* option will be selected. If the information is correct, the software will produce a visual map of orography and elevation including the met masts and the turbines used, such as the one in figure 5.19 for Korpinen.
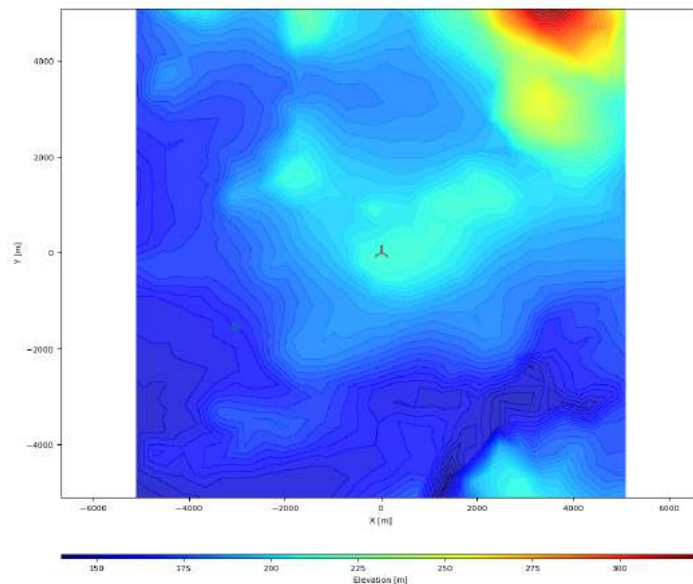

Figure 5.19: Orography map in Zephy TOOLS

Analyze and mesh modules

In the *ANALIZE* module, the parameter *zs* is given by default, and it is possible to select the climatology in case the RIX index should be evaluated. After analyzing the terrain, the software will calculate the complexity of the terrain with a *ZIX* value, as seen in figure 5.20.
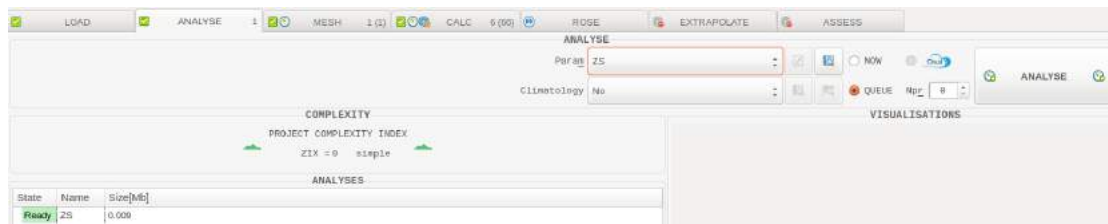

Figure 5.20: Analyze module in Zephy TOOLS

Subsequently, in the *MESH* module a fine or a coarse mesh can be selected, considering 180 or 72 directions, respectively. An estimation of the number of cells for each mesh can be previously calculated, as seen in figure 5.21.

Figure 5.21: Mesh module in Zephy TOOLS

Calculate and rose modules

Once the mesh is created, the calculations for the wind rose can be performed. This is the most time-consuming module in Zephy TOOLS, so it is crucial to select the correct parameters for the calculations from the beginning. Firstly, the type of mesh has to be selected in order to set the wind directions to be calculated. It is possible to select a *rose* direction, considering all the sectors of the map, but a longer computing time will be required. It is recommended to select every 2 degrees for super-prevalent directions; every 4 degrees for prevalent directions and every 10 degrees for non-prevalent directions and this has to be selected one by one in the set list menu. Then the calculation is ready to start, as seen in figure 5.22.
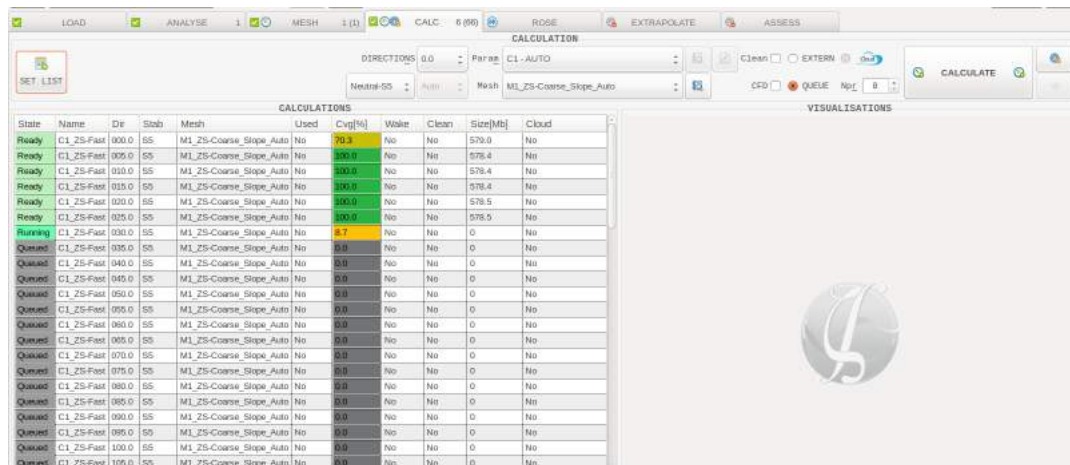
Figure 5.22: Calculation module in Zephy TOOLS

When the calculations are ready, in the *ROSE* module it is possible to select the met mast, the reference height and the calculations previously obtained (figure 5.23). 5 kinds of visualizations can be obtained, either in the rose shape or as a chart for the horizontal speed-up, the TI variation, direction variation, flow inclination and turbulence intensity.
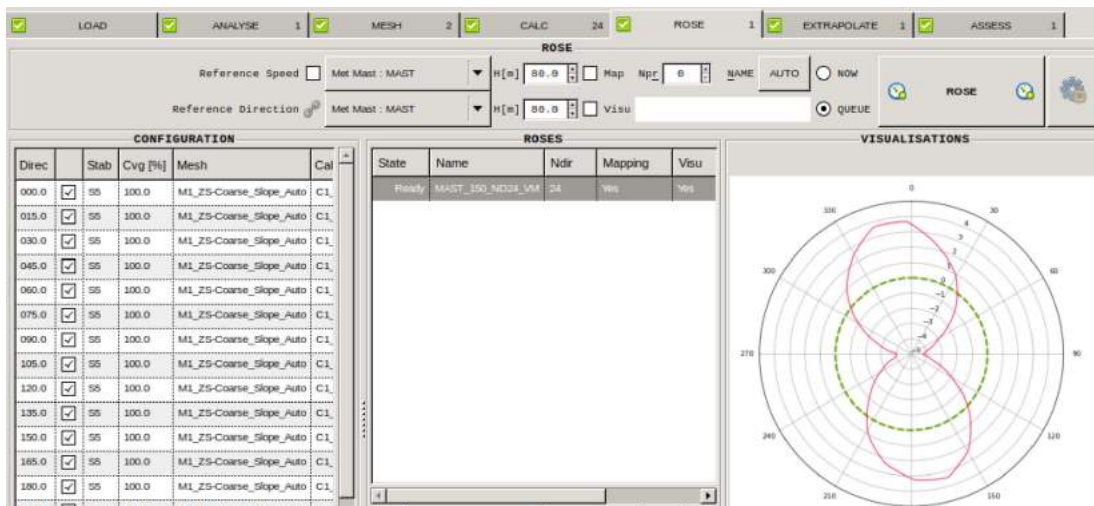

Figure 5.23: Rose module in Zephy TOOLS

Extrapolate and assess

In *EXTRAPOLATE*, seven different visual maps can be generated with the rose information previously calculated as well as the information of the climatology (figure 5.24).
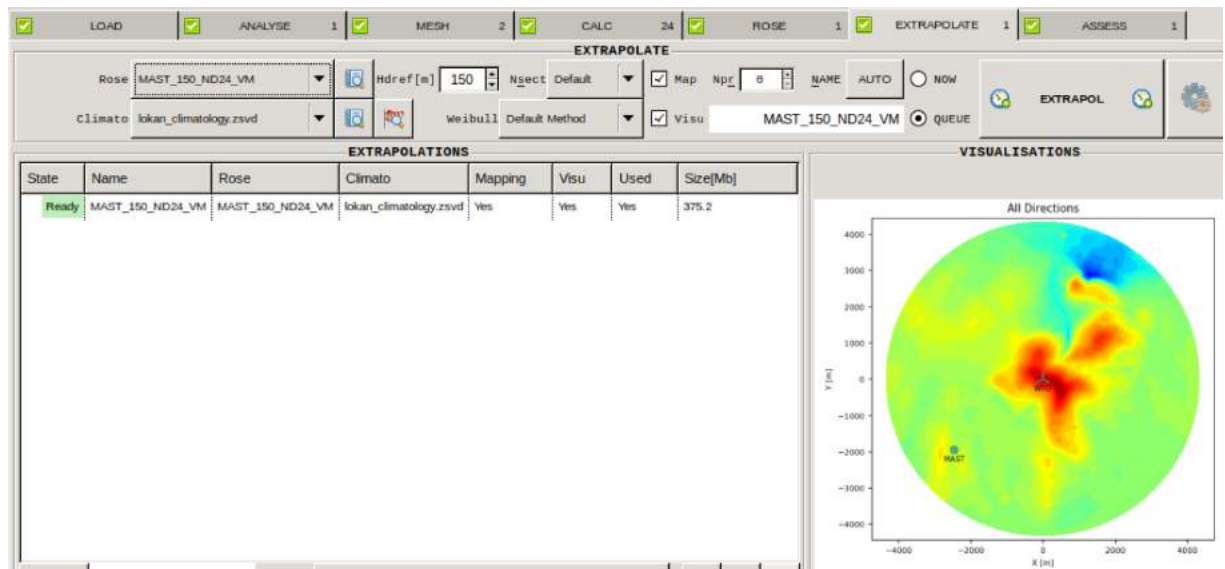
Figure 5.24: Extrapolate module in Zephy TOOLS

Finally, in the *ASSESS* module, it is possible to get in a *.csv* file all the numerical information about the wind farm, including:

- Information for each wind turbine:

  - Elevation/hub height [m]
  - Free and waked mean wind speed [m/s]
  - Wake loss [%]
  - Capacity Factor

  - Power Density [W/m^2]
  - Average and maximum shear
  - Direction of maximum shear [°]
  - Air density [kg/m^3]
  - Weibull A [m/s] and k

- Information about turbine-wise uncertainties and productions:

  - Gross, array and net production [$MWh/year$]
  - Nearest reference horizontal distance [km]
  - Nearest reference vertical distance [m]

  - Model extrapolation uncertainty (Base) [%]
  - Model extrapolation uncertainty (Add) [%]
  - Total uncertainty [%]

- Information about input losses and uncertainties:

  - Future uncertainty [%]
  - Total uncertainty [%]
  - P50 production [$MWh/year$]

  - P75 production [$MWh/year$]
  - P90 production [$MWh/year$]
  - P95 production [$MWh/year$]

Figure 5.25 provides an overview over the logical sequence of the simulation process described in the above sections, from preparation to simulation in Zephy TOOLS.
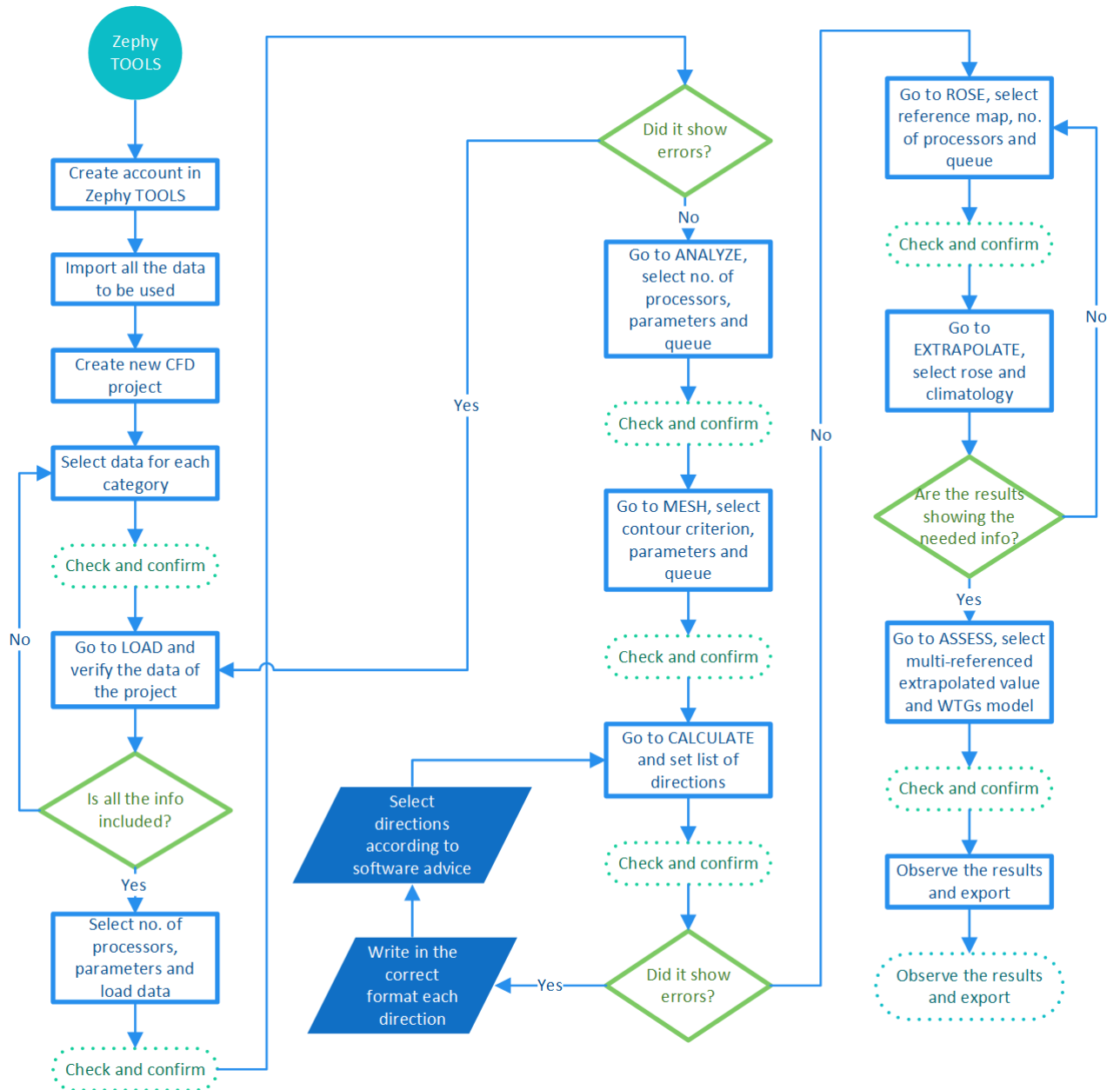
Figure 5.25: Methodology followed to get wind maps in Zephy TOOLS

Chapter 6

Results analysis

6.1 Results of WindPRO

6.1.1 Korpinen

In the case of Korpinen, two wind turbines were placed in the terrain, displayed in figure 6.1, in order to measure exactly the wind speed at both positions. The main result is based on the met mast located in the Southern location, in this case where the turbine 2 is located. An average wind speed of $7.5m/s$ was registered for the site as well as an average density of $1.24kg/m^3$.
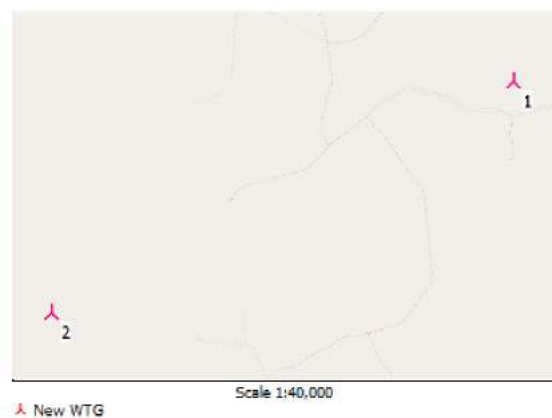

Figure 6.1: Location of wind turbines in Korpinen

In figure 6.2, a 3D map for the elevation of the terrain was created in WindPRO, and the colors of the surface represent the wind speeds obtained for each location. A height difference of 50m separate each of the turbines, defining this site as with a quite gentle slope. From this map, it can be seen that the position of the objects register the highest wind speed for this area, which can be suitable for the development of a wind farm in such location.
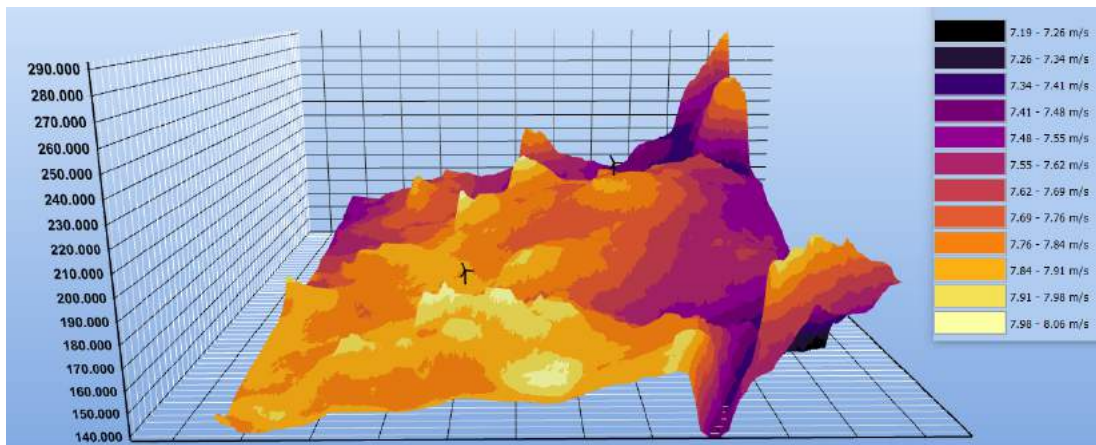
Figure 6.2: 3D map of the elevation and wind speeds in Korpinen

6.1.2 Lokan Tekojärvi

The same principle was applied to Lokan Tekojärvi, which shows two wind turbines placed in the terrain, as shown in figure 6.3. The met mast was placed in the location of wind turbine number 1. An average wind speed of $7.66m/s$ was registered for the site as well as an average density of $1.237kg/m^3$.
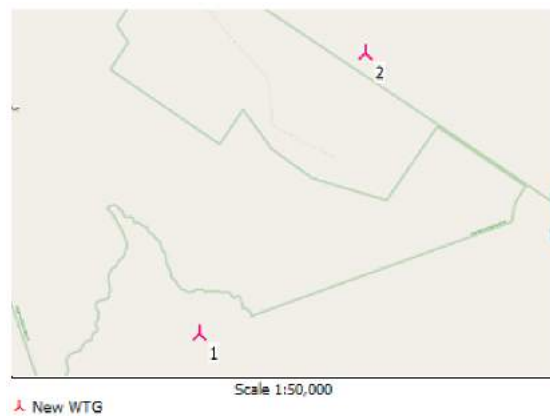

Figure 6.3: Location of two wind turbines in Lokan Tekojärvi

In figure 6.4, a 3D map for the elevation of the terrain was generated in WindPRO, where the colors of the surface depict the wind speeds obtained for each location. A height difference of 87m separate each of the turbines, defining this site as with a moderate slope. From this map, it can be seen that the met mast is positioned on a flat terrain, while the wind turbine is in the top of the hill, which registers high wind speeds of around $7.86m/s$.
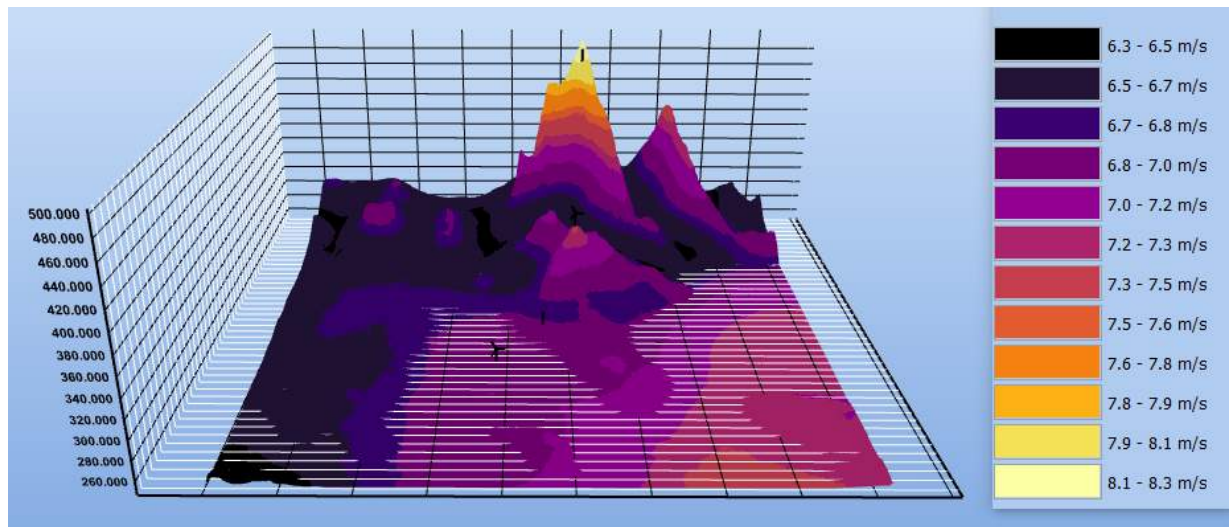
Figure 6.4: 3D map of the elevation and wind speeds in Lokan Tekojärvi

As this location contains both flat and hilly terrain, it was interesting to investigate what would be the outcome of wind speeds when many turbines are placed around the met mast, so they were placed in different terrain heights, as seen in figure 6.5, ranging from 246 to 400m above sea level. All of them registered an average wind speed of $7.55m/s$ for the area and a slightly lower density of $1.236kg/m^3$.
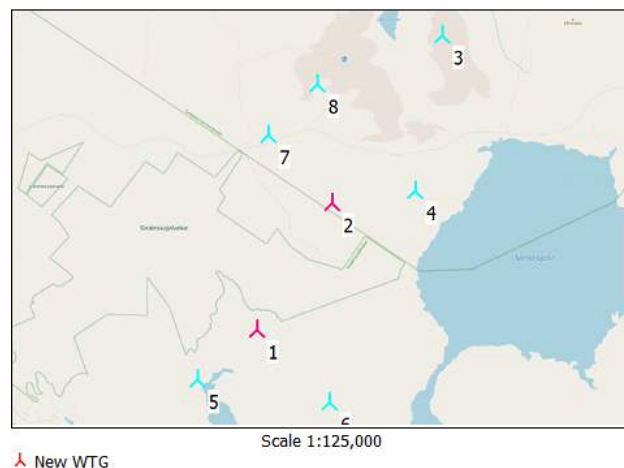

Figure 6.5: Location of several wind turbines in Lokan Tekojärvi

6.1.3 Ylläs

In the case of Ylläs, the main wind turbine to be analyzed is placed in the very top of the hill, in the position number 2 displayed in figure 6.6, while the met mast is located in the flat terrain (turbine number 1). An average wind speed of $7.89m/s$ was registered for the site as well as an average density of $1.206kg/m^3$.
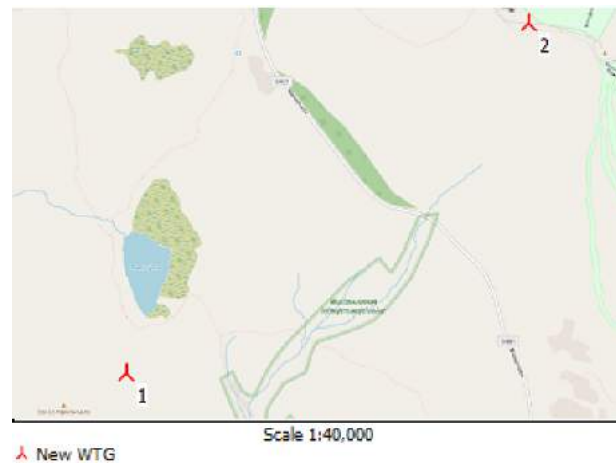
Figure 6.6: Location of wind turbines in Ylläs

A 3D map of the terrain in Ylläs is shown in figure 6.7, where the complexity of the terrain is evident. 387m of height difference separate both the wind turbine and the met mast. WindPRO registered wind speeds ranging from $6.71m/s$ to $9.07m/s$.
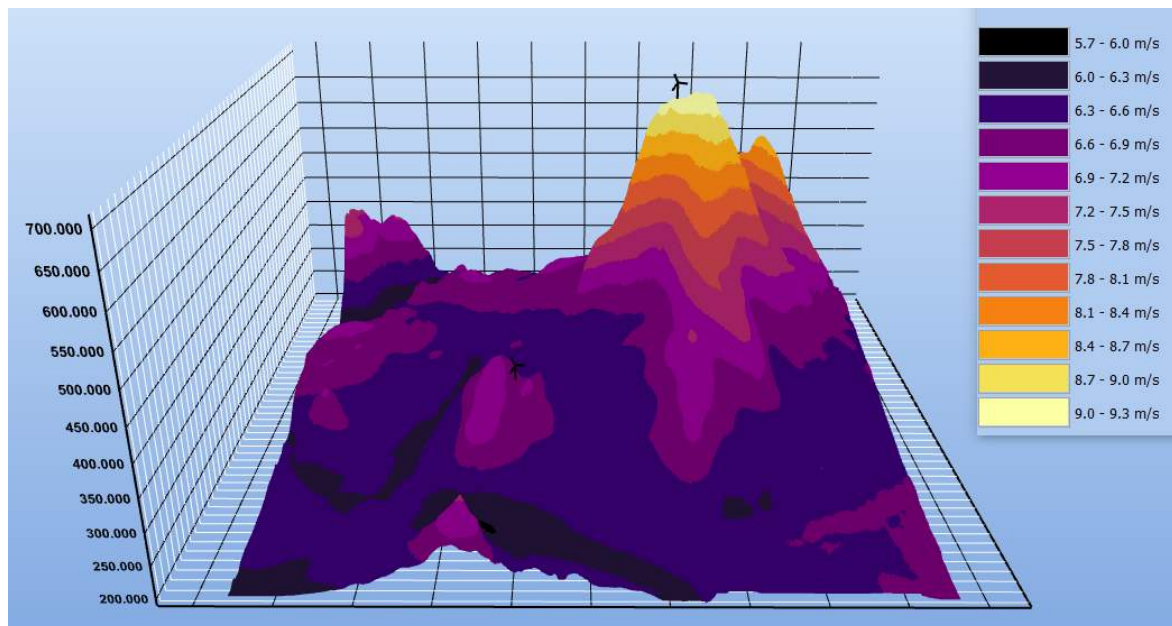

Figure 6.7: 3D map of the elevation and wind speeds in Ylläs

6.1.4 Finlandia

In the case of Finlandia, three wind turbines were located in the terrain, as seen in figure 6.8. In order to get the exact wind speed at each location, a met mast was placed in the same location as each wind turbine. The terrain is mainly flat, as only a height difference of 27m separate the wind turbines.
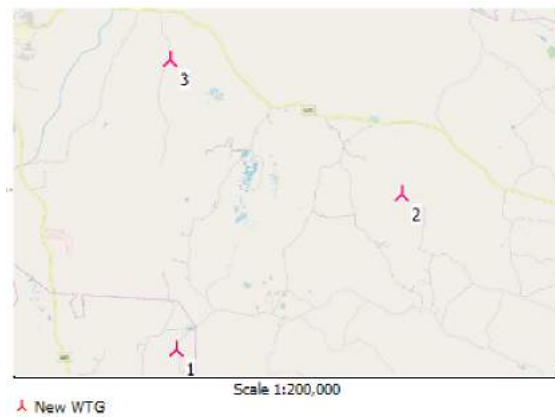
Figure 6.8: Location of wind turbines in Finlandia

Figure 6.9 shows a 3D map of Finlandia´s terrain and the surface colors reveal the wind speeds registered for the area, which range from $7.45m/s$ to $8.50m/s$. More information of the wind speeds obtained for each met mast are in table 6.1.

Figure 6.9: 3D map of the elevation and wind speeds in Finlandia
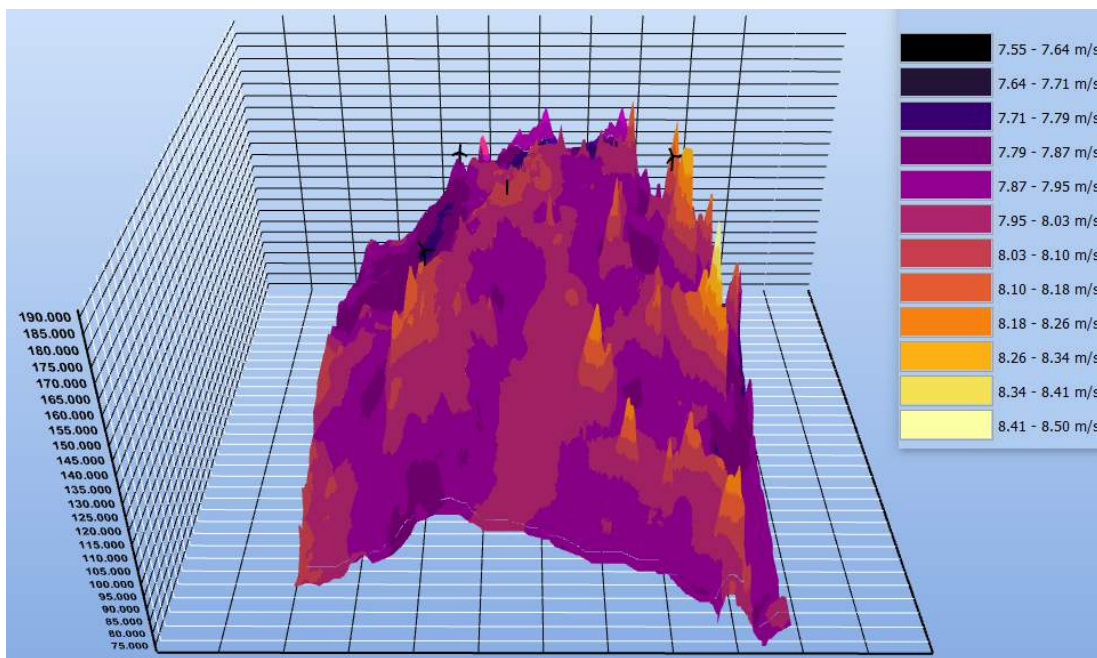
Table 6.1: Wind speed for Finlandia obtained by WindPRO

		Finlandia WindPRO			
		Real met mast	LOW	MIDDLE	HIGH
	Elevation [m]	Wind speed [m/s]			
Turbine 1	173.4	**7.58**	7.58	7.71	7.69
Turbine 2	176.9	**7.6**	7.58	7.7	7.69
Turbine 3	150	**7.45**	7.42	7.46	7.45

6.2 Results of WindSim

6.2.1 Korpinen

In the 2D model, under the terrain module, the forest was regarded by associating a baseline roughness height, as mentioned in section 5.3.2. A forest was generated at all locations with a given roughness height of $0.7m$. Figure 6.10a displays the forested areas identified by the software, where the colors in the scale show the underlying roughness height [m]. In the terrain module it is possible to visualize a variation for the digital terrain model, including the roughness height [m], where the variation in vegetation is modelled with a roughness height given on the same grid as the elevation data. The roughness height for Ylläs is presented in figure 6.10b.
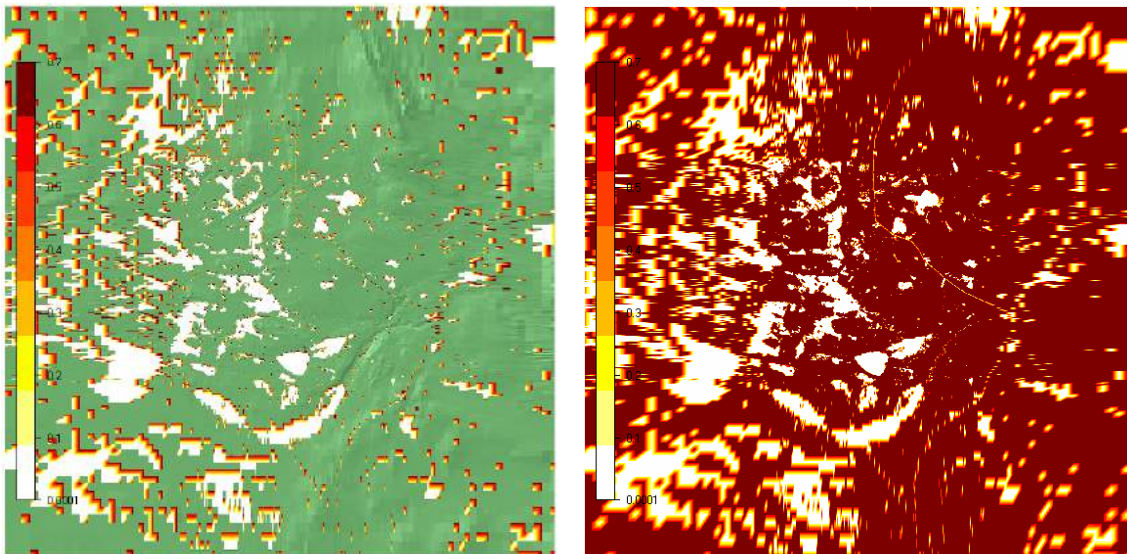
(a) Forest map   (b) Roughness height

Figure 6.10: Forest and roughness for Korpinen in WindSim

A digital terrain model of elevation was created based on the elevation and roughness data given in the initial *.gws* file grid, showing the different heights of the terrain (figure 6.11a). Also, information about the numerical grid is presented including possible blocking effects. For the digital terrain module with the refined grid, body fitted co-ordinates were used in grid generation. The following plot (figure 6.11b) displays the resolution at ground level, using a total number of cells of 4,998,380.
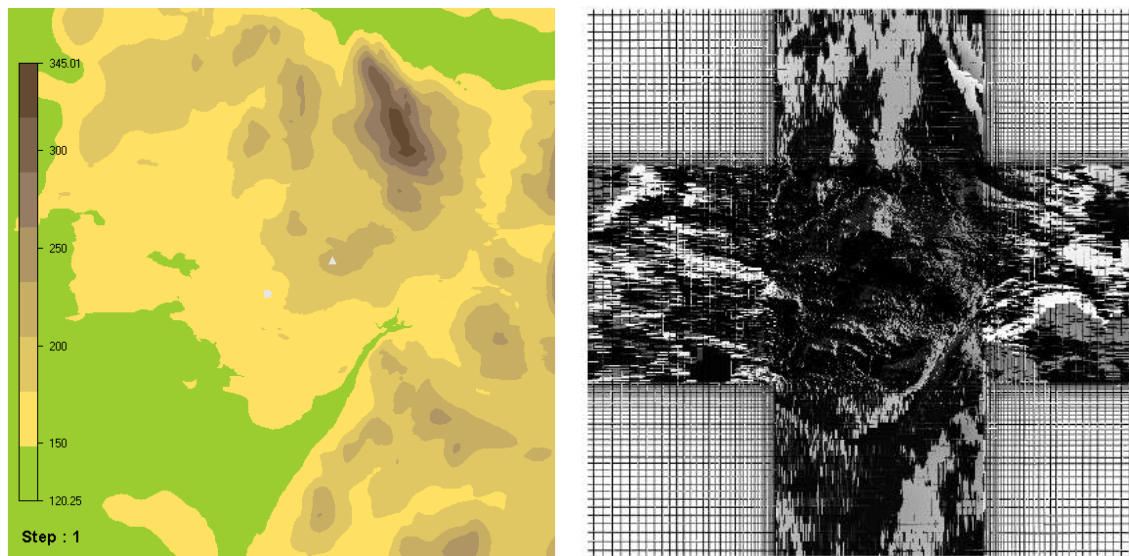
(a) Orography map

(b) Refinement area

Figure 6.11: Terrain and refinement area for Korpinen in WindSim

Based on the generation of the 3D model in the preceding terrain module, the simulation of the wind fields started. The wind fields were determined by solving the RANS equations, applying the standard $k - \epsilon$ model as turbulence closure. Since the equations are non-linear, the solution procedure is iterative. Starting with the initial conditions, which were guessed estimations, the solution was progressively resolved by iteration until a converged solution was achieved. Figure 6.13a shows the mean wind speed applied for all the terrain. Figure 6.13b plots the power density. Figure 6.13c is the power intensity and finally figure 6.13d is the inclination angle along with derived field data. Besides, wind data from the climatology station was used in calibration of the wind resources and in the energy calculations. Figure 6.12 shows a frequency table fitted to a Weibull distribution, as well as the wind rose created for Korpinen.
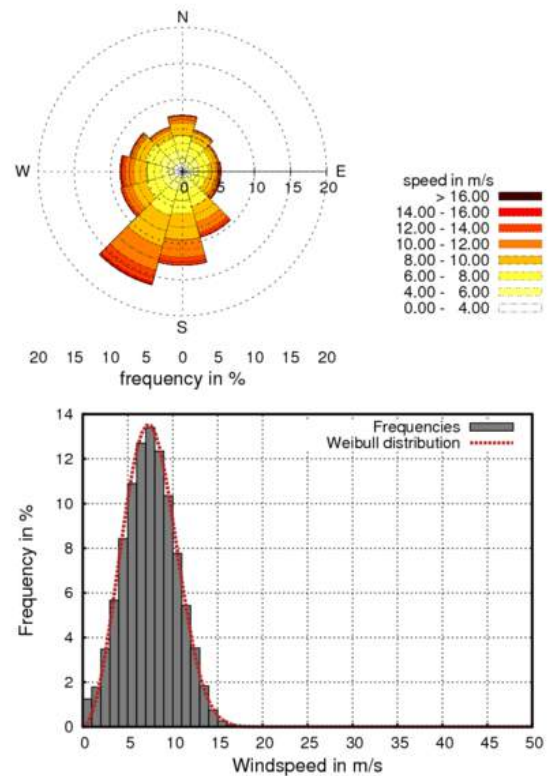

Figure 6.12: Wind statistics Korpinen

(a) Mean wind speed [m/s]

(b) Power density [W/m^2]

(c) Turbulent Intensity

(d) Inclination angle [deg]
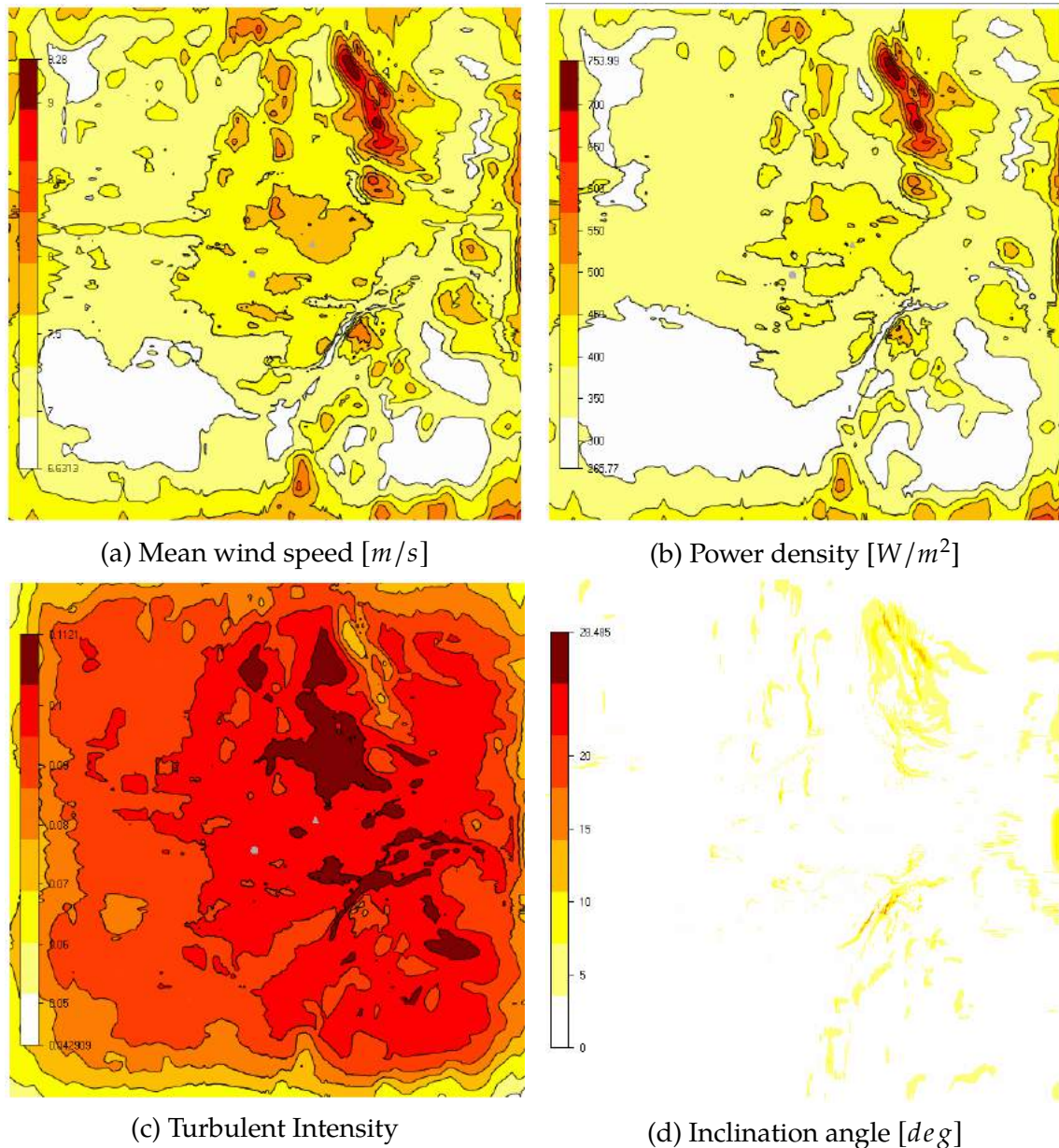
Figure 6.13: Wind resources for Korpinen in WindSim

6.2.2 Lokan Tekojärvi

In the 2D model, a forest was generated at all locations with a given roughness height of $0.7m$ (as seen in section 5.2.3). Figure 6.14a displays the forested areas identified by the software. In the terrain module it is possible to observe a variation for the digital terrain model, containing the roughness height [m], where the difference in vegetation is modelled with a roughness height given on the same grid as the elevation data. The roughness height for Lokan Tekojärvi is presented in figure 6.14b.

(a) Forest map

(b) Roughness height

Figure 6.14: Forest and roughness for Lokan Tekojärvi in WindSim
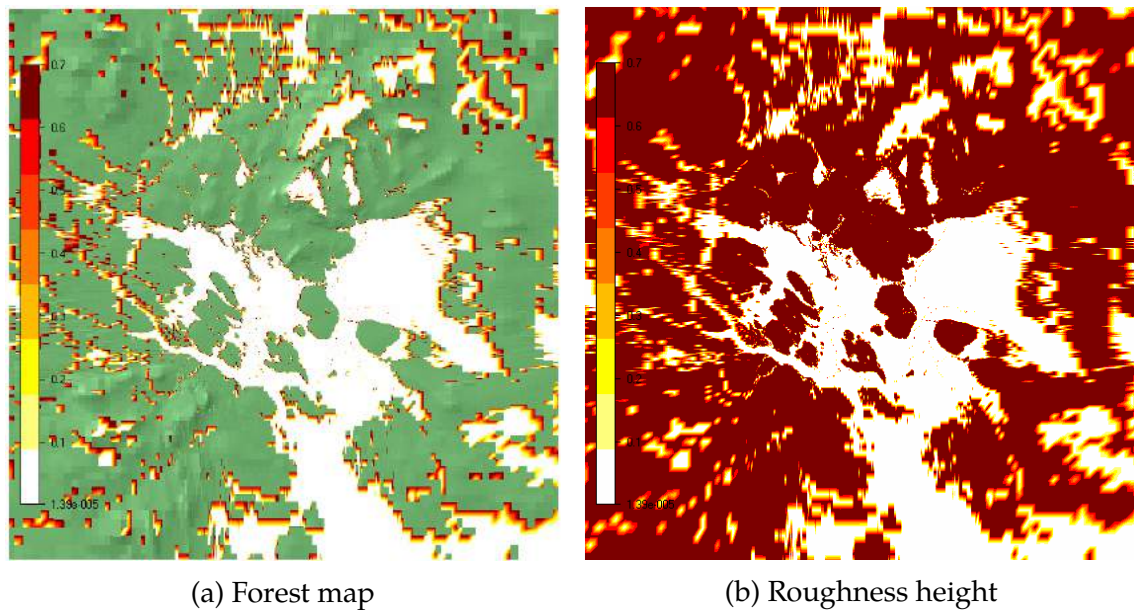
A digital terrain model of elevation was created based on the elevation and roughness data given in the initial *.gws* file grid, showing the different heights of the terrain (figure 6.15a). It can also be observed the placement of 8 wind turbine generators as well as the met mast placed in the Southern position. Both cases with a single turbine and 8 turbines were modelled in order to analyze the differences. For the digital terrain module with the refined grid, body fitted co-ordinates were used in grid generation. Figure 6.15b) shows the resolution at ground level, using a total number of cells of 4,998,380.
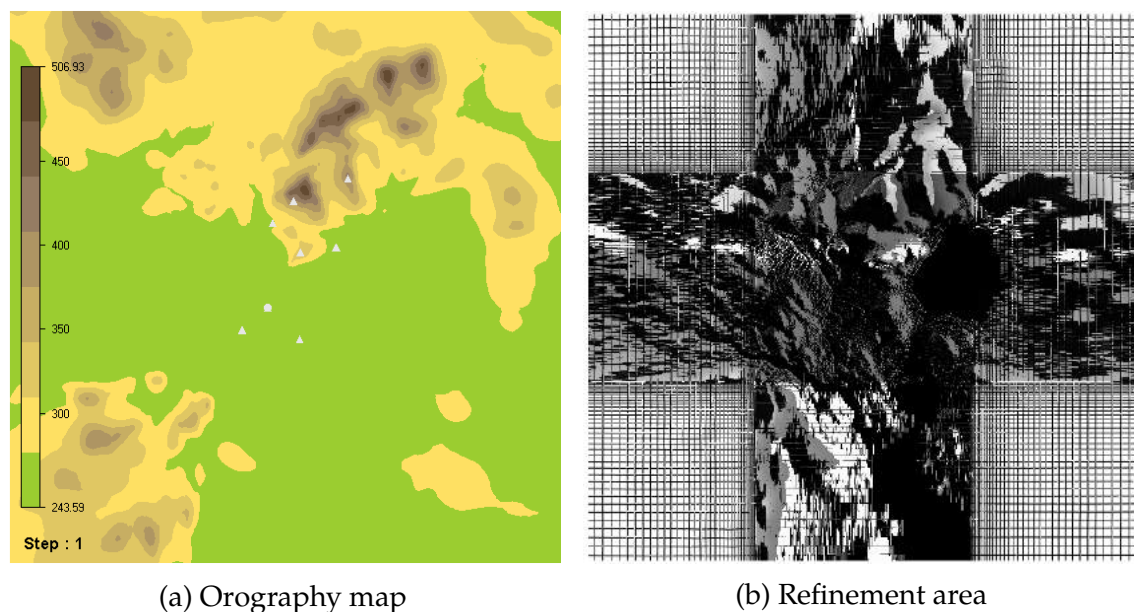

(a) Orography map

(b) Refinement area

Figure 6.15: Terrain and refinement area for Lokan Tekojärvi in WindSim

The wind fields calculations were based on the generation of the 3D model in the preceding terrain module, where such wind fields were determined by solving the RANS equations, applying the standard $k - \epsilon$ model as turbulence closure. Since the equations are non-linear, the solution procedure is iterative. Starting with the initial conditions, which were guessed estimations, the solution was progressively resolved by iteration until a converged solution was achieved. Figure 6.17a shows the mean wind speed applied for all the terrain. Figure 6.17b plots the power density. Figure 6.17c is the power intensity and lastly, figure 6.17d is the inclination angle along with derived field data. Furthermore, wind data from the climatology station was used in calibration of the wind resources and in the energy calculations. Figure 6.16 displays a frequency table fitted to a Weibull distribution, along with the wind rose created for Lokan Tekojärvi.
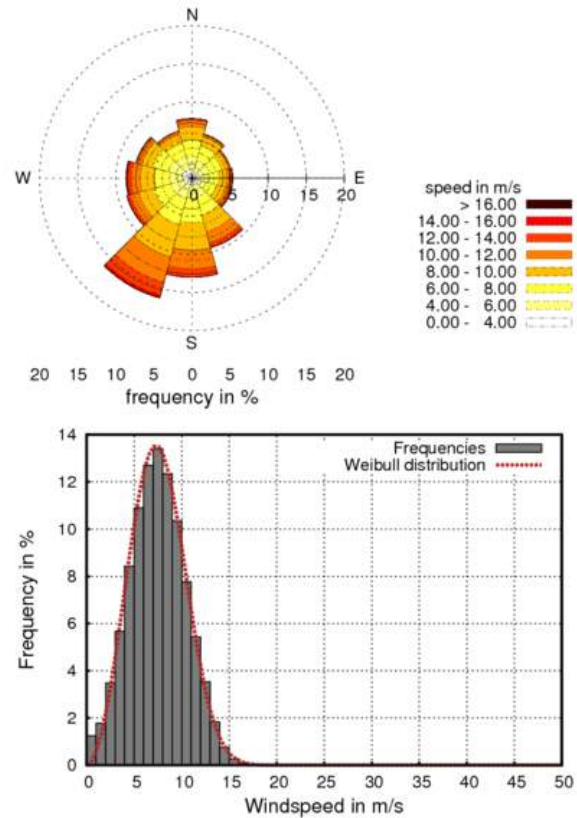

Figure 6.16: Wind statistics Lokan Tekojärvi

(a) Mean wind speed [m/s]

(b) Power density [W/m^2]

(c) Turbulent Intensity

(d) Inclination angle $[deg]$
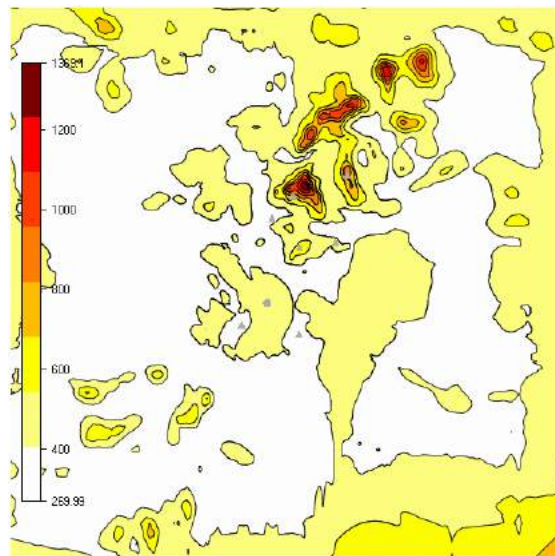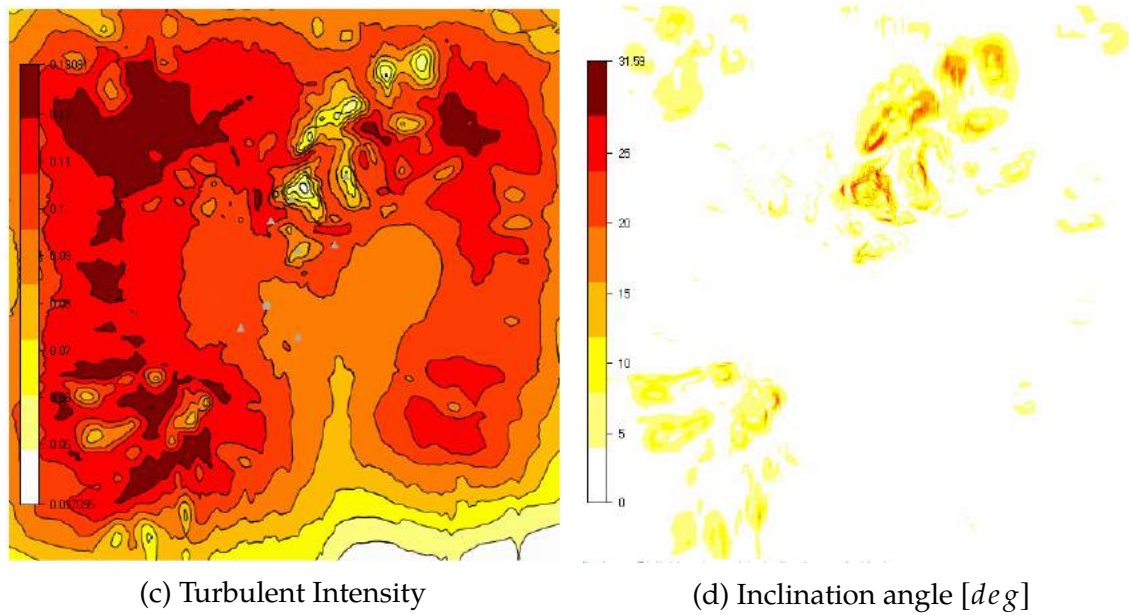
Figure 6.17: Wind resources for Lokan Tekojärvi in WindSim

6.2.3 Ylläs

In the 2D model, a forest was generated at all locations with a given roughness height of $0.7m$. Figure 6.18a displays the forested areas identified by the software. Also, a variation for the digital terrain model is shown, including the roughness height [m], where the variation in vegetation is designed with a roughness height given on the same grid as the elevation data. The roughness height for Ylläs is displayed in figure 6.18b.

(a) Forest map
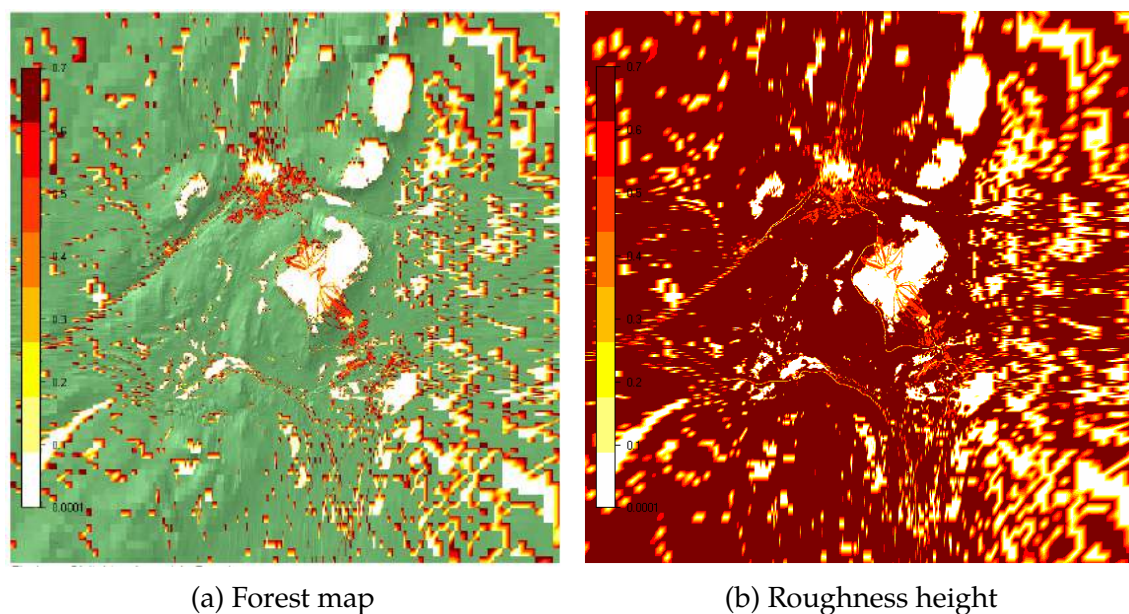
(b) Roughness height

Figure 6.18: Forest and roughness for Ylläs in WindSim

A digital terrain model of elevation was created based on the elevation and roughness data given in the initial *.gws* file grid, showing the different heights of the terrain (figure 6.19a). Figure 6.19b shows the resolution at ground level, using a total number of cells of 4,999,680.
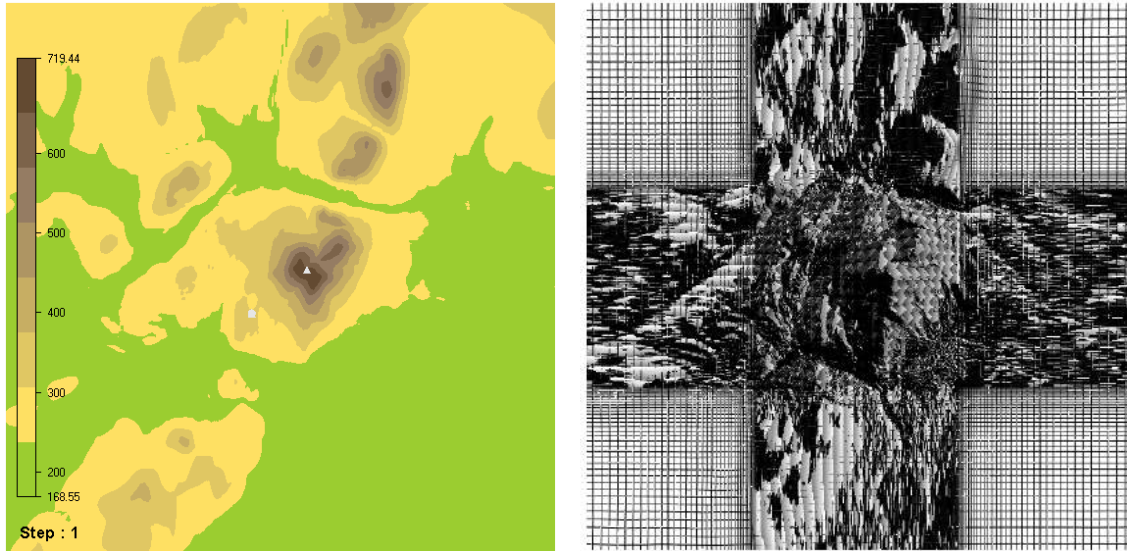
(a) Orography map

(b) Refinement area

Figure 6.19: Terrain and refinement area for Ylläs in WindSim

Figure 6.20: Wind statistics Ylläs

The wind field module is based on the generation of the 3D model in the preceding terrain module. Starting with the initial conditions, which were guessed estimations, the solution was progressively resolved by iteration until a converged solution was achieved by solving the RANS equations and applying the standard $k - \epsilon$ model as turbulence closure. Figure 6.21a shows the mean wind speed applied for all the terrain. Figure 6.21b plots the power density. Figure 6.21c is the power intensity and finally figure 6.21d is the inclination angle along with derived field data. Additionally, wind data from the climatology station was used in calibration of the wind resources and in the energy calculations. Figure 6.20 shows a frequency table fitted to a Weibull distribution, as well as the wind rose created for Ylläs.
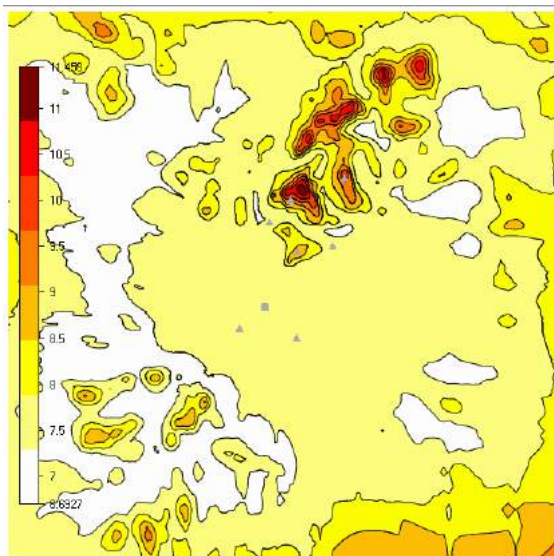
(a) Mean wind speed [m/s]

(b) Power density [W/m^2]

(c) Turbulent Intensity

(d) Inclination angle [deg]
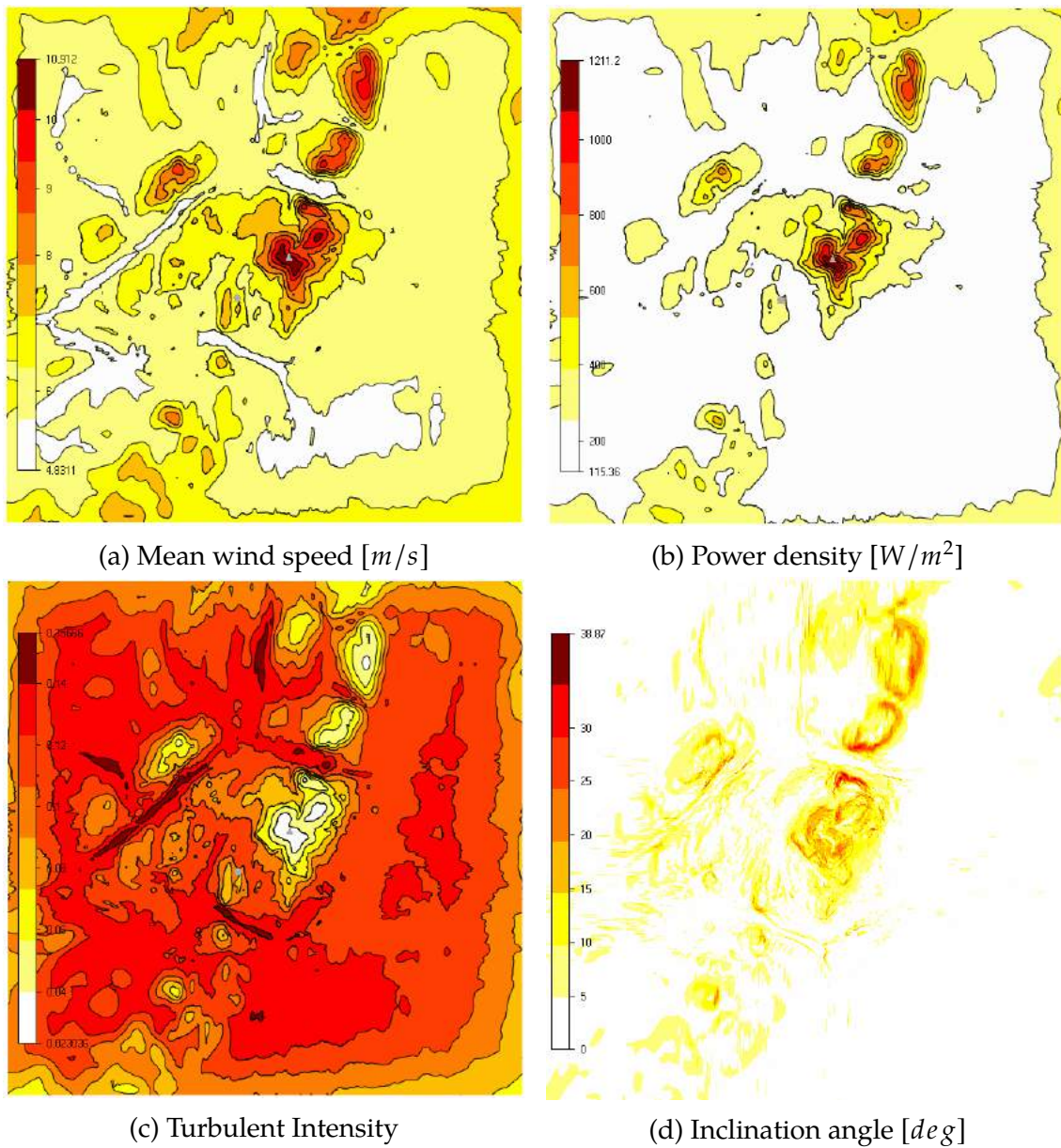
Figure 6.21: Wind resources for Ylläs in WindSim

6.2.4 Finlandia

In the 2D model, a variation for the digital terrain model is shown where the variation in vegetation is designed with a roughness height of $0.7m$ given on the same grid as the elevation data. The roughness height for Finlandia can be seen in figure 6.22.

A digital terrain model of elevation was created based on the elevation and roughness data given in the initial *.gws* file grid, showing the different heights of the terrain (figure 6.23a). Figure 6.23b) shows the resolution at ground level, using a total number of cells of 4,999,540.
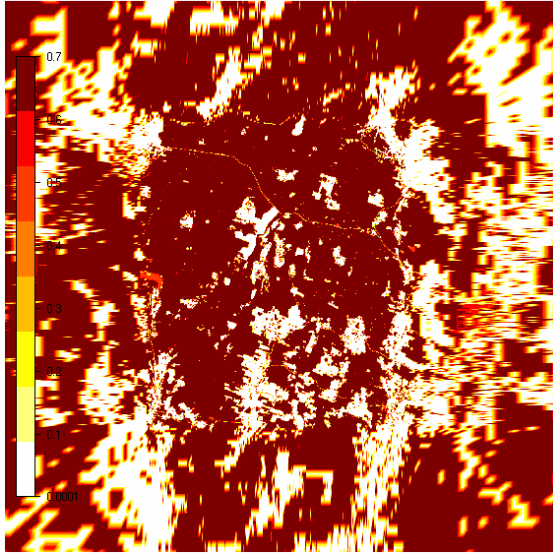
Figure 6.22: Roughness height
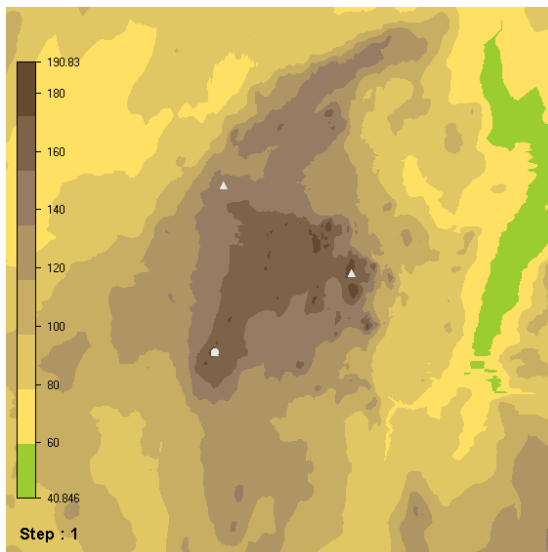
(a) Orography map
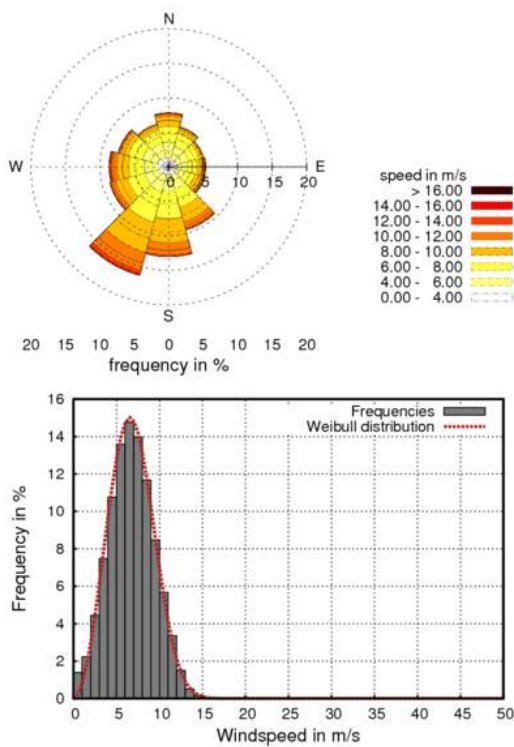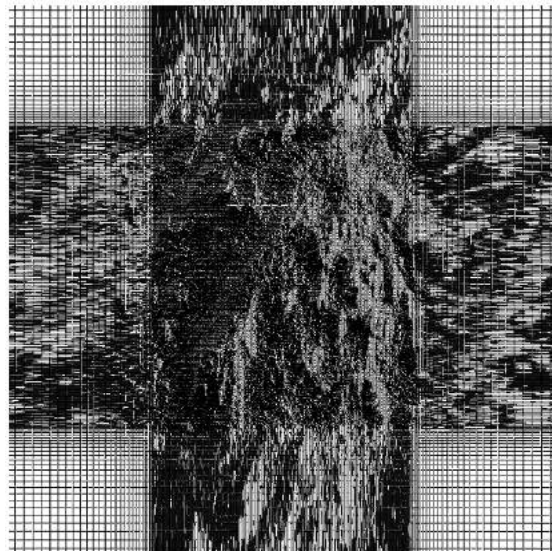

(b) Refinement area

Figure 6.23: Terrain and refinement area for Finlandia in WindSim

The wind field module is based on the generation of the 3D model in the preceding terrain module. Starting with the initial conditions, which were guessed estimations, the solution was progressively resolved by iteration until a converged solution was achieved by solving the RANS equations and applying the standard $k - \epsilon$ model as turbulence closure. Figure 6.25a shows the mean wind speed applied for all the terrain. Figure 6.25b plots the power density. Figure 6.25c is the power intensity and finally figure 6.25d is the inclination angle along with derived field data. Additionally, wind data from the climatology station was used in calibration of the wind resources and in the energy calculations. Figure 6.24 shows a frequency table fitted to a Weibull distribution, as well as the wind rose created for Finlandia.


(a) Wind rose

(b) Weibull distribution
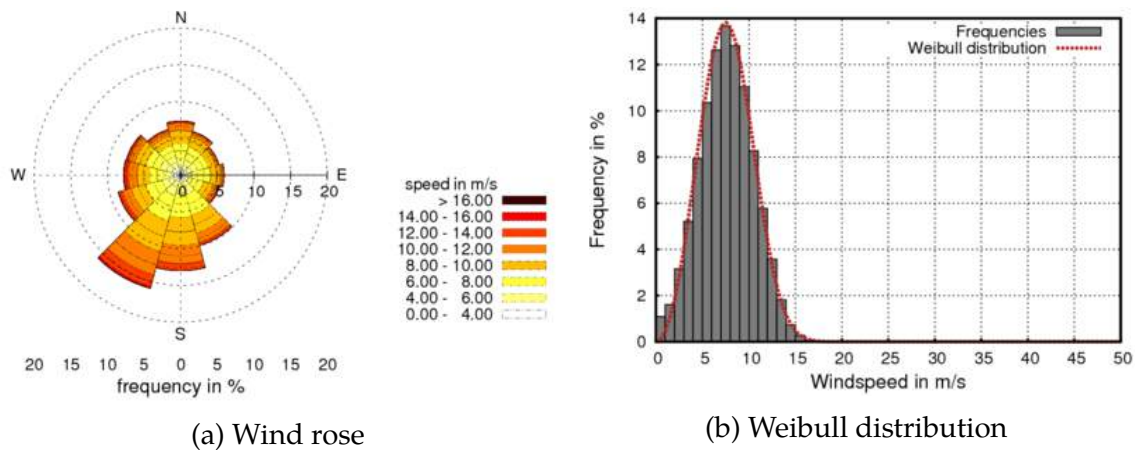
Figure 6.24: Wind statistics Finlandia

(a) Mean wind speed [m/s]

(b) Power density [W/m^2]

(c) Turbulent Intensity

(d) Inclination angle [*deg*]
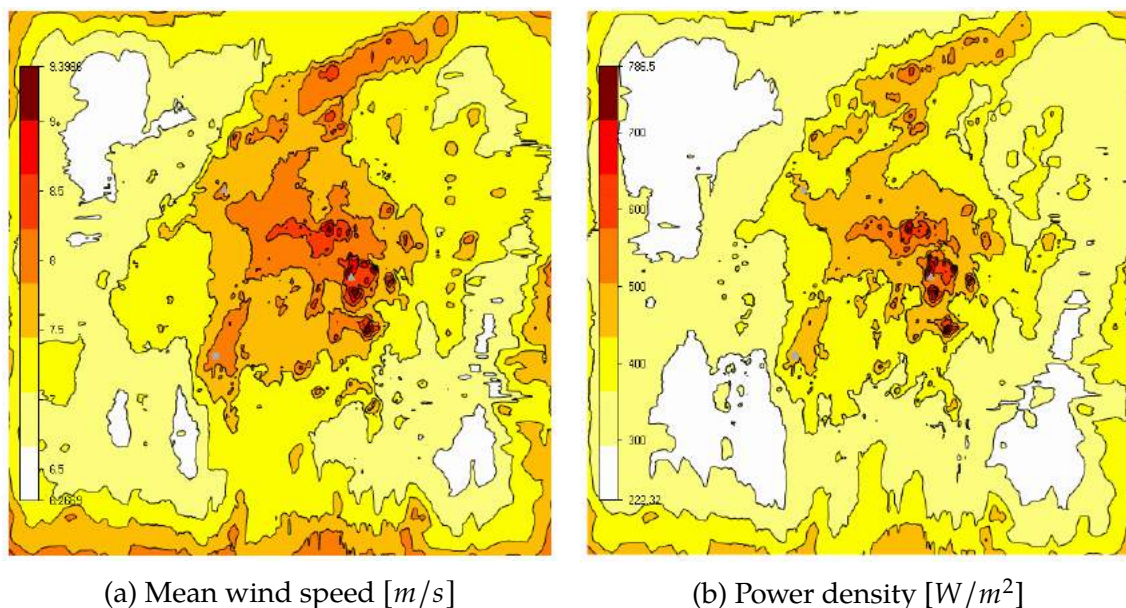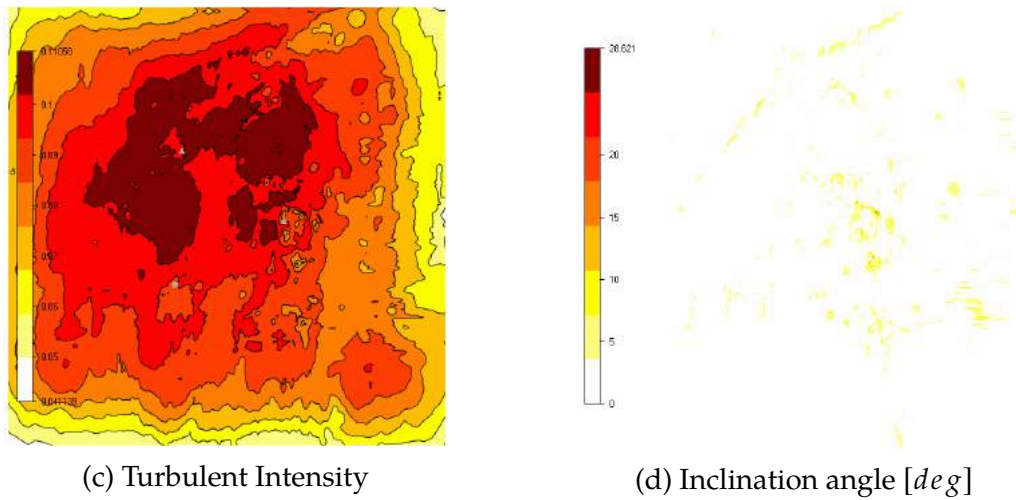
Figure 6.25: Wind resources for Finlandia in WindSim

6.3 Results of Zephy Tools

6.3.1 Korpinen

Korpinen was the first location to be simulated in Zephy TOOLS. An orography map modelled in the software is displayed in figure 6.26a, showing the position of both the met mast and the WTG. it can be seen that the heights variate from 150 to 300m above sea level. Subsequently, in the *ANALYZE* module, a project complexity index **ZIX = 0** was designated, meaning that the complexity of the terrain is simple. Figure 6.26b shows the average slope *[deg]* obtained for the site.

(a) Elevation map
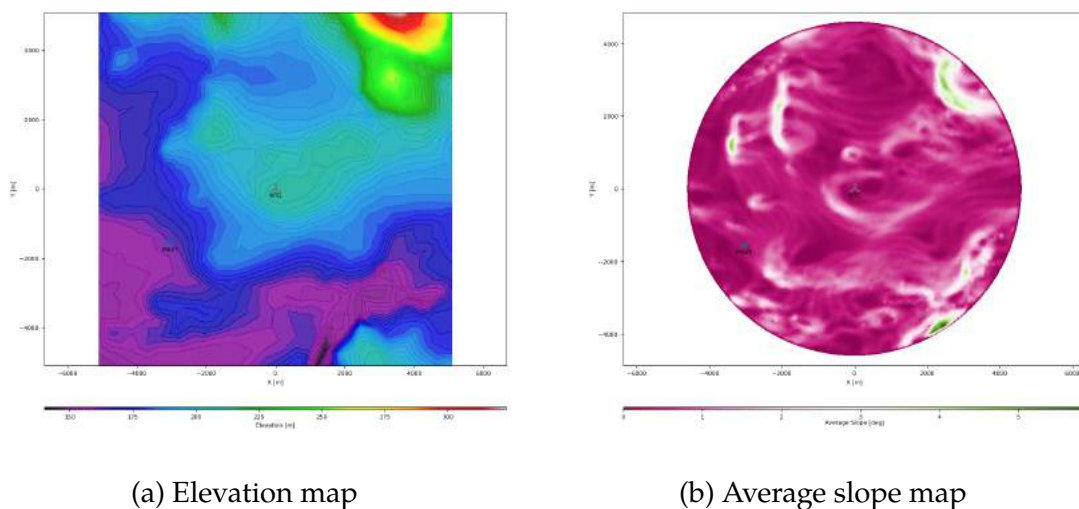
(b) Average slope map

Figure 6.26: Elevation and average slope for Korpinen in Zephy TOOLS

As a prior step before commencing the calculations, a *MESH* in the terrain was created. A coarse mesh with 72 directions (figure 6.27a) and a fine mesh with 180

directions (figure 6.27b) were generated. Similarly, a map with the orography of Korpinen as a background, with the coarse mesh on top is shown in figure 6.27c.

(a) Coarse mesh

(b) Fine mesh

(c) Coarse mesh + elevation
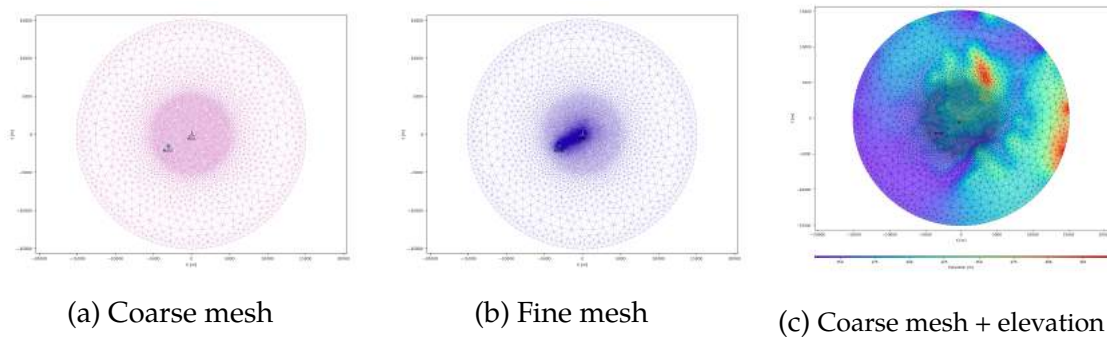
Figure 6.27: Different meshes for Korpinen in Zephy TOOLS

After selecting the coarse mesh and 72 sectors for the rose, the following roses where created for Korpinen, including the flow inclination (6.28a), direction variation (6.28b), TI variation (6.28c), turbulent intensity (6.28d) and horizontal speed-up (6.28e) all of them displayed in figure 6.28.

(a) Flow inclination

(b) Direction variation

(c) TI variation

(d) Turbulent intensity

(e) Horizontal speed-up
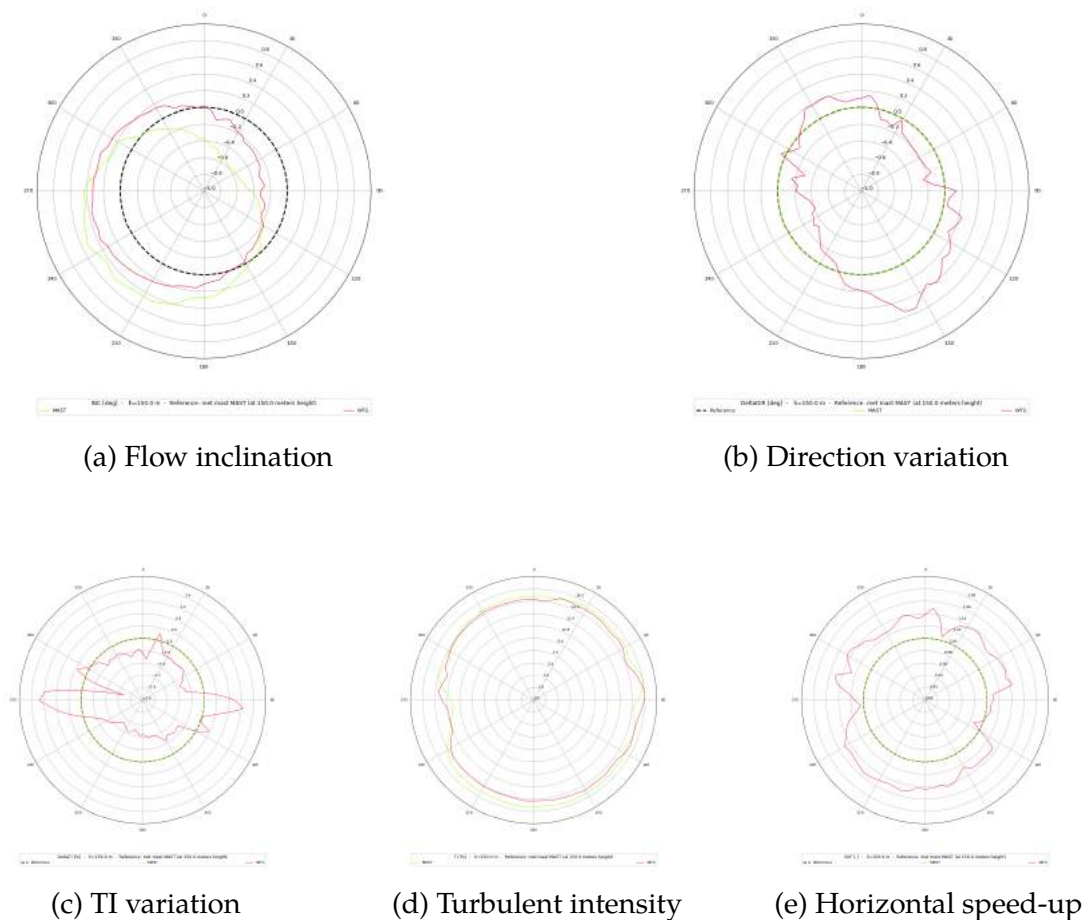
Figure 6.28: Different roses for Korpinen in Zephy TOOLS

Six types of maps can visualized with the following variables: Wind Power Density (6.29a), Flow Inclination (6.29b), Weibull Scale Parameter (6.29c), CFD Turbulent Intensity (6.29d), Extrapolated Turbulent Intensity (6.29e) and Weibull Shape Parameter (6.29f). All of them displayed for all directions in the rose.

(a) Wind Power Density

(b) Flow Inclination

(c) Weibull Scale Parameter

(d) CFD Turbulent Intensity

(e) Extrapolated Turbulent Intensity

(f) Weibull Shape Parameter
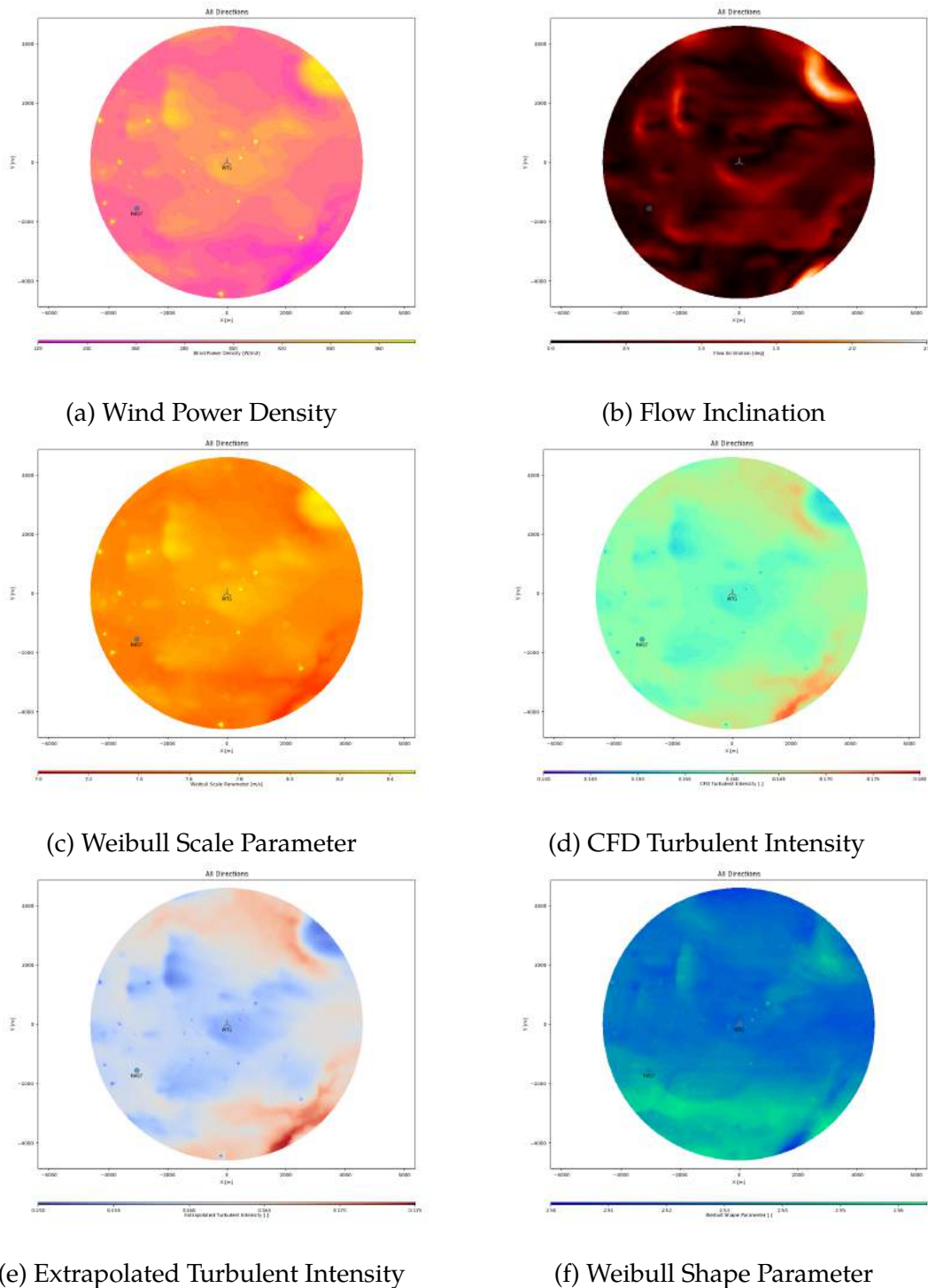
Figure 6.29: Different maps for Korpinen in Zephy TOOLS

6.3.2   Lokan Tekojärvi

Once all the files are uploaded and selected, in the *LOAD* module it is possible to visualize the orography and roughness of the site, as well as the location of the met mast and turbines. Figure 6.30a shows the map created for the elevation in Lokan Tekojärvi. Then, in the *ANALYZE* module, a project complexity index **ZIX = 0** was assigned, meaning that the complexity of the terrain is simple. Figure 6.30b shows the average slope *[deg]* obtained for the site.
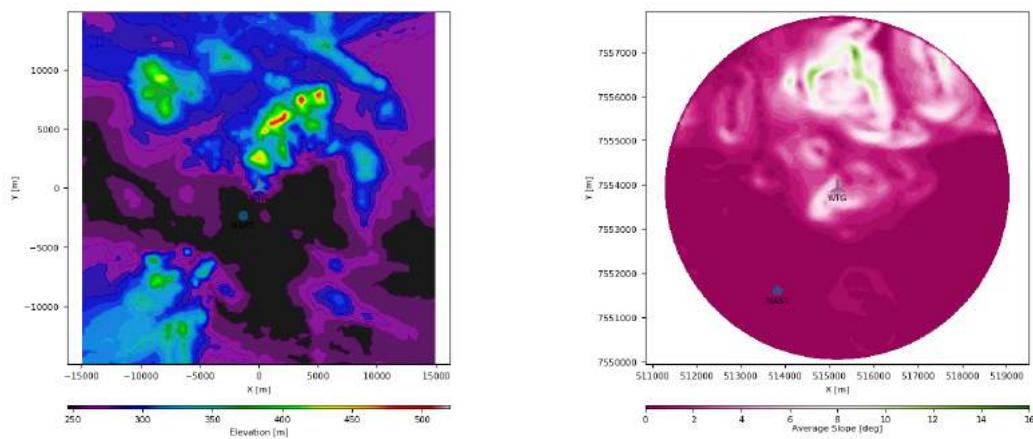

(a) Elevation map (b) Average slope map

Figure 6.30: Elevation and average slope for Lokan Tekojärvi in Zephy TOOLS

Before initiating the calculations, a *MESH* in the terrain has to be created. A coarse mesh with 72 directions (figure 6.31a) and a fine mesh with 180 directions (figure 6.31b) were created. It can also be seen in figure 6.31c a map with the orography of Lokan Tekojärvi as a background, with the coarse mesh on top.

(a) Coarse mesh (b) Fine mesh

(c) Coarse mesh + elevation

Figure 6.31: Different meshes for Lokan Tekojärvi in Zephy TOOLS

After selecting a mesh and the number of sectors for the rose, similar roses to the case of Korpinen in figure 6.28 were created (see figure 6.32):

(a) Flow inclination · · · · · (b) Direction variation · · · · · (c) TI variation

Figure 6.32: Different roses for Lokan Tekojärvi in Zephy TOOLS

Similarly to the case of Korpinen, some maps can visualized with the following variables: Wind Power Density (6.33a), Weibull Scale Parameter (6.33b), CFD Turbulent Intensity (6.33c) and Weibull Shape Parameter (6.33d).
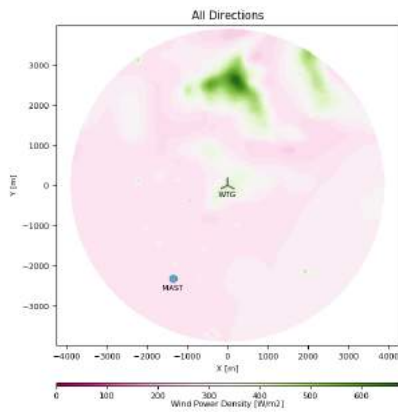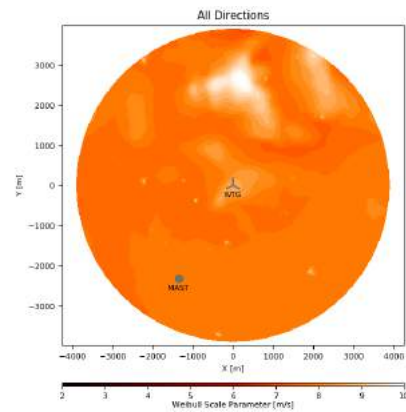
(a) Wind Power Density · · · · · (b) Weibull Scale Parameter
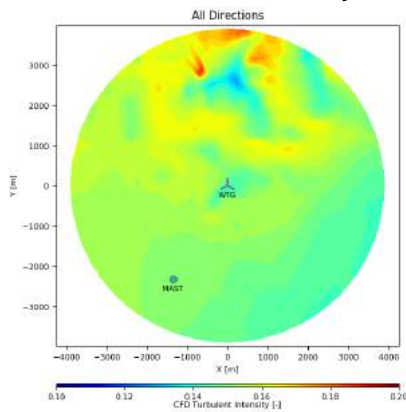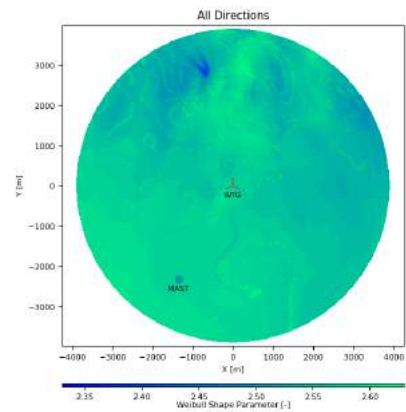
(c) CFD Turbulent Intensity · · · · · (d) Weibull Shape Parameter

Figure 6.33: Different maps for Lokan Tekojärvi in Zephy TOOLS

6.3.3 Ylläs

In the *LOAD* module of Zephy TOOLS, the elevation and roughness of Ylläs is presented, along with the location of the met mast and turbines. Figure 6.34a shows the map produced for the orography in Ylläs. Likewise, in the *ANALYZE* module, a project complexity index **ZIX = 2** was assigned, explaining that the complicatedness of the terrain is complex. Figure 6.34b shows the average slope *[deg]* obtained for the site.
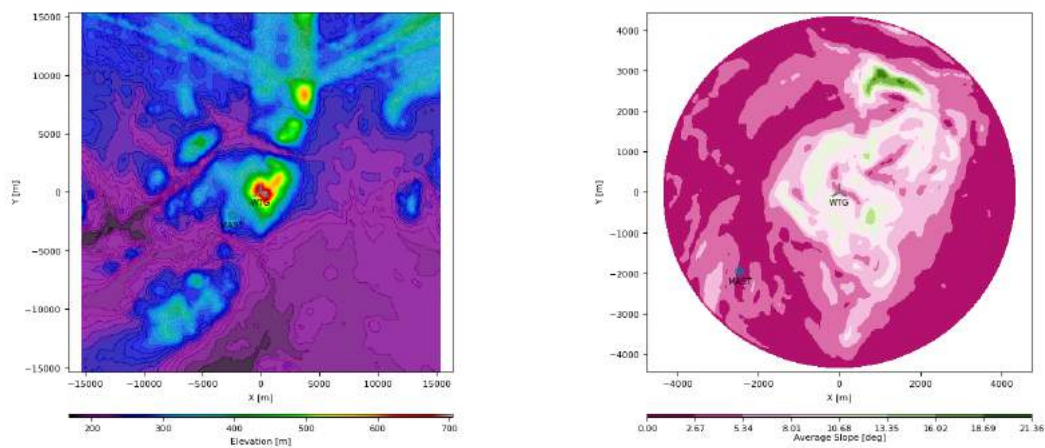
(a) Elevation map   (b) Average slope map

Figure 6.34: Elevation and average slope for Ylläs in Zephy TOOLS

Two *meshes* were created; a coarse mesh with 72 directions (figure 6.35a) and a fine mesh with 180 directions (figure 6.35b). Figure 6.35c displays a map with the orography of Ylläs as a background, with the coarse mesh on top.
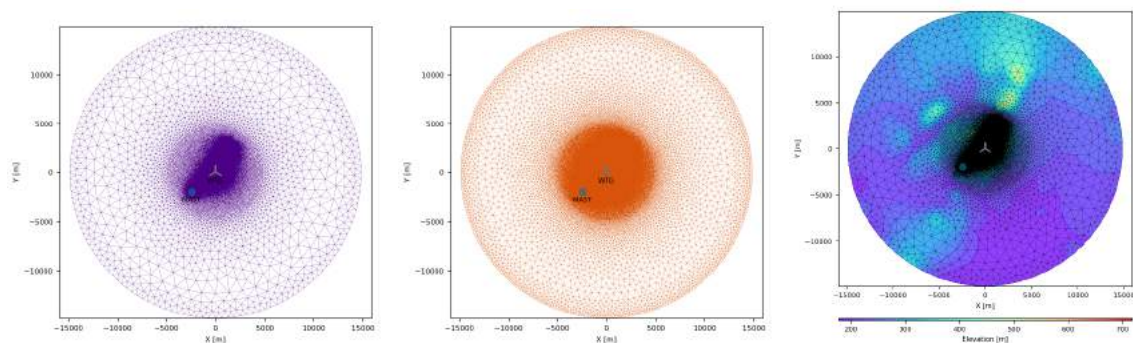
(a) Coarse mesh   (b) Fine mesh   (c) Coarse mesh + elevation

Figure 6.35: Different meshes for Ylläs in Zephy TOOLS

The coarse mesh was selected, generating roses such as the direction variation (6.36a), TI variation (6.36b) and horizontal speed-up (6.36c), shown in figure 6.36.

(a) Direction variation (b) TI variation (c) Horizontal speed-up
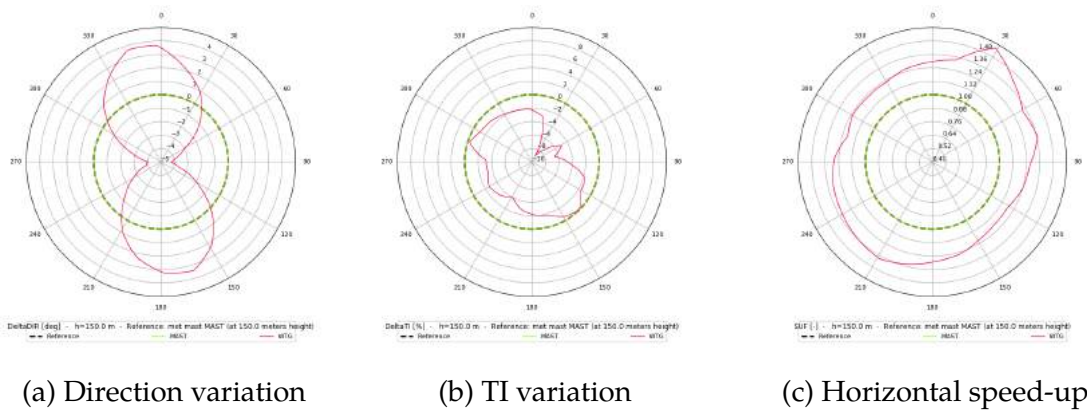
Figure 6.36: Different roses for Ylläs in Zephy TOOLS

For all directions in the rose after a CFD simulation, various maps were generated with the following variables: Wind Power Density (6.37a), Flow Inclination (6.37b), Weibull Scale Parameter (6.37c), CFD Turbulent Intensity (6.37d), Extrapolated Turbulent Intensity (6.37e) and Weibull Shape Parameter (6.37f).
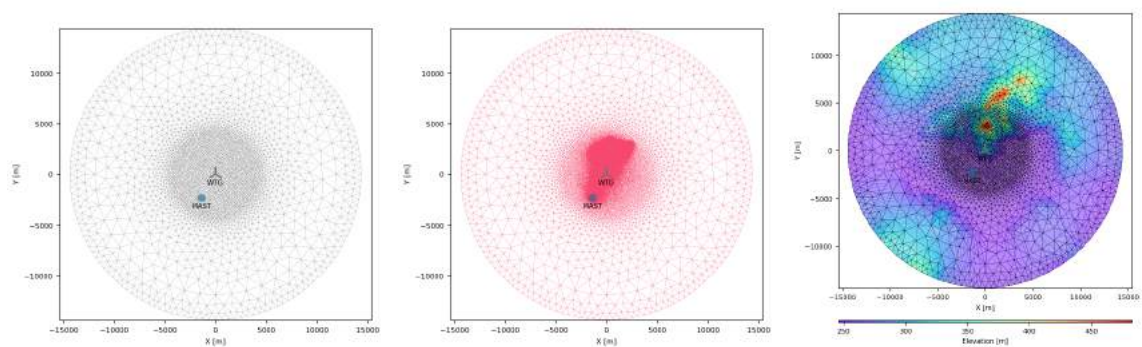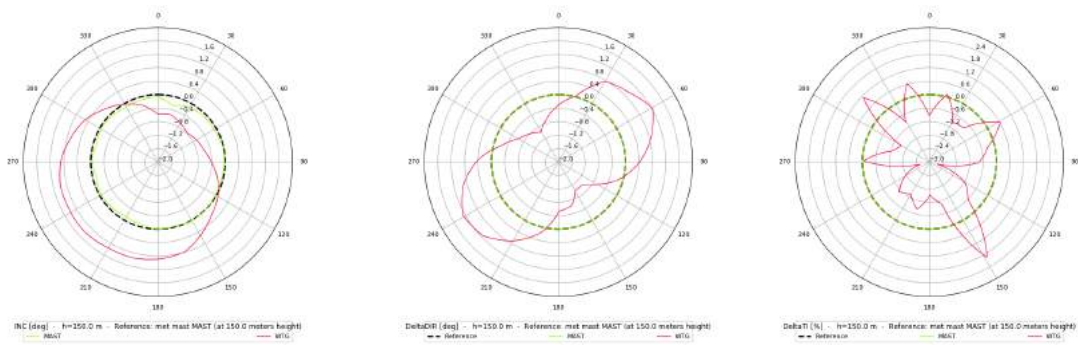

(a) Wind Power Density (b) Flow Inclination (c) Weibull Scale Parameter

(d) CFD Turbulent Intensity (e) Extrapolated Turbulent Intensity (f) Weibull Shape Parameter
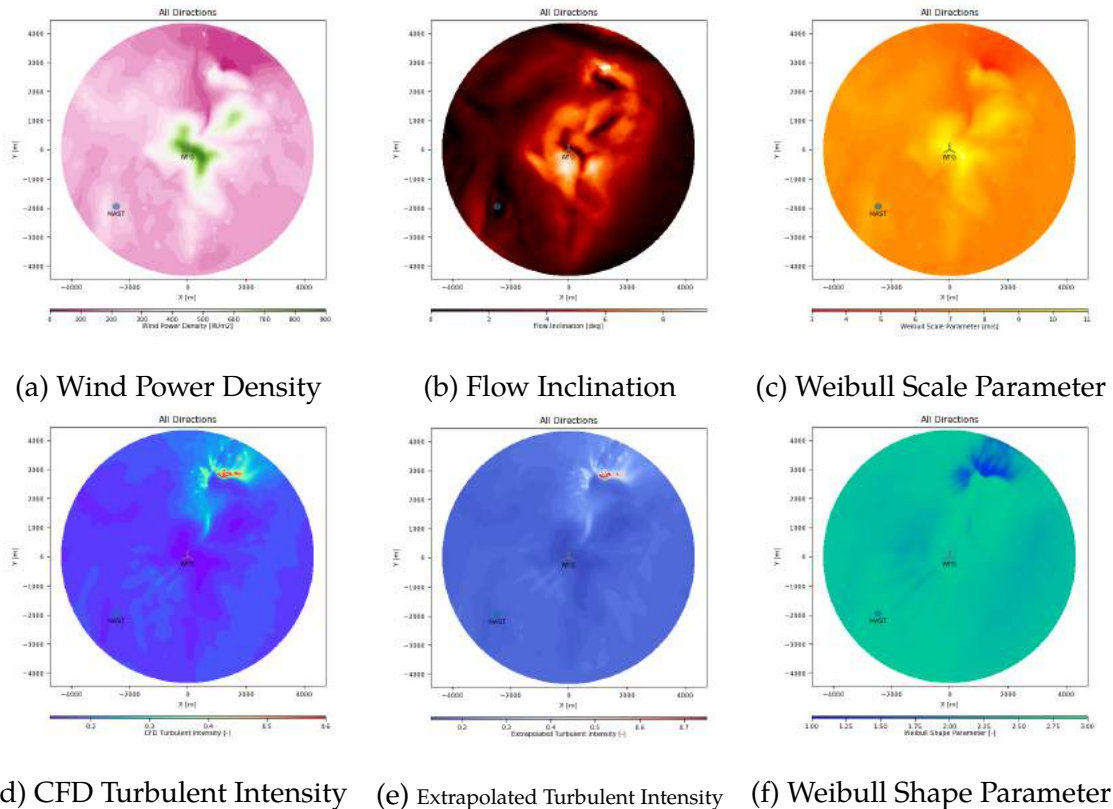
Figure 6.37: Different maps for Ylläs in Zephy TOOLS

6.3.4 Finlandia

The elevation and roughness of Finlandia is presented, along with the location of the met mast and turbines. Figure 6.38a shows the map produced for the orography in Finlandia. Likewise, in the *ANALYZE* module, a project complexity index **ZIX = 0** was assigned, explaining that the complexity of the terrain is simple. Figure 6.38b shows the average slope *[deg]* obtained for the site.

(a) Elevation map   (b) Average slope map
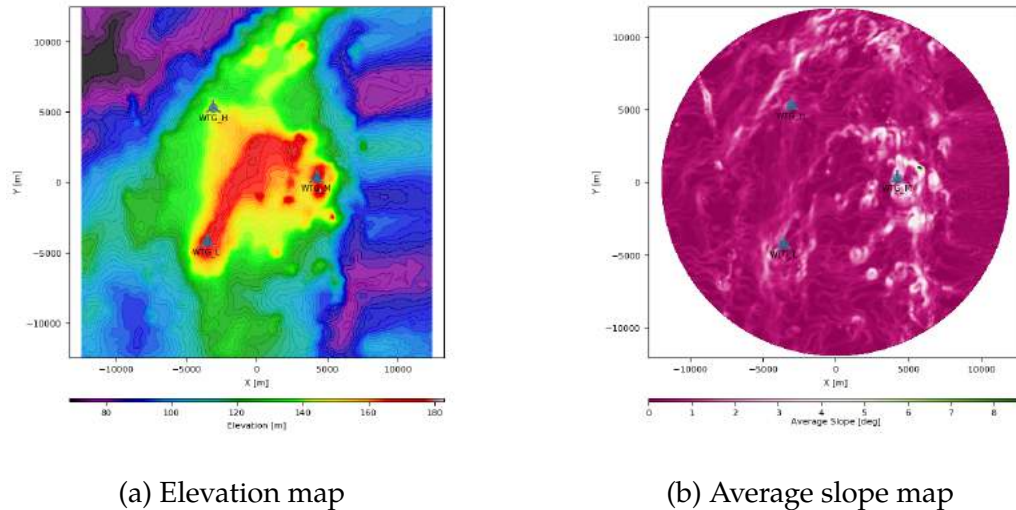
Figure 6.38: Elevation and average slope for Finlandia in Zephy TOOLS

Afterwards, A *MESH* in the terrain of Finlandia was created. A coarse mesh with 72 directions (figure 6.39a) and a fine mesh with 180 directions (figure 6.39b) were created. It can also be seen in figure 6.39c a map with the orography of Finlandia as a background, with the coarse mesh on top.

(a) Coarse mesh   (b) Fine mesh

(c) Coarse mesh + elevation
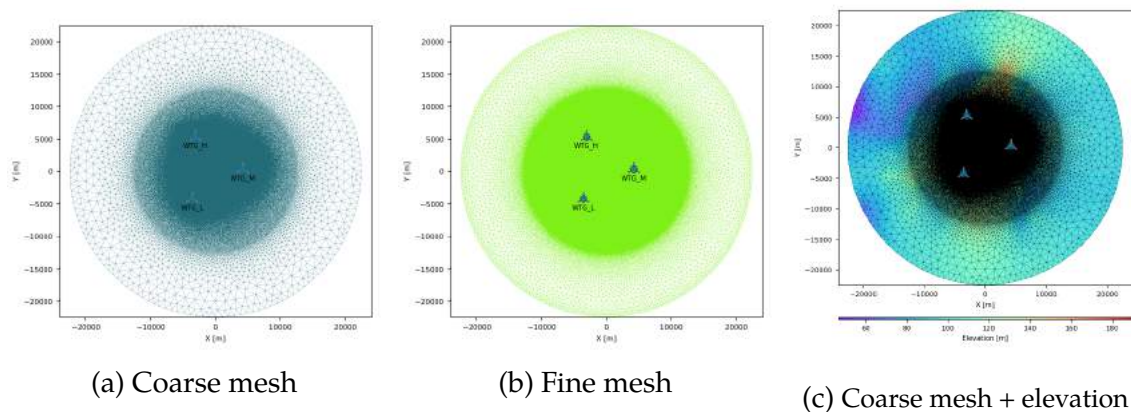
Figure 6.39: Different meshes for Finlandia in Zephy TOOLS

The coarse mesh was selected in order to generate some roses including the flow inclination (6.40a), direction variation (6.40b) and TI variation (6.40c) shown in figure 6.40.

(a) Flow inclination   (b) Direction variation   (c) TI variation
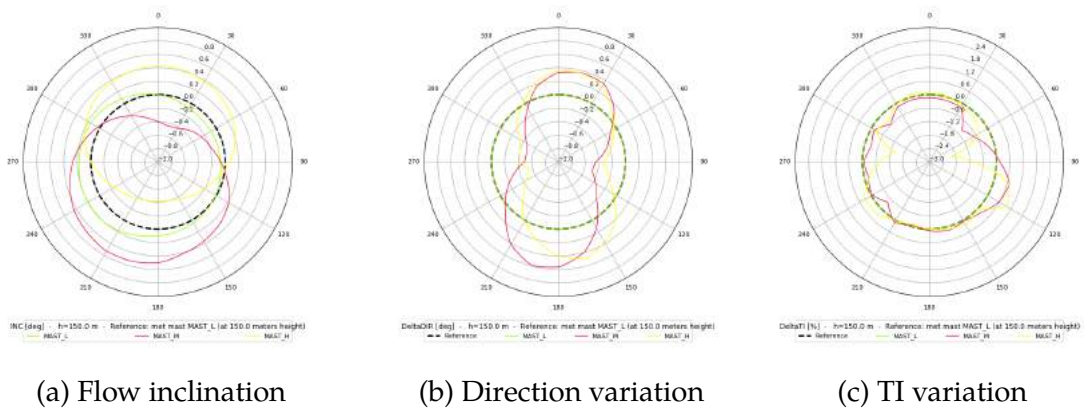
Figure 6.40: Different roses for Finlandia in Zephy TOOLS

For all directions in the rose, after a CFD simulation, different maps were generated with the following variables: Wind Power Density (6.41a), Flow Inclination (6.41b), Weibull Scale Parameter (6.41c), CFD Turbulent Intensity (6.41d), Extrapolated Turbulent Intensity (6.41e) and and Weibull Shape Parameter (6.41f)

(a) Wind Power Density   (b) Flow Inclination   (c) Weibull Scale Parameter

(d) CFD Turbulent Intensity   (e) Extrapolated Turbulent Intensity   (f) Weibull Shape Parameter
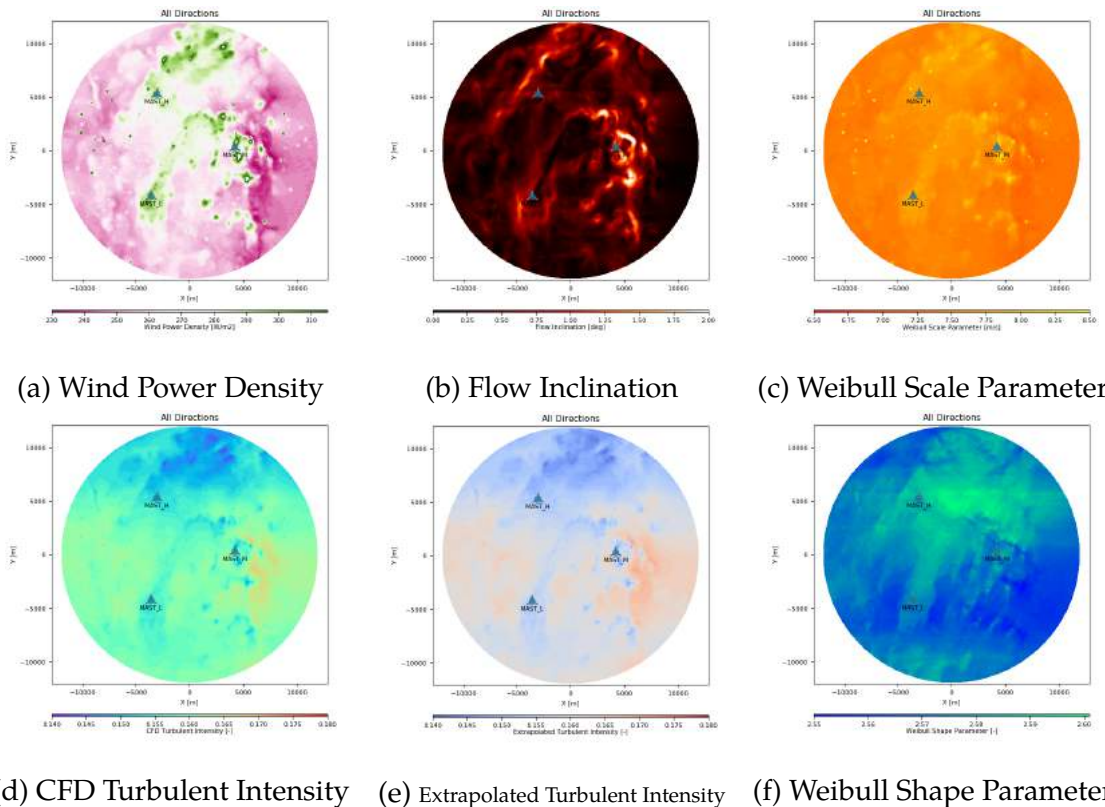
Figure 6.41: Different maps for Finlandia in Zephy TOOLS

6.4 Comparison of the software

In order to have comparable results, the different maps for the wind resource obtained by the three software were modified so that there was a clearly visible distinction or similarity between them. In such maps, the colors towards the yellow scale indicate higher wind speeds while colors towards the black suggest lower wind speeds.

6.4.1 Korpinen
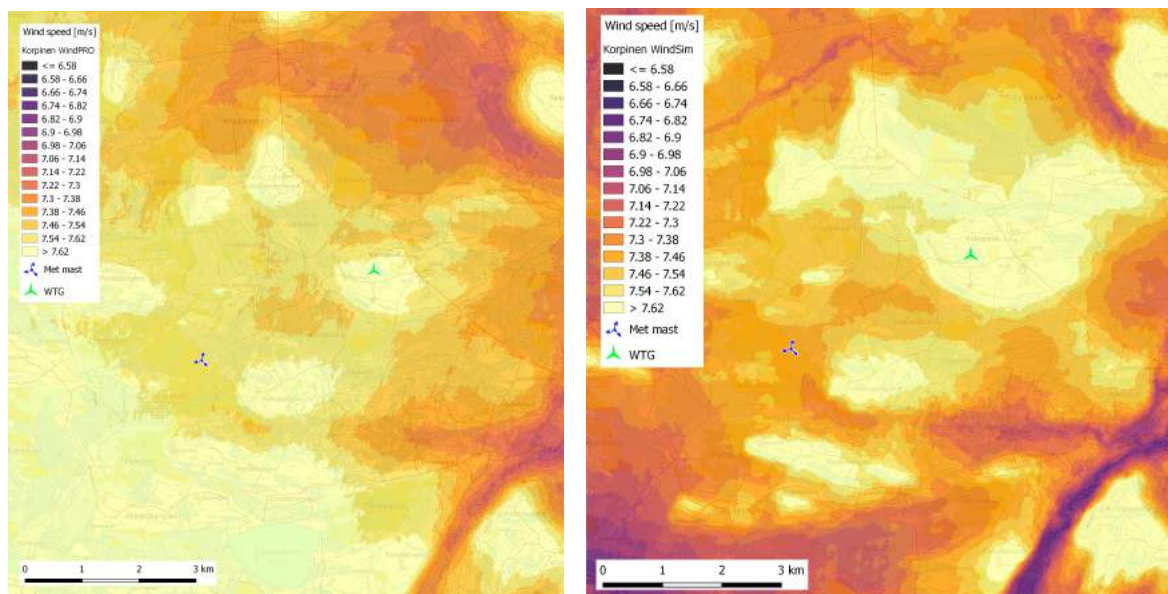
(a) Wind resource map from WindPRO

(b) Wind resource map from WindSim
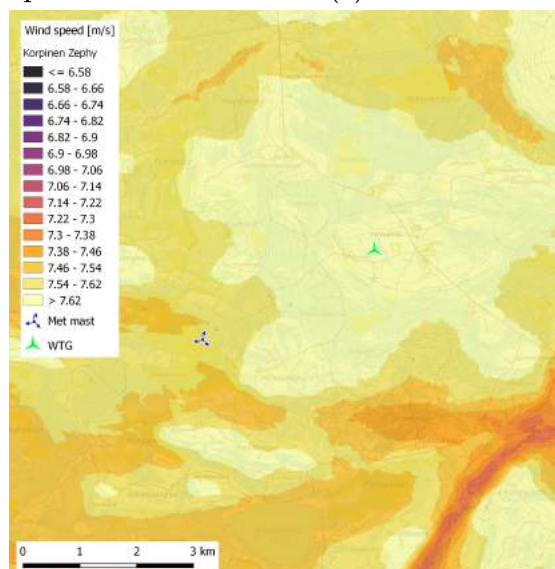
(c) Wind resource map from Zephy TOOLS

Figure 6.42: Wind resource maps generated for Korpinen in different software

Figure 6.42a shows the map generated in WindPRO for the wind speed in Korpinen using speeds from $6.58m/s$ to $7.62m/s$. The met mast has an average wind speed of $7.45m/s$, which corresponds to the measurements calculated by WindPRO using a met mast height of 150m, as seen in table 6.2. Similarly, figure 6.42b shows the same results for Korpinen modeled in WindSim, where the met mast coincides as well with the average wind speed measured for this case. Figure 6.42c shows the map generated in Zephy TOOLS. All the software show in the LOW met mast position the same color scale towards the orange, but starts differing in the scale when it moves towards the wind turbine position. The wind speed predicted by WindPRO in the met mast shows an deviation of 0.00%, meaning that it coincides totally with the average wind speed from the climatology file, while the wind speed in the met mast in WindSim is 0.13% higher than the real. Zephy TOOLS overestimates the wind speed in the met mast by 0.40%.

Table 6.2: Wind speed for Korpinen in the met mast

				KORPINEN						
				WindPRO		WindSim		Zephy TOOLS		
	Elevation [m]	East	North	Deviation	Wind speed [m/s]	Deviation	Wind speed [m/s]	Deviation	Wind speed [m/s]
Met mast	161.3	525,014	7,213,486	0.00%	**7.45**	0.13%	**7.46**	0.40%	**7.48**

The WTG is located 50m above the met mast and reaches wind speeds of roughly $7.84m/s$. In table 6.3, the wind speed predicted in the turbine in WindSim is only 3.84% larger than the one predicted by WindPRO and 2.52% bigger for Zephy TOOLS. In all cases, the comparison of the results were compared with respect to the one obtained in WindPRO. Same principle applies for all the following sites.

Table 6.3: Wind speed for Korpinen obtained by different software

				KORPINEN					
				WindPRO	WindSim		Zephy TOOLS		
	Elevation [m]	East	North	Wind speed [m/s]	Deviation	Wind speed [m/s]	Deviation	Wind speed [m/s]
Turbine 1	212.1	528,056	7,215,038	**7.55**	**7.84**	3.84%	**7.74**	2.52%

6.4.2 Lokan Tekojärvi

Figure 6.43a shows the map generated in WindPRO for the wind speed in Lokan Tekojärvi using speeds from $6.2m/s$ to $8.8m/s$. The met mast measured an average wind speed of $7.45m/s$, which corresponds to the measurements calculated by WindPRO using a met mast height of 150m. The same applies for WindSim, where the met mast concur as well with the average wind speed measured for this case, measuring a wind speed of $7.46m/s$ (figure 6.43b). In the case of Zephy TOOLS, for the same location a wind speed of $7.48m/s$ is registered (figure 6.43c). Table 6.4 shows the different wind speeds estimated in the met mast by the different software, and the deviation is obtained by comparing the measured data to the real measured speed in the met mast of 7.45m/s. WindPRO predicts such speed with no error, while WindSim overestimates the speed with only 0.13% and Zephy TOOLS with 0.40%.

Table 6.4: Wind speed for Lokan Tekojärvi in the met mast

				WindPRO		WindSim		Zephy TOOLS	
	Elevation [m]	East	North	Deviation	Wind speed [m/s]	Deviation	Wind speed [m/s]	Deviation	Wind speed [m/s]
Met mast	246	513,821	7,551,603	0.00%	**7.45**	0.13%	**7.46**	0.40%	**7.48**

For this site, the main WTG is located 87m above the met mast. Zephy TOOLS was closer to the WindPRO results than those of WindSim for the wind speeds in the majority of the locations, even though in the wind maps generated by the software, lower Wind speeds are registered by WindPRO whereas WindSim and Zephy TOOLS look quite similar (figure 6.43).
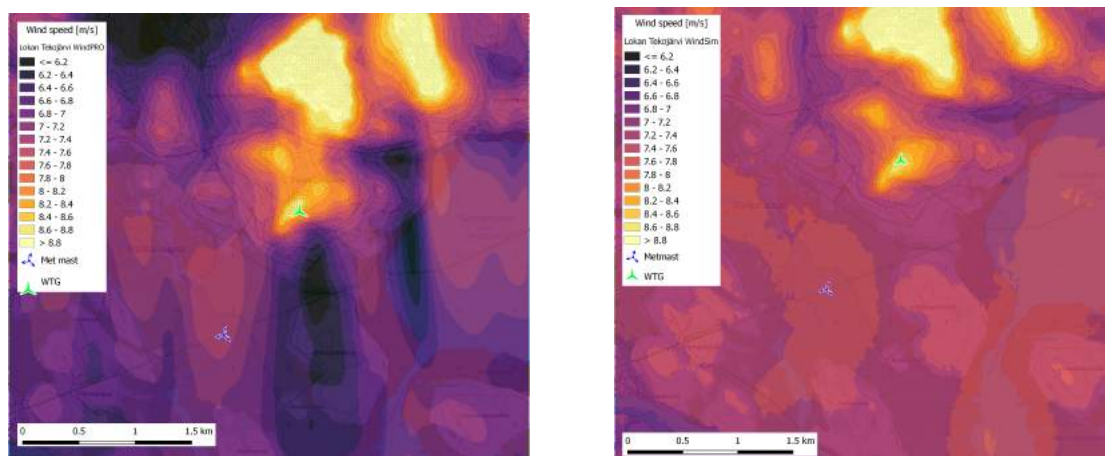
(a) Wind resource map from WindPRO

(b) Wind resource map from WindSim
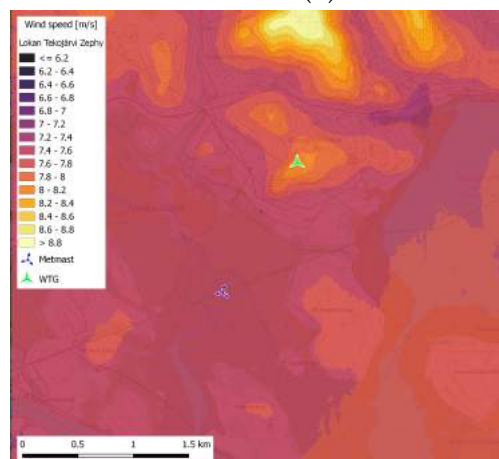
(c) Wind resource map from Zephy TOOLS

Figure 6.43: Wind resource maps generated for Lokan Tekojärvi in different software

Table 6.5 displays the different positions for the proposed wind turbines (as seen in figure 6.5) as well as the different wind speeds obtained by the different software. The percentages shown in the *deviation* column contrast the results obtained for both WindSim and Zephy TOOLS against the results of WindPRO as a baseline for comparison. For instance, for the turbine 2, 10.81% indicates that WindSim

is such rate bigger than the one predicted by WindPRO and 2.67% indicates that Zephy TOOLS is such percentage larger than in WindPRO. It can be observed that the deviation becomes larger when the elevation increases and the three software differ quite a bit.

Table 6.5: Wind speed for Lokan Tekojärvi obtained by different software

				WindPRO	WindSim		Zephy TOOLS	
	Elevation [m]	East	North	Wind speed [m/s]	Deviation	Wind speed [m/s]	Deviation	Wind speed [m/s]
Turbine 2	333	515,181	7,553,925	7.86	10.81%	8.71	2.67%	8.07
Turbine 3	400	517,162	7,556,990	7.9	19.49%	9.44	7.22%	8.47
Turbine 4	273	516,687	7,554,148	7.4	2.97%	7.62	3.65%	7.67
Turbine 5	246	512,746	7,550,682	7.33	-0.14%	7.32	2.18%	7.49
Turbine 6	246	515,153	7,550,281	7.52	-2.13%	7.36	-0.13%	7.51
Turbine 7	273	514,015	7,555,150	7.04	1.56%	7.15	6.11%	7.47
Turbine 8	400	514,896	7,556,074	7.91	14.92%	9.09	4.42%	8.26

6.4.3 Ylläs
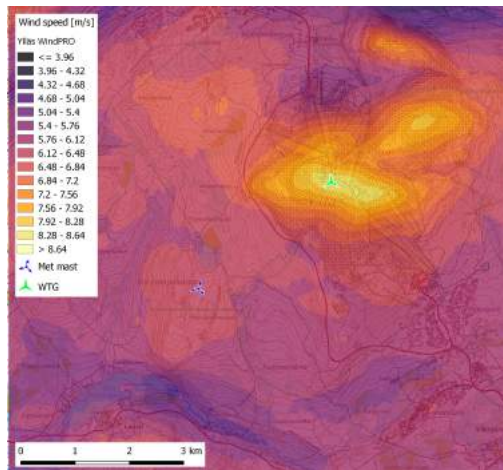
(a) Wind resource map from WindPRO
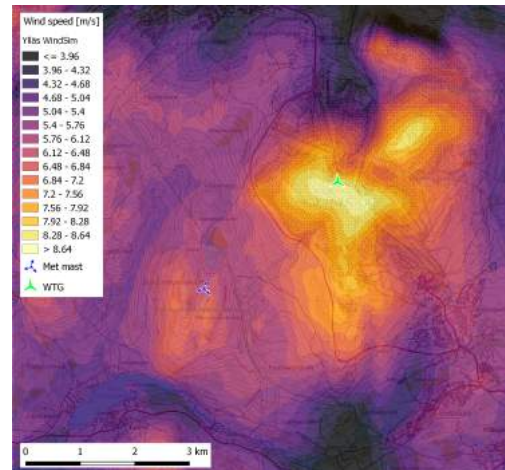
(b) Wind resource map from WindSim
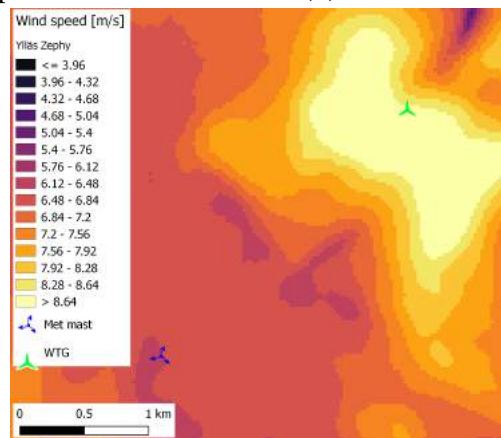
(c) Wind resource map from Zephy TOOLS

Figure 6.44: Wind resource maps generated for Ylläs in different software

Figure 6.44a shows the map generated in WindPRO for the wind speed in Ylläs using speeds from $3.96m/s$ to $8.64m/s$. The met mast has an average wind speed of $6.7m/s$, which corresponds to the measurements calculated by WindPRO using a met mast height of 150m. Similarly, figure 6.44b shows the same results for Ylläs modelled in WindSim, and it can be seen that the met mast also coincides with the average wind speed measured for this case. Figure 6.44c was generated in Zephy TOOLS. The software show similar colors around the hilly area where the wind turbine is located, but differ in the flat terrain around this area. In table 6.6 the wind speed predicted by WindPRO in the met mast has a 0.00% deviation, meaning that it coincides totally with the average wind speed from the climatology file, whereas the wind speed in the met mast in WindSim is 0.15% higher than the real value. Zephy TOOLS estimates this speed as 6.8m/s, corresponding to a 1.34% overestimation from the real measurement.

Table 6.6: Wind speed for Ylläs by different software in the met mast

				YLLÄS						
				WindPRO		WindSim		Zephy TOOLS		
	Elevation [m]	East	North	Deviation	Wind speed [m/s]	Deviation	Wind speed [m/s]	Deviation	Wind speed [m/s]
Met mast	317.4	378,913	7,495,220	0.00%	**6.71**	0.15%	**6.72**	1.34%	**6.8**

The WTG is located in the top of the hill, which reaches very high wind speeds of around $9.7m/s$. In the case of the turbine 2, located at 705m above sea level the wind speed predicted in WindSim is 14.88% higer than the one predicted by WindPRO and 7.39% larger for Zephy TOOLS.

For this extreme case, the height difference between the met mast and the generator is of 387m; therefore it was expected to have different results of the prediction of wind speeds for the different software, due to the flow separation generated and the speed up effect, explained in section 3.2.

Table 6.7: Wind speed for Ylläs by different software in the turbine

				YLLÄS					
				WindPRO	WindSim		Zephy TOOLS		
	Elevation [m]	East	North	Wind speed [m/s]	Deviation	Wind speed [m/s]	Deviation	Wind speed [m/s]
Turbine 2	705	381,373	7,497,164	**9.07**	**10.42**	14.88%	**9.74**	7.39%

6.4.4 Finlandia

In the case of Finlandia, 3 different met mast were placed in the area, and in order to register the exact wind speed at each side, a wind turbine was placed in the same location for each one. Figure 6.45 shows the different maps generated in WindPRO for each met mast, named *HIGH met mast* for the Northern position, *MIDDLE met mast* for the one placed between the 2 other met masts and *LOW met mast* the one located in Southern position in the map. As expected, the 3 maps registered the same wind speeds even though they are generated with different climatology files. The real wind speeds measured for each met mast are, for

the LOW met mast, an average wind speed of $7.58m/s$, for the MIDDLE met mast, $7.6m/s$ and for the HIGH met mast $7.45m/s$. These values are the base for comparison with the results obtained for the other software.

HIGH met mast　　　　　　　MIDDLE met mast　　　　　　　LOW met mast
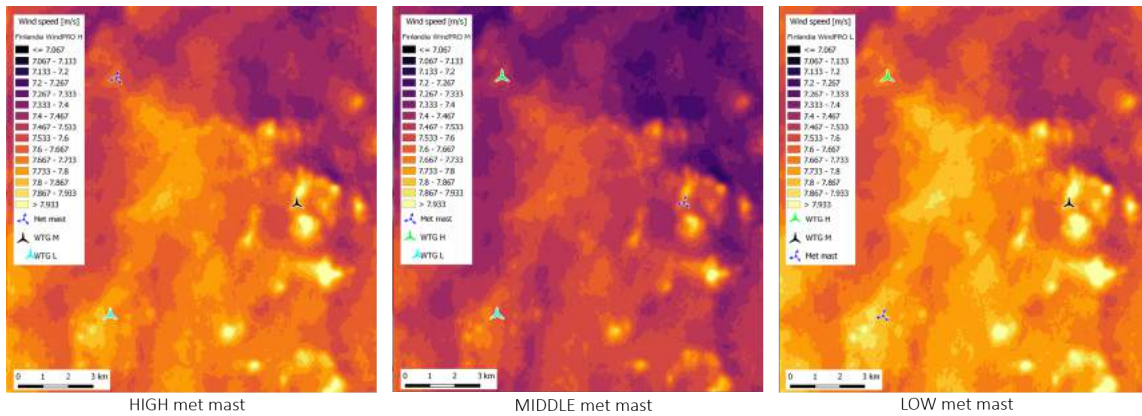
Figure 6.45: Wind resource maps for Finlandia in WindPRO

(a) Wind resource map WindSim　　　　(b) Wind resource map Zephy TOOLS
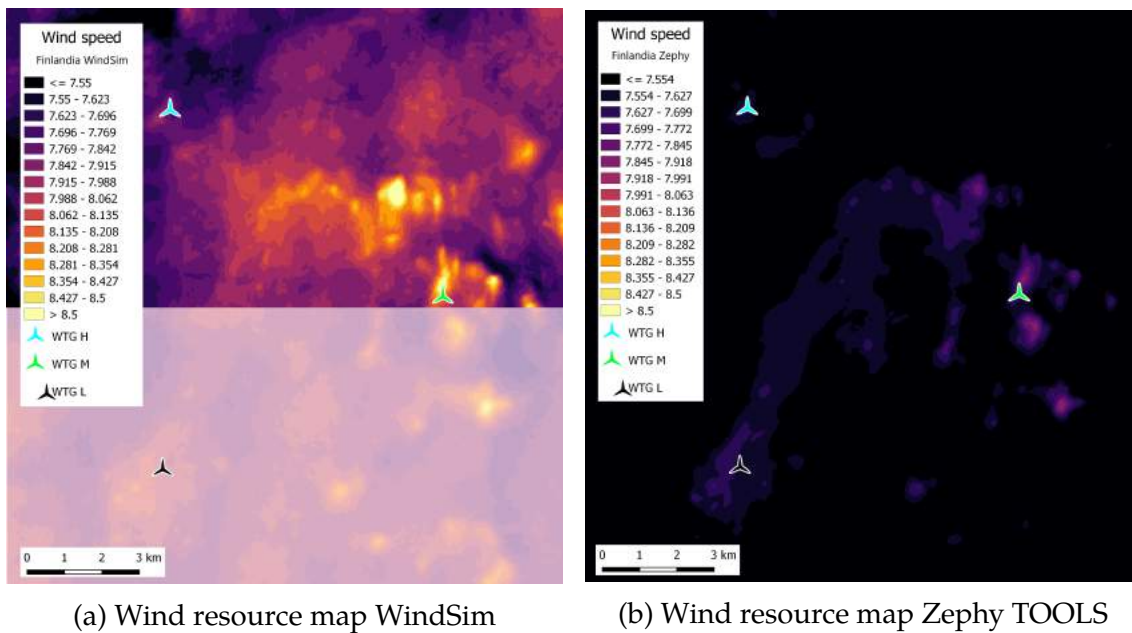
Figure 6.46: Wind resource maps for Finlandia in WindSim and Zephy TOOLS

Figure 6.46 displays the wind maps obtained for Finlandia with both WindSim and Zephy TOOLS, with the same color scale so that a clear comparison can be performed. Figure 6.46a was obtained in WindSim, but as it can be seen in the top, only half of the map could be generated by the software despite having run simulations with the three met mast. The lower part is displayed so that the reader has an idea of the location of the LOW turbine position. Figure 6.46b was obtained with Zephy TOOLS and it is clear that the software is overestimating the real wind speeds with around 0.38%. To have a better understanding of the

comparison between the software, figure 6.47 shows the same wind resource map for both WindPRO and Zephy TOOLS with the equivalent scale. In this case, WindPRO is the software showing the most accurate results.

Finlandia WindPRO   Finlandia Zephy TOOLS
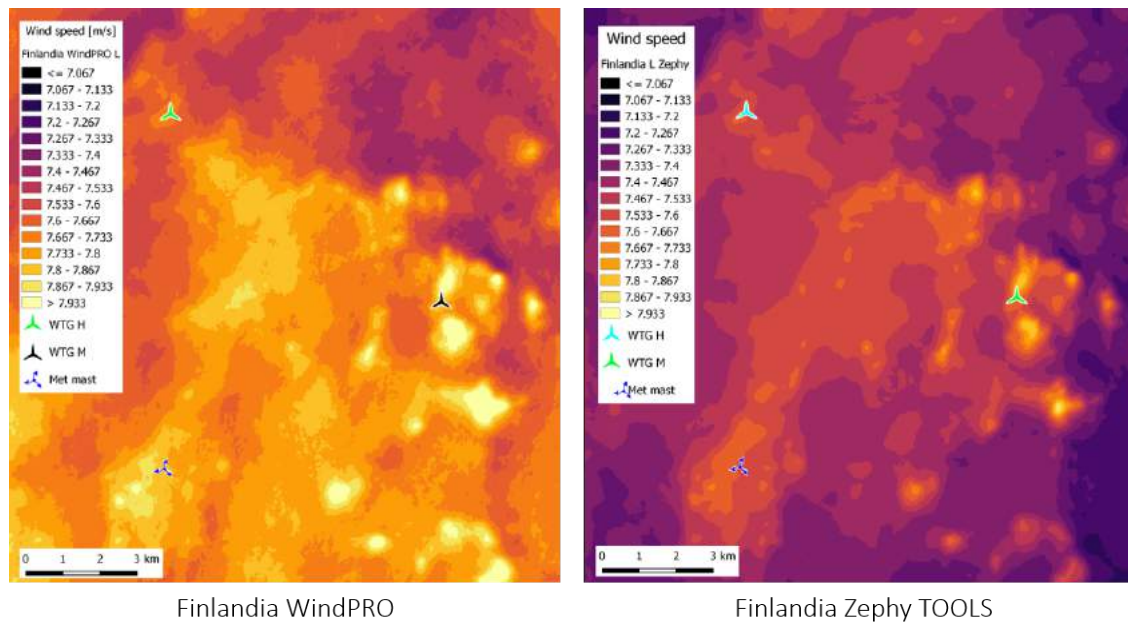
Figure 6.47: Wind resource maps for Finlandia in WindPRO and Zephy TOOLS

Table 6.8 contains the wind speeds obtained by WindPRO, WindSim and Zephy TOOLS at each location for the *LOW met mast*. At the met mast position, WindPRO estimates accurately the wind speed of 7.58m/s, while WindSim overestimates it with 0.13% and Zephy TOOLS overestimates it with 0.26%. Figure 6.48 shows the location of the wind turbines in question.
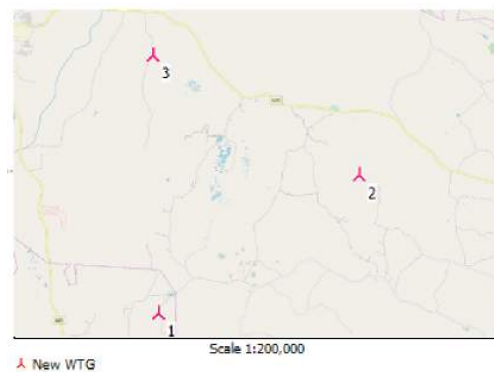
Figure 6.48: WTGs in Finlandia

Table 6.8: Wind speed for Finlandia LOW met mast obtained by different software

		Real met mast	WindPRO		WindSim		Zephy TOOLS	
	Elevation [m]	Wind speed [m/s]	Deviation	Wind speed [m/s]	Deviation	Wind speed [m/s]	Deviation	Wind speed [m/s]
Met mast	173.4	**7.58**	0.00%	7.58	0.13%	7.59	0.26%	7.6
Turbine 2	176.9	**7.6**	-0.26%	7.58	2.50%	7.79	0.53%	7.64
Turbine 3	150	**7.45**	-0.40%	7.42	0.94%	7.52	1.74%	7.58

LOW MAST FINLANDIA

Table 6.9 contains the wind speeds obtained by WindPRO, WindSim and Zephy TOOLS at each location for the *MIDDLE met mast*. At the met mast position, Wind-

PRO overestimates the real wind speed of 7.6m/s with a 1.32%, while WindSim overestimates it with only 0.13%. Zephy TOOLS overestimates it with 0.39%.

Table 6.9: Wind speed for Finlandia MIDDLE met mast obtained by different software

		MIDDLE MAST FINLANDIA							
		Real met mast	WindPRO		WindSim		Zephy TOOLS		
	Elevation [m]	Wind speed [m/s]	Deviation	Wind speed [m/s]	Deviation	Wind speed [m/s]	Deviation	Wind speed [m/s]	
Turbine 1	173.4	**7.58**	1.72%	7.71	-3.03%	7.35	0.13%	7.59	
Met mast	176.9	**7.6**	1.32%	7.7	0.13%	7.61	0.39%	7.63	
Turbine 3	150	**7.45**	0.13%	7.46	-2.28%	7.28	1.48%	7.56	

Finally, table 6.10 contains the wind speeds obtained by WindPRO, WindSim and Zephy TOOLS at each location for the *HIGH met mast*. At the met mast position where the wind speed is 7.45m/s, WindPRO predicts it accurately with no error, whereas WindSim overestimates it with only 0.13% and Zephy TOOLS overestimates it with just 0.40%.

Table 6.10: Wind speed for Finlandia HIGH met mast obtained by different software

		HIGH MAST FINLANDIA							
		Real met mast	WindPRO		WindSim		Zephy TOOLS		
	Elevation [m]	Wind speed [m/s]	Deviation	Wind speed [m/s]	Deviation	Wind speed [m/s]	Deviation	Wind speed [m/s]	
Turbine 1	173.4	**7.58**	1.45%	7.69	-0.26%	7.56	-0.92%	7.51	
Turbine 2	176.9	**7.6**	1.18%	7.69	3.16%	7.84	-0.66%	7.55	
Met mast	150	**7.45**	0.00%	7.45	0.13%	7.46	0.40%	7.48	

6.5 Overall comparison

An overall personal comparison over the software has been provided by the author according to her experience with the use of the different software in table 6.11. The scale goes from 1, meaning **very unsatisfied** to 5, **very satisfied** (figure 6.49). In the *accuracy of results in the met mast*, WindPRO showed better results, as well as in the results for *simple terrain*, while WindSim and Zephy TOOLS had similar results. WindSim was the less accurate in *complex terrain*. The *prior data treatment* considers the effort invested to convert the data into the correct extension. The *user experience* refers to the emotions and attitudes about using a particular software, and includes the practical, experiential, meaningful and valuable aspects of human–computer interaction. The *computational time* refers of how fast the calculations performed and for the *visual results*, the graphs and result obtained at the end of the simulations.

Figure 6.49: Satisfaction scale for the qualitative comparison

Table 6.11: Qualitative comparison for different characteristics of the software

Quality comparison for different software			
	WindPRO	WindSim	Zephy TOOLS
Accuracy of results in the met mast	5	4	3
Accuracy of results in simple terrain	5	4	4
Accuracy of results in complex terrain	4	3	4
Prior data treatment	4	3	3
User experience	3	4	1
Computational time	5	2	2
Visual results	3	3	5
Total	**29**	**23**	**22**

Chapter 7

Wind power generation costs

Wind power has experienced a significantly unforeseen revolution since 2008. Between 2008 and 2017, improved technologies have increased capacity factors for a given wind resource and installed costs have fallen as wind turbine prices have declined from their peak in 2008. Balance of project costs have as well lowered, resulting in a decline in the LCOE of wind and arousing increased deployment. From 2000 to 2016, cumulative installed wind capacity raised at a compound annual rate of 15%, and by the end of 2016, total installed wind capacity had reached 467 GW, being 454 GW onshore. [8]

7.1   Wind Power technology trends

The greatest share of the total installed cost of a wind project is related to the wind turbines, and these usually include the towers, installation and delivery. The range of the share of wind turbines in total installed costs has historically varied from 64 - 84% for onshore wind and 30 - 50% for offshore wind.

The total installed costs of a wind project are driven by 5 principal cost categories:

- **Turbine cost**: gearbox, generator, rotor blades, nacelle, power converter, transformer and tower

- **Construction works** for the preparation of the site and foundations

- **Grid connection**: comprising transformers and substations and connection to the local distribution or transmission network

- **Planning and project costs**: these can represent a considerable share of the balance of project costs depending on the project complexity and can include development costs and fees, licenses, financial costs, development and feasibility studies, legal fees, right of way, insurance, debt service reserves, and construction management not associated with the engineering, procurement and construction contract

- **Land**: cost of land is one of the littlest shares of total costs. Land is normally leased through long-term contracts to diminish the high administrative costs associated with land ownership, but it is sometimes purchased outright.
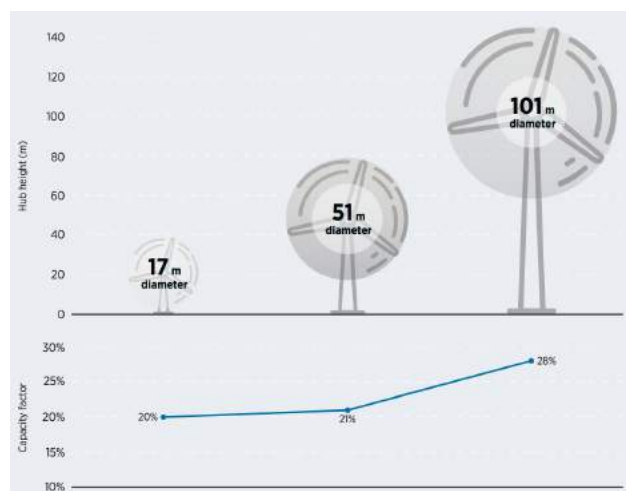
Figure 7.1: Global weighted average hub height, rotor diameter and capacity factors for onshore wind, 1983 (20%) - 2016 (28%) [8]

Some trends work together in synergy to trim the cost of electricity from wind power. As blade lengths have grown, a continuous increase in the average capacity of turbines, hub-heights and swept areas is seen. Higher wind speeds can be accessed with higher hub-heights, while larger swept areas from longer blades also boost the yield of a wind turbine. Larger projects can be allowed with higher turbine capacities, which can amortize project development costs over a larger output. The settlement for these developments is that taller towers supporting larger weight generally cost more, so the impact in some markets might be cost-neutral for installed costs, but leading to a lower LCOE due to the higher yields. For instance, hub heights increased from around 20 metres in 1983 to over 100 metres in 2016, while capacity factors increased from 23% in 1983 to 28% in 2016 (figure 7.1). Another question is that longer blade lengths imply extra engineering challenges, as loads on turbines increase noticeably with longer blades, thus needing a diverse structural design.

7.2   Wind turbine costs

Wind turbine prices fluctuate with demand and supply, together with economic cycles. The latter can affect the cost of the materials used in wind turbine manufacturing, since these have a crucial disclosure to commodity [4] prices. The increasing costs of wind turbines has been driven by 3 factors:

- Initially, the *increase in construction costs* with materials (such as steel, copper and cement), labour and civil engineering costs

- Then, for a few years, *demand outstripped supply* as many countries adopted policies favourable to wind deployment, allowing manufacturers to operate with higher margins

---

[4]Reasonably interchangeable good or material, bought and sold freely as an article of commerce. Commodities include agricultural products, fuels, and metals and are traded in bulk on a commodity exchange or spot market.

- Finally, a trend that has continued ever since is the distinctly *improved technology*; wind turbine manufacturers introduced larger, more expensive turbines, with higher hub heights.

Hence, more capital-intensive foundations and towers were required, although higher energy output were delivered, largely offsetting the higher installed costs and thus delivering a lower LCOE. The total installed costs of onshore wind projects and global weighted average can be seen in figure 7.2.
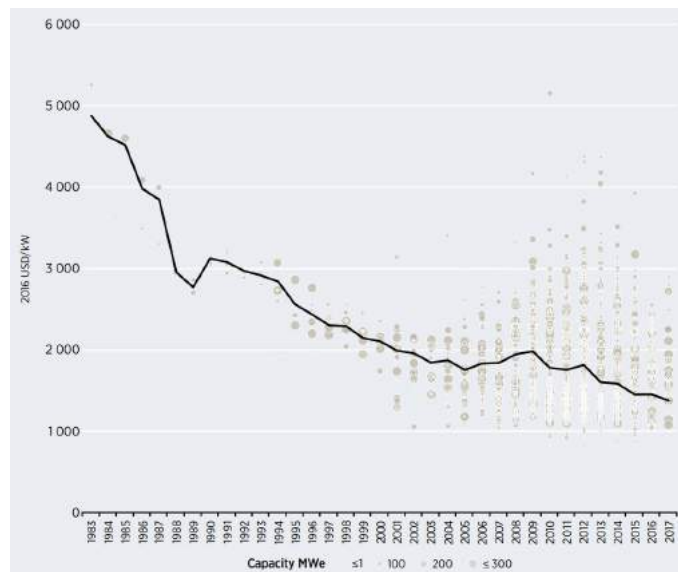
Figure 7.2: Total installed costs of onshore wind projects and global weighted average, 1983-2017 [8]

7.2.1 Total installed costs for onshore wind

Onshore wind installed costs have declined markedly, over 70% from 1983 - 2016, as costs fell from 4,880 USD to 1,477 USD/kW. The lowest installed costs for onshore wind projects were found in China and India, with weighted average total installed costs approximated to 1,245 USD/kW and 1,121 USD/kW respectively in 2016. In terms of zones, Asia, Oceania, Central America and the Caribbean and South America were the most expensive regions, with weighted averages of between 1,884 USD and 2,256 USD/kW in 2016. Between 2010 and 2016, costs fell by 36% in Oceania, 22% in North America, 19% in Europe and between 13% and 19% in other zones. Cost ranges also represent the natural variation of renewable power projects, given the site-specific characteristics that can influence total installed costs, such as the level of existing infrastructure to enable access to sites, the distance from ports or manufacturing hubs, the distance from a major grid-interconnection point, labour costs among others. [8]

7.3 Capacity factors

The capacity factors of wind projects are driven by the quality of the wind resource and the technology used. There has been a trend towards the use of more advanced turbine technologies as previously discussed. Consequently, a consistent trend towards bigger capacity factors globally is seen, but with significant variations by market, which has been determined by the growth in the average hub height, turbine rating and rotor diameters of installed turbines, but also by the trends in resource quality at new projects in individual markets. The global weighted average capacity factor for onshore wind increased from 20% in 1983 to about 29% in 2017. Figure 7.3 addresses the change in the weighted average capacity factor of onshore wind projects that were commissioned in 2010 and 2016 in different countries.
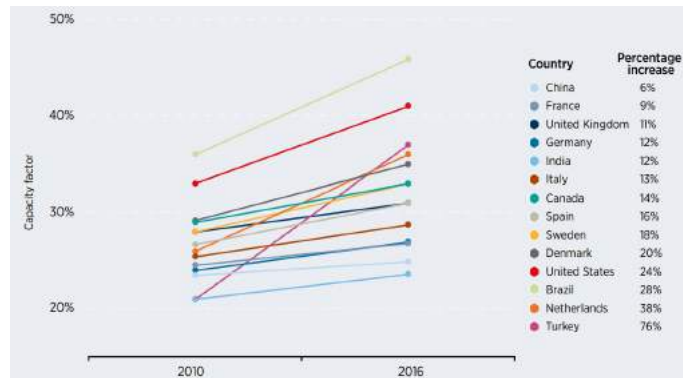
Figure 7.3: Country-specific weighted average capacity factors for new wind projects, 2010 and 2016 [8]

7.4 Operation and maintenance costs
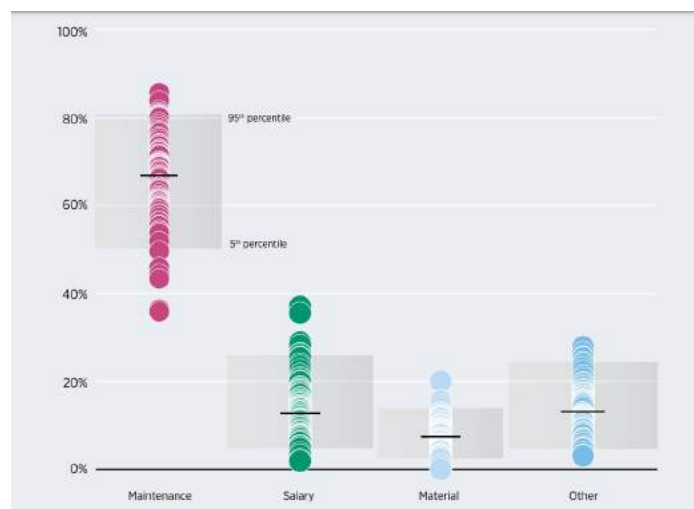
Figure 7.4: O&M costs by component, 2008-2016 [8]

Operations and maintenance costs (O&M), both fixed and variable, are a important part of the LCOE of wind power. O&M costs vary depending on the year. The largest share of O&M costs is represented by maintenance operations, which have a weighted average of 67%, followed by salaries at 14% and materials at 7% (Figure 7.4). Initial full service contracts varied from 14 USD to 30 USD/kW/year between 2008 and 2017, while full-service renewal contracts varied from 22 USD to 44 USD/kW/year.

In China, costs ranging from 0.008 USD to 0.028 USD/kWh can be typical, while the average is 0.017 USD/kWh. In India, weighted average O&M costs range from 0.005 USD to 0.027 USD/kWh. The weighted average O&M costs for Central and South America is 0.014 USD/kWh.

7.5   Levelised Cost of Electricity

The LCOE of a wind power project is driven by total installed costs, wind resource quality, the technical characteristic of the wind turbines used, O&M costs, the cost of capital and the economic life of the project. Thus, the LCOE depends principally on 4 factors:

- **Capacity factor**: which depends on many variables, among which the most critical is the nature and quality of the wind resource, followed by wind turbine design and operational availability, including potential curtailment

- **Total installed costs**: depending on the complexity of the project, the turbine cost is generally the single biggest cost part in a wind project

- **WACC**: the cost of debt, the equity premium of the investors and the share of debt and equity in a project all go towards the final value of the Weighted Average Cost of Capital

- **O&M costs**: operational expenses comprise both fixed and variable costs and can represent up to 20 - 25% of LCOE.
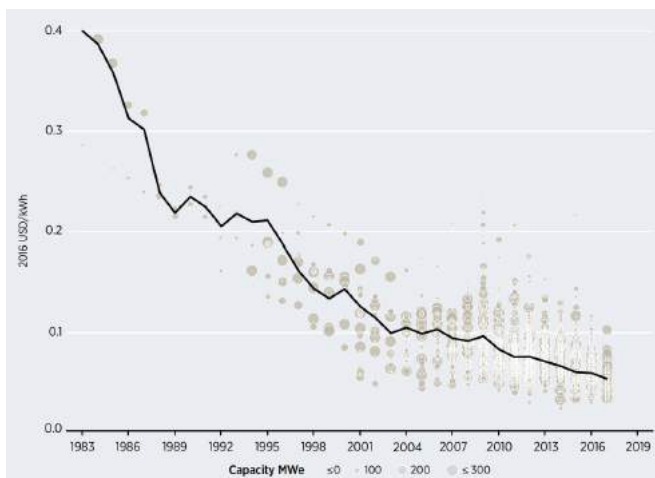
Figure 7.5: The global weighted average LCOE of onshore wind, 1983-2017 [8]

Figure 7.5 shows the evolution of the LCOE of onshore wind between 1983 and 2017. The global weighted average LCOE declined from 0.40 USD/kWh in 1983 to 0.06 USD/kWh in 2017, meaning an 85% decline. The data suggests that every time cumulative installed capacity doubles, the LCOE of onshore wind drops by 15%. This trend includes the impact of lower O&M costs over time, but not the impact of a reduced cost of capital, as technology matures and financial markets become more comfortable with wind power development. [8]

7.5.1 LCOE of different energy sources

One of the parameters to compare costs of energy across various technologies is the LCOE. As future investment decisions are largely influenced by costs, estimates in the research of Ram et al. (2018) prove renewables and storage to be far cheaper than fossil and nuclear sources by 2030, even without considering external costs. Renewable energy technologies offer the lowest LCOE ranges across G20 countries in 2030. Utility-scale solar PV generally shows the lowest values ranging from 16 to 117 $€/MWh_{el}$ and onshore wind LCOE range is from 16 to 90 $€/MWh_{el}$. Rooftop solar PV generally offers the next lowest LCOE ranging from 31 to 126 $€/MWh_{el}$, followed by LCOE of offshore wind power ranging from 64 to 135 $€/MWh_{el}$. Solar PV and battery systems are highly competitive on an LCOE basis at utility-scale ranging from 21 to 165 $€/MWh_{el}$ and at residential scale from 40 to 204 $€/MWh_{el}$. Such numbers have been calculated with the LCOE formula, described in eq. (7.1)

$$LCOE = \frac{capex_{Real} * opex_{fixed} + \frac{decomissioning\ costs}{N}}{FLH} + opex_{variable} + LCOS$$
$$+ fuel\ costs + waste\ disposal\ costs + external\ costs + GHG\ costs$$

$$(7.1)$$

Where $capex_{Real}$ is the annual capital expenditures ($€/MW_{el}$), which include a low and high estimate for investments and budget overruns; $opex_{fixed}$ are fixed O&M costs (% of capex/year); Decommissioning costs are given as a percentage of capex for all technologies except nuclear power plants, for which they are expressed as a value in $€/MW_{el}$; N is the operational lifetime of the technology; $opex_{variable}$ is the annual variable O&M costs ($€/MWh_{el}$); LCOS is the levelised cost of storage in $€/MWh_{el}$ (see eq. (7.3)); Fuel costs are expressed in $€/MWh_{el}$; Waste disposal costs are given in $€/MWh_{el}$; External costs include a range of socio-economic costs related to energy generation ($€/MWh_{el}$); GHG costs include the full socio-economic costs of GHG emissions ($€/MWh_{el}$).

The capital recovery factor *(crf)* is calculated according to equation (7.2).

$$crf = \frac{WACC * (1 + WACC)^N}{(1 + WACC)^N - 1}$$

$$(7.2)$$

Where *WACC* is the weighted average cost of capital and N is the operational lifetime of the technology. Also, the *LCOS* is calculated according to equation (7.3).

$$LCOS = \frac{storage\ capacity * \left[(capex_{Real} * crf) + opex_{fixed}\right]}{System\ output} + \frac{costs\ of\ battery\ losses}{System\ output}$$

$$(7.3)$$

Chapter 8

Potential impact of wind farms on the environment

The use of wind power has a minor environmental footprint compared to the severe effects of conventional electricity generation, which affects climate change and disturbs the natural balance. Wind power does not generate harmful emissions or hazardous waste, it does not deplete natural resources, nor causes environmental damage through resource extraction, transport and waste management. Wind turbines occupy less than 1% of the land area and once up and running, existing activities, such as agriculture can continue around them.

8.1 Finnish policies for wind power generation

8.1.1 Land use and building act

In accordance with the *Land Use and Building act* in **section** 77, the use of a *master plan* (see section 8.3) as a basis for a wind turbine building permit is briefly stipulated. A building permit for the construction of a wind turbine may be granted if the binding master plan clearly provides specific content requirements for a general plan for wind power construction, including:

- An adequate guidance of the construction and other uses of the area

- The planned wind power construction and other land use adapted to the landscape and environment

- The technical maintenance of turbines and the transmission of electricity.

Also, in **section** 137, special conditions for planning permission in the planning area in addition to what is otherwise provided for in a building permit, requires that the building:

- does not interfere with town planning or any other projected area use

- is suitable for the construction of infrastructure networks and transport corridors and for road safety and accessibility of services

- is suitable from a landscape point of view and does not hinder the preservation of the special values of the natural or cultural environment.

Regional decisions on the special conditions of the building permit may happen if there is a valid master plan in the area. The municipality may decide on the presence of the special conditions of a building permit provided for more than one site at a time. Such a decision may be made in an area designated as a village or otherwise suitable for construction in a legally binding master plan. [55]

8.1.2 Act on Environmental Impact Assessment Procedure 252/2017

Finnish legislation in the Act on Environmental Impact Assessment (EIA) Procedure applies to all projects that may be expected to have considerable negative environmental impacts. Appendix 1 of the EIA Act entitles WTGs with a nominal output of no more than 45MW to be exempted from performing an EIA, which is a change from the previous limit of 30MW. Projects with turbines exceeding 9 are obliged to perform an EIA, regardless of the MW output. [56]

8.2 Decision regarding the need of planning (STR)

STR or *Rakennusluvan erityiset edellytykset suunnittelutarvealueella* in Finnish is the first permit for small projects from 1 up to 5 turbines, defined in *section 137* in the Land Use and Building act for granting a building permit in areas where planning is required. Necessary environmental field studies and impact assessment are carried out before or within the process. The steps are shown in figure 8.1. [9]

Figure 8.1: Decision regarding the need of planning [9]

8.3 Master Plan

Also known as the *zoning* or *land use planning* is for projects with a total power below 45 MW where necessary environmental field studies and impact assessment are carried out within the process. The Master plan for wind power projects is

defined in *section 77* in the Land Use and Building act. Only *public display* (PD) for a master plan proposal is obligatory, but typically 3 PD are carried out. A typical overall timetable without appeals is of 12-18 months (see figure 8.2). [9]
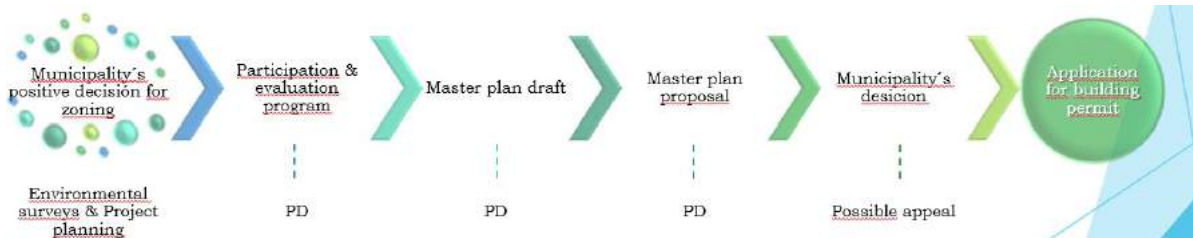
Figure 8.2: Master plan [9]

8.4   Environmental Impact Assessment

A wind farm development is subject to EIA to ensure that the potential effects on the immediate environment are carefully considered before allowing the construction of the facility, and applies to projects of over 45 MW. Usually, impacts can be avoided or reduced by adjusting the location of the whole development (at the planning stage), the number of turbines or by relocating the wind turbines within the existing boundaries of the development. EIA process is commonly synchronized with the master plan and it is defined in the *Finnish Act on Environmental Impact Assessment Procedure 252/2017*. A typical overall timetable without appeals is of roughly 18 months. EIA steps are summarized in figure 8.3. [56]
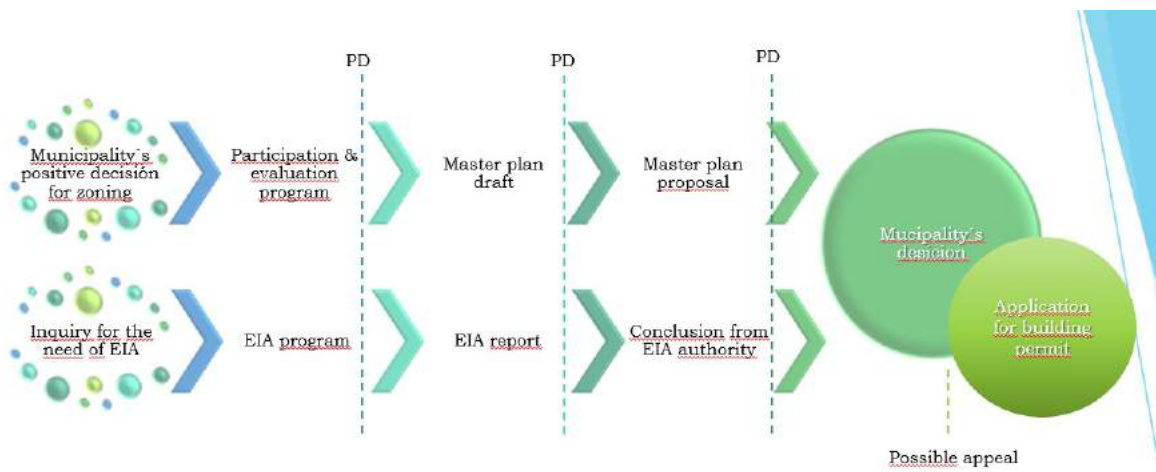
Figure 8.3: Master plan and Environmental Impact Assessment Procedure [9]

8.5   Environmental impacts of wind power

Wind farms could impact the natural and urban environment, but with an optimal design of such facilities, it is possible to avoid or reduce the negative environmental impacts. Therefore, existing municipality development plans shall be designed in relation to the natural, built and geological heritage, especially if these are protected by law, and they should consider the following aspects:

- **Natural heritage**: it refers to habitats and species of flora and fauna located within protected sites. Habitats that may be impacted by wind projects are peat lands (blanket bog, temporary ponds, flushes, flood zones and various other wetland habitats with water courses and lakes), sand dune systems, steppes, grasslands and woodlands. The degree at which birds will have a repercussion by wind energy developments will depend on species, season and location, being either temporary or permanent impacts. Among the species at most risk, birds of prey, swans, geese and divers are found, as well as endangered morass birds in the brooding stage and water birds in flocks. Deliberate awareness is required for potential impacts on migratory birds and local bird movements between egg-laying, feeding and brooding areas.

- **Geology**: a geological and hydrogeological assessment of the suitability of the site holds a site map of areas of important mineral or combined potential, an appraisal of the potential impact of the facility on groundwater, a geotechnical stability analyses of the structure as well as the potential effect of the disposal of excavated materials.

- **Archaeology**: the potential impact of the proposed developments on the archaeological heritage of the site should be assessed, addressing the direct repercussions on the integrity and visual amenity of monuments, including proper protection measures.

- **Noise**: the noise of wind turbines arise from the aerodynamic noise of the blades and the individual parts of the electricity generation machinery, such as the gear box, generators and cooling systems. The noise caused by wind power is roughly 40 dB at a distance of 500–700 metres from the wind turbine and is comparable to that of a modern dishwasher. Normal household noises range from 40–45 dB and in offices the noise level rises to almost 50–60 dB. In a moving car, the noise level is roughly 70 dB. [57]

- **Proximity to roads, railways and power lines**: although wind turbines erected in accordance with standard engineering practice are stable structures, best practice indicates that it is advisable to achieve a safety set back from roads and railways of a distance equal to the height of the turbine and length of the blade. Furthermore, adequate clearance between structures and overhead power lines shall be provided as required by the competent electricity company and aligned with the Finnish regulations.

- **Interference with communication systems**: wind turbines, like all electrical

devices, produce electromagnetic radiation that can interfere with broadcast communications. Such interference can be overcome through the installation of deflectors or repeaters. Turbines must not create electromagnetic interference with the operation of telecommunication networks and must harmonize with the measures for the elimination of electromagnetic interference in the operation of telecommunication networks and signal reception.

- **Air traffic safety**: the siting of wind turbines may have implications for the operations of the communications, navigation and surveillance systems used for air traffic control and aircraft safety as well as in flight corridors. Further, in order to assure the safety and efficiency of aircraft operations nearby airports, the *International Civil Aviation Organization* (ICAO) has defined a volume of air space above which new objects are not permitted [5]. No part of the wind turbine should penetrate this space. [58]

- **Shadow flicker**: the rotor blade creates moving shadows as it rotates when the sun shines behind the wind turbine. Such shadow results from the movement of the blades and is called the *shadow flicker*. The effect can be noticed up to 1–2 km from the wind turbine. Withal, the flicker can exclusively be perceived on the sunniest of days and only on specific hours of the day. [57]

- **Landscape and social concerns**: as part of the planning stage, it is important to consider the resident´s opinion regarding the change in the visual environment, since it may arise controversy among them. [9]

- **Decommissioning**: usually, the operational life of a wind turbine is around 20-25 years. Issues to be addressed when decommissioning include the removal of above ground structures and equipment, landscaping and reinstatement of roads and vegetation, as well as measures for the restoration of the environment to its original state to the greatest possible extent. Each case is different depending on the size of the development and geographic properties of the locality. [58]

---

[5]https://www.icao.int/safety/Pages/default.aspx

Chapter 9

Discussions and Conclusions

Three different sites located in Finland were analyzed in terms of the wind resource with three different wind simulation software: WindPRO, WindSim and Zephy TOOLS. The places were Korpinen with a quite gentle slope, Lokan Tekojärvi with a moderate slope and Ylläs with a steep slope, all of them simulated using real wind data obtained from the site Finlandia.

In the case of the *quite gentle* slope it is evident that both WindPRO and WindSim predicted quite precisely the wind speed of the met mast, the latter differing with only 0.13% while Zephy TOOLS overestimated this value in 0.40%. Results are in line with what is stated in section 3.2 about distinctness in the models. Both WindPRO and WindSim manage to estimate the wind resource accurately when the the terrain has a low orographic complexity (there is no flow separation since there are only low angle slopes). Namely, the need for modeling turbulence is irrelevant in low orographic situations. In this case, the linear model, without the ability to model turbulence is as good as the non-linear model in wind resource estimation terms. Moreover, the linear model is in this case much more time efficient than the non-linear model.

In the case of the *moderate slope*, the same results as in the case of the gentle slope were obtained for both WindPRO and WindSim in the met mast position, whereas Zephy TOOLS over-predicted such value 0.40%. Here, when the elevation difference becomes greater between the met mast and the turbines, the software differ significantly, as explained in table 6.5. Yet, when the height difference is between 100m, results are still acceptable.

For the *steep slope*, WindPRO estimated correctly the wind speed in the met mast position, while WindSim overestimated it with only 0.15% and Zephy TOOLS with 1.34%. These results were expected because of the flat terrain at which the met mast is located. Nonetheless, for the wind turbine located in the top of the mountain, the three software produced different results, differing in around 1.35m/s between them. In general, most of the software will have issues predicting the wind speed when a steep slope comes into question since flow separation may occur, so placing the met mast closer to the potential wind turbine position could

lower the uncertainties.

In the case of WindSim, the simulation cases performed to investigate the influence of the *Obukhov length* showed that this is indeed an important parameter that can influence the results considerably. Also, the number of *iterations* is crucial to reach a convergence in the calculations, considering that the number of iterations is proportional to the computational times. Also, increased *complexity* leads to a need for an increased grid size to reach convergence which is dependent on both the number of iterations as well as the grid size.

Overall, WindPRO and WindSim are the preferred software for wind assessment when it comes to gentle and moderate slopes. Zephy TOOLS is still under development and their results can still be questionable, even though they were not far from the results obtained by the others software. In terms of computing times, WindPRO is way faster than both WindSim and Zephy TOOLS. Regarding user experience, WindPRO has a pretty visual interface but many of the useful commands are hidden unless the user has some experience with the software. WindSim is very straightforward and easy to use when the input values are available. Zephy TOOLS has also an user-friendly interface but does not show any information when an error appears, so the user cannot know what is wrong.

Finally, for the results output, WindPRO generates an elegant PDF with the production results and has a charming graphic interface for 3D graphics with interchangeable colors. WindSim generates autumn-colors graphics that cannot be modified unless exported to a 3rd software. Zephy TOOLS generates as well a detailed report with all the parameters used and the results obtained, together with several neat visualizations with delightful colour combinations.

9.1   Recommendations for further investigation

It is recommended to increase the number of simulation sites to cover for different orographic complexities and roughness heights. Also, adding more wind turbines and different hub heights to investigate the energy production.

For WindSim, developing clear guidelines for defining which values are appropriate for treating the atmospheric stability, specifically, for the height distribution factor, as well as for the forest module, including the forest height, forest resistive and the roughness height. In the wind fields, the height of the boundary layer has to be further investigated, as well as the Monin-Obukhov length as it can change results considerably. The number of iterations can produce different results even though the same parameters are applied.

In Zephy TOOLS, many questions may arise when running a simulation. Creating a support forum with developers would save a lot of time, as well as a user guideline with solutions to all the possible errors that a user may encounter.

Bibliography

[1] Miroslav Petrov. *Green aircraft propulsion C-Seminar*. `Wind%20Turbines%201.4%20Practical%20aerodynamics%20&%20characteristics.pdf`. (Accessed on 08/02/2019). 2017.

[2] *Wind energy: On the grid, off the checkerboard*. `https://phys.org/news/2014-04-energy-grid-checkerboard.html`. (Accessed on 08/06/2019).

[3] Weijun Wang, Stéphane Caro, Fouad Bennis, and Oscar Roberto Salinas Mejia. "A Simplified Morphing Blade for Horizontal Axis Wind Turbines". In: *Journal of Solar Energy Engineering* 136 (Feb. 2013), p. 011023. DOI: `10.1115/1.4025970`.

[4] *Don't be fooled: there is no such thing as wind speed*. `https://www.rechargenews.com/wind/1769531/dont-be-fooled-there-is-no-such-thing-as-wind-speed`. (Accessed on 08/15/2019).

[5] *WindSim Write Up - Validation study.docx*. `https://www.windsim.com/documentation/papers_presentations/thesis/080512trw%20WindSim%20Write%20Up%20-%20Validation%20study.pdf`. (Accessed on 07/17/2019).

[6] *Korpinen - Järviwiki*. `https://www.jarviwiki.fi/wiki/Korpinen_(61.721.1.007)`. (Accessed on 07/09/2019).

[7] *Vestas signs V150 blade deal with TPI | Windpower Monthly*. `https://www.windpowermonthly.com/article/1459778/vestas-signs-v150-blade-deal-tpi`. (Accessed on 08/22/2019).

[8] The International Renewable Energy Agency. *Renewable power generation costs in 2017*. `https://www.irena.org/-/media/Files/IRENA/Agency/Publication/2018/Jan/IRENA_2017_Power_Costs_2018.pdf`. (Accessed on 08/28/2019). 2018.

[9] Etha Wind Oy Ab. "Wind power projects – Permitting summary in Finland". `http://cloud.etha.fi/index.php/apps/files/?dir=/1sales/0SalesSupport/Presentations&fileid=652188`. (Accessed on 08/26/2019).

[10] H. K. Versteeg and W. Malalasekera. *An introduction to computational fluid dynamics - the finite volume method 2nd edition.pdf*. `http://ftp.demec.ufpr.br/disciplinas/TM702/Versteeg_Malalasekera_2ed.pdf`. (Accessed on 07/18/2019). 2007.

[11] Eric Johansson. "En jämförelse av vindresursberäkningar i kuperad skogsterräng med programmet WAsP (linjär modellering) och CFD-programmet WindSim". swe ; eng. MA thesis. Uppsala universitet, Teknisk-naturvetenskapliga vetenskapsområdet, Geovetenskapliga sektionen, Institutionen för geovetenskaper, 2013.

[12] Carlos Díaz-Asensio Mancebo. "Comparison study for wind resource assessment in complex domain using Meteodyn and WindSim". eng. MA thesis. 2014.

[13] Kunal Kushal Dayal. "Offshore wind resource assessment, site suitability and technology selection for bligh waters Fiji using WindPRO". eng. MA thesis. Uppsala universitet, Teknisk-naturvetenskapliga vetenskapsområdet, Geovetenskapliga sektionen, Institutionen för geovetenskaper, 2015.

[14] Karl Nilsson. "Estimation of wind energy production in relation to orographic complexity". (Accessed on 07/18/2019). MA thesis. Gotland University, 2010.

[15] Nikolaos Simisiroglou. "Wind resource assessment comparison on a complex terrain employing WindPRO and WindSim". MA thesis. Gotland University, School of Culture, Energy and Environment, 2012, p. 48.

[16] Tobias Timander and Jimmy Westerlund. "Reliability of wind farm design tools in complex terrain: A comparative study of commercial software". eng ; swe. MA thesis. KTH, Skolan för industriell teknik och management (ITM), Energiteknik, Kraft- och värmeteknologi, 2012.

[17] Jae-Kyoon Woo, Hyeon-Gi Kim, Byeong-Min Kim, Il-Han Gwon, In-Su Baek, and Neung-Soo Yoo. "AEP Prediction of a Wind Farm in Complex Terrain - WindPRO Vs. WindSim". In: *Journal of the Korean Solar Energy Society* 32 (Dec. 2012). DOI: `10.7836/kses.2012.32.6.001`.

[18] Shafiul Murshed Maruf. "Wind resource assessment and site suitability in Bangladesh using WindPRO and WindSim". MA thesis. Uppsala University, Department of Earth Sciences, 2015, p. 75.

[19] Steven A. Ackerman and John A. Knox. *Meteorology: Understanding the Atmosphere*. Pacific Grove, CA: Thomson Brooks/Cole, 2012.

[20] *Coriolis Effect - an overview*. `https://www.sciencedirect.com/topics/earth-and-planetary-sciences/coriolis-effect`. (Accessed on 07/20/2019).

[21] *Centrifugal Force - an overview*. `https://www.sciencedirect.com/topics/earth-and-planetary-sciences/centrifugal-force`. (Accessed on 07/20/2019).

[22] *Friction - an overview*. `https://www.sciencedirect.com/topics/materials-science/friction`. (Accessed on 07/20/2019).

[23] C. Donald Ahrens. *Meteorology Today : an Introduction to Weather, Climate, and the Environment*. Belmont, CA: Thomson/Brooks/Cole, 2007.

[24] *Virtual temperature - AMS Glossary*. `http://glossary.ametsoc.org/wiki/Virtual_temperature`. (Accessed on 08/06/2019).

[25] Monica Górska, J Arellano, Margaret A. LeMone, and Chiel van Heerwaarden. "Mean and Flux Horizontal Variability of Virtual Potential Temperature, Moisture, and Carbon Dioxide: Aircraft Observations and LES Study". In: *Monthly Weather Review 136 (2008)* 136 (Nov. 2008). DOI: `10.1175/2008MWR2230.1`.

[26] A.R. Jha. *Wind Turbine Technology*. CRC Press, 2010. ISBN: 9781439815076. URL: `https://books.google.fi/books?id=cKDMBQAAQBAJ`.

[27] Lalit Anjum. "Wind Resource Estimation Techniques-An Overview". In: *International Journal of wind and Renewable Energy* Volume 3 (Jan. 2014), pp. 26–38.

[28] Ioannis Kastanas, Andreas Georgiou, Panagiotis Zavros, and Evangelos Akylas. "An integrated GIS-based method for wind-power estimation: Application to western Cyprus". In: *Central European Journal of Geosciences* 6 (Mar. 2014), pp. 79–87. DOI: `10.2478/s13533-012-0162-3`.

[29] *Roughness classes and associated roughness lengths.* `https://barani.biz/apps/wind-height/`. (Accessed on 07/20/2019).

[30] Ib Troen and Erik Lundtang Petersen. *European Wind Atlas.* English. Risø National Laboratory, 1989. ISBN: 87-550-1482-8.

[31] *EMD International A/S Energy Modules.* `https://www.emd.dk/windpro/windpro-modules/energy-modules/`. (Accessed on 06/20/2019).

[32] *How Do Wind Turbines Work? | Department of Energy.* `https://www.energy.gov/eere/wind/how-do-wind-turbines-work`. (Accessed on 07/31/2019).

[33] *Vestas | Options & Solutions.* `https://www.vestas.com/en/products/options_and_solutions#!power-and-load-optimised-modes-`. (Accessed on 07/31/2019).

[34] *Wake effect.* `http://mstudioblackboard.tudelft.nl/duwind/Wind%20energy%20online%20reader/Static_pages/wake_effect.htm`. (Accessed on 07/31/2019).

[35] K G. Rados, John Prospathopoulos, Evangelos Politis, P.K. Chaviaropoulos, and A Zervos. "CFD modeling issues of wind turbine wake under stable atmospheric conditions". In: vol. 6. Jan. 2009.

[36] *European Wind Turbine Standards II.* `https://publicaties.ecn.nl/PdfFetch.aspx?nr=ECN-C--99-073`. (Accessed on 07/31/2019).

[37] *Development of a New Wake Model Based on a Wind Tunnel Experiment.* `http://windeng.t.u-tokyo.ac.jp/ishihara/e/posters/2004_gwp_poster.pdf`. (Accessed on 07/31/2019).

[38] V. Quaschning. *Understanding Renewable Energy Systems.* Earthscan, 2005. ISBN: 9781844071289. URL: `https://books.google.fi/books?id=tNelPKdQxoMC`.

[39] Sathyajith Mathew. *Wind energy: Fundamentals, resource analysis and economics.* Jan. 2007, pp. 1–246. DOI: `10.1007/3-540-30906-3`.

[40] H. Nfaoui. "Wind Energy Potential". In: *Comprehensive Renewable Energy.* Ed. by Ali Sayigh. Oxford: Elsevier, 2012, pp. 73 –92. ISBN: 978-0-08-087873-7. DOI: `https://doi.org/10.1016/B978-0-08-087872-0.00204-3`. URL: `http://www.sciencedirect.com/science/article/pii/B9780080878720002043`.

[41] Steven Lang and Eamon Mckeogh. "LIDAR and SODAR Measurements of Wind Speed and Direction in Upland Terrain for Wind Energy Purposes". In: *Remote Sensing* 3 (Dec. 2011), pp. 1871–1901. DOI: `10.3390/rs3091871`.

[42] *met mast | Wind farms construction.* `http://www.windfarmbop.com/tag/met-mast-2/`. (Accessed on 08/06/2019).

[43] *Wind resources for energy production of wind turbines - WAsP.* `https://www.wasp.dk/wasp`. (Accessed on 06/17/2019).

[44] *WindSim :: WindSim | Technical Basics.* `http://www.windsim.com/software/windsim---technical-basics.aspx`. (Accessed on 06/20/2019).

[45] *WindSim :: WindSim | Module Overview.* `http://www.windsim.com/software/windsim---module-overview.aspx`. (Accessed on 06/20/2019).

[46] *Global Settings and Interface — Documentation.* `http://documentation.zephy-science.com/ZephyTOOLS/en/2_Global/global.html`. (Accessed on 08/07/2019).

[47] *Input Files — Documentation.* `http://documentation.zephy-science.com/ZephyTOOLS/en/4_Input_Files/files.html`. (Accessed on 08/07/2019).

[48] *ZephyCFD — Documentation.* `http://documentation.zephy-science.com/ZephyTOOLS/en/7_ZephyCFD/zephycfd.html`. (Accessed on 08/07/2019).

[49] *Geography of Finland, Landforms - World Atlas.* `https://www.worldatlas.com/webimage/countrys/europe/finland/filand.htm`. (Accessed on 07/04/2019).

[50] *Lake Lokka - Järviwiki.* `https://www.jarviwiki.fi/wiki/Lokan_tekoj%C3'%A4rvi_(65.931.2.001)`. (Accessed on 07/08/2019).

[51] *Ylläs | Ski.fi.* `https://www.ski.fi/keskukset/yllas/`. (Accessed on 07/09/2019).

[52] *File service of open data.* `https://tiedostopalvelu.maanmittauslaitos.fi/tp/kartta?lang=en`. (Accessed on 07/03/2019).

[53] *Paikkatietoaineistojen latauspalvelu - LAPIO.* `http://paikkatieto.ymparisto.fi/lapio/latauspalvelu.html`. (Accessed on 07/03/2019).

[54] Manish Ram, Michael Child, Arman Aghahosseini, Dmitrii Bogdanov, Alena Lohrmann, and Christian Breyer. "A comparative analysis of electricity generation costs from renewable, fossil fuel and nuclear sources in G20 countries for the period 2015-2030". In: *Journal of Cleaner Production* 199 (Oct. 2018), pp. 687–704. DOI: `10.1016/j.jclepro.2018.07.159`.

[55] *Land Use and Building Act 132/1999 - Up-to-date legislation - FINLEX.* `https://www.finlex.fi/fi/laki/ajantasa/1999/19990132`. (Accessed on 08/25/2019).

[56] *Updated Environmental Impact Assessment Rules for Wind Power Projects.* `https://www.castren.fi/blogandnews/news-2019/updated-environmental-impact-assessment-rules-for-wind-power-projects/`. (Accessed on 08/24/2019).

[57] *Suomen Hyötytuuli – Environmental impacts of wind power.* `https://hyotytuuli.fi/en/wind-power/environmental-impacts-of-wind-power/`. (Accessed on 08/24/2019).

[58] United Nations Development Programme (UNDP) Serbia. *Guidelines of the environmental impact assessment for wind farms.* `https://www.unece.org/fileadmin/DAM/env/eia/documents/EIAguides/Serbia_EIA_windfarms_Jun10_en.pdf`. (Accessed on 08/24/2019).